PROCESS CHARACTERIZATION OF COMPOSITE STRUCTURES MANUFACTURED USING RESIN IMPREGNATION TECHNIQUES

A THESIS SUBMITTED TO
THE GRADUATE SCHOOL OF NATURAL AND APPLIED SCIENCES
OF
MIDDLE EAST TECHNICAL UNIVERSITY

BY

ADEM ONUR MİSKBAY

IN PARTIAL FULFILLMENT OF THE REQUIREMENTS
FOR
THE DEGREE OF MASTER OF SCIENCE
IN
MECHANICAL ENGINEERING

DECEMBER 2008

Approval of the thesis:

PROCESS CHARACTERIZATION OF COMPOSITE STRUCTURES MANUFACTURED USING RESIN IMPREGNATION TECHNIQUES

submitted by **ADEM ONUR MİSKBAY** in partial fulfillment of the requirements for the degree of **Master of Science in Mechanical Engineering Department, Middle East Technical University** by,

Prof. Dr. Canan Özgen _____
Dean, Graduate School of **Natural and Applied Sciences**

Prof. Dr. Süha Oral _____
Head of Department, **Mechanical Engineering**

Prof. Dr. Levend Parnas _____
Supervisor, **Mechanical Engineering Dept., METU**

Examining Committee Members:

Prof. Dr. Sahir Arıkan _____
Mechanical Engineering Dept., METU

Prof. Dr. Levend Parnas _____
Mechanical Engineering Dept., METU

Assist. Prof. Dr. Merve Erdal _____
Mechanical Engineering Dept., METU

Assoc. Prof. Dr. Altan Kayran _____
Aerospace Engineering Dept., METU

Fikret Şenel _____
R&D Manager, Barış Electric Ind. Inc.

Date: _____

I hereby declare that all information in this document has been obtained and presented in accordance with academic rules and ethical conduct. I also declare that, as required by these rules and conduct, I have fully cited and referenced all material and results that are not original to this work.

Name, Last name : Adem Onur Miskbay

Signature :

ABSTRACT

PROCESS CHARACTERIZATION OF COMPOSITE STRUCTURES MANUFACTURED USING RESIN IMPREGNATION TECHNIQUES

Adem Onur Miskbay

M.S., Department of Mechanical Engineering

Supervisor: Prof. Dr. Levend Parnas

December 2008, 123 pages

The aim of this study is to investigate and compare the properties of two layer carbon epoxy composite plates manufactured using various resin impregnation techniques; Resin Transfer Molding (RTM), Light RTM (LRTM), Vacuum Assisted RTM (VARTM) and Vacuum Packaging (VP). Throughout the study a different packaging method was developed and named Modified Vacuum Packaging (BP). The mechanical properties of composite plates manufactured are examined by tensile tests, compressive tests, in-plane shear tests and their thermal properties are examined by Differential Scanning Calorimetry (DSC) and Thermo Gravimetric Analysis (TGA) tests. All tests were performed according to suitable ASTM standards. The performance of specimens from each process was observed to vary according to the investigated property; however the VP process showed the highest performance for most properties. For most of the tests, VARTM, LRTM and RTM methods were following VP process in terms of performance, having close results with each other.

Keywords: Resin Transfer Molding, Vacuum Assisted Resin transfer Molding, RTM, Light RTM, process characterization, mechanical properties, testing of composites

ÖZ

REÇİNE EMDİRME YÖNTEMLERİ İLE ÜRETİLMİŞ KOMPOZİT YAPILARIN PROSES KARAKTERİZASYONU

Adem Onur Miskbay
Yüksek Lisans, Makina Mühendisliği Bölümü
Tez Yöneticisi: Prof. Dr. Levend Parnas

Aralık 2008, 123 sayfa

Bu çalışmanın amacı, Reçine Transfer Kalıplama (RTM), Hafif RTM (LRTM), Vakum Yardımlı RTM (VARTM) ve Vakum Paketleme (VP) üretim yöntemleri ile üretilmiş iki katlı karbon epoksi kompozit plakaların incelenmesi ve özelliklerinin deneysel olarak belirlenmesidir. Bu çalışma esnasında farklı bir üretim tekniği geliştirilmiş ve Modifiye Vakum Paketleme (BP) olarak adlandırılmıştır. Üretilen kompozit plakaların mekanik özellikleri; çekme, basma ve düzlemsel kayma testleri ile belirlenmiş, ısıl özellikleri ise *Differential Scanning Calorimetry* (DSC) ve *Thermo Gravimetric Analysis* (TGA) testleri ile belirlenmiştir. Bütün testler uygun ASTM standartlarına göre yapılmıştır. Plakaların performanslarının incelenen malzeme özelliğine göre değiştiği gözlenmişse de; VP yönteminin birçok malzeme özelliği için en yüksek performansı sunduğu görülmüştür. LRTM, VARTM ve RTM yöntemlerinde elde edilen değerler, birçok test sonucunda VP yönteminde elde edilen değerleri birbirlerine yakın sonuçlarla takip etmiştir.

Anahtar Kelimeler: Reçine Transfer Kalıplama, Vakum Yardımlı RTM, Hafif RTM, proses karakterizasyonu, mekanik özellikler, kompozit malzeme deneyleri

ACKNOWLEDGEMENT

I would like to express my appreciation and thankfulness to Prof. Dr. Levend Parnas for his encouragement and support that created this study. I also wish to thank my professors in the thesis committee for their suggestion and comments.

Thanks to all my colleagues in Barış Elektrik, leading Fikret Şenel, Bora Balya and Gökhan Güven for their collaboration and support.

I owe Aysu for her precious help, support and friendship.

I would like to thank Çağrı, Mecit and Ilgar for being good friends; and the thanks extend to Ufuk, Onursal, Emre, Günay and Erkal for being great companions in the quest for graduation. Also the logistic support provided by Melis is greatly appreciated.

The special thanks go to my parents Ferdi and Pelin Miskbay for their infinite support, and to my uncle Altan Yazıcı.

TABLE OF CONTENTS

LIST OF TABLES

LIST OF FIGURES

CHAPTER 1

INTRODUCTION

Within the years, composites have become the preferred materials mainly used in high technology industries. The reason composite materials are favored over conventional materials is mostly due to their superior mechanical and chemical properties as well as their ability to be tailored specifically for the object at hand. That is, properties of composite structures being a function of its composing materials, their distribution, the interaction in between, etc. enables the designer to select individual materials; combine them together with a specific alignment and therefore manufacture a product with definite properties.

Polymer matrix composites are highly favored materials in the wide variety of composites because they are relatively easy of manufacture and are lower in weight. In addition, mostly fiber reinforced composites are preferred for high technology applications due to their superior mechanical properties. A fibrous reinforcement is determined by their high aspect ratio. Fiber reinforced polymer matrix (FRP) composites have a wide application range due to their orthotropic nature that is; their mechanical properties are different in different direction axes. This property results in much flexible designs that cannot be obtained with conventional isotropic materials or particle reinforced composites.

However these features come with a price; these materials are difficult to design and characterize; high performance composites are also expensive to manufacture. Within the years study was performed to lower the costs while maintaining – if not developing –

the performance. Several new manufacturing processes were developed; some expensive and high performance some cheap but low performance and some in between.

Within the quest for the cheaper yet high performance processes; resin impregnation methods were developed. The dozens of different impregnation techniques mostly differ in small details. These different processes are usually patented by various companies and are thoroughly studied and characterized.

This study was aimed to make a comparison between the most common resin impregnation techniques using the same tooling and keeping the process parameters as constant as the nature of different processes allow.

1.1. Production Methods

Dozens of resin impregnation methods that are patented by different companies are currently used in composites industry. All of them have slight differences from each other depending to the field of use of the process. Some are developed for very large products such as nautical vehicles therefore are mainly interested in lowering the mold costs and hastening the impregnation process. Whereas some are developed for smaller scale products but require higher strength and better surface quality. Table 1.1 is given to provide an idea of the variety of these impregnation methods.

Table 1.1: Some of the Best Known Resin Impregnation Techniques [1]

Acronym	Name of the Process
RTM	*Resin Transfer Molding*
VARTM	*Vacuum Assisted RTM*
LRTM/RTML	*Light RTM/ RTM Light (A Hybrid RIFT/RTM [Plastech])*
CIRTM	Co-Injection RTM
Crystic VI	Vacuum Infusion (Scott Bader)
DRDF	Double RIFT Diaphragm Forming (University of Warwick)
LRI	Liquid Resin Infusion

Table 1.1 (continued)

Acronym	Name of the Process
MVI	Modified Vacuum Infusion (Airbus)
RFI	Resin Film Infusion
RIFT	Resin Infusion Under Flexible Tooling (ACMC Plymouth)
RIRM	Resin Injection Recirculation Molding
SCRIMP	Seeman Composites Resin Infusion Molding Process
VAIM	Vacuum-Assisted Injection Molding
VAP	Vacuum Assisted Process (EADS)
VARI	Vacuum Assisted Resin Injection System (Lotus Cars)
VARIM	Vacuum Assisted Resin Injection Molding
VIM	Vacuum Infusion Molding
VIMP	Vacuum Infusion Molding Process
VIP	Vacuum Infusion Process

Note that the processes listed in Table 1.1 are only a fraction of all the resin impregnation processes in use.

With this situation in mind three of the most common resin impregnation methods were selected for this study. While selecting which methods to use; manufacturing infrastructure available and common details with other widespread processes are considered. Finally Resin Transfer Molding (RTM), Vacuum Assisted RTM (VARTM) and Light RTM (LRTM) were decided to be used. After the main processes were decided, a more primitive method was introduced to provide some more data for comparison. This process was determined to be Vacuum Packaging (VP) due to its ease of manufacturing and low cost. While the production continued another process was introduced by Barış Elektrik End. A.Ş. engineers, as an alternative to VP process (BP), to provide more data to compare.

All the methods used are briefly explained in the following pages.

1.1.1. Resin Transfer Molding (RTM)

This process is a resin impregnation process in which closed mold tools are used and the resin is injected by means of positive pressure. In this study this process is selected to provide the control data since it is known to be the most advanced and controlled process that results in very high performance products.

At the beginning of the process the dry reinforcements are laid, usually bound together to have the shape of the mold cavity and called preform. Later the two mold tools are clamped to each other and vacuum is applied from exit ports. The resin is injected with a pressure of 1-5 bars depending on the resin-woven type and part size (Figure 1.1).

With RTM, it is possible to obtain higher fiber to resin ratios and very low void content. Moreover, the process is highly automated, thus reducing labor and increasing process reliability. Additionally, the emitted volatiles are reduced to a great extent. Since both sides are in contact with mold, the surface quality is nearly perfect for both sides. The main drawback is the weight and cost of molding which constrains the production to relatively small components [2].

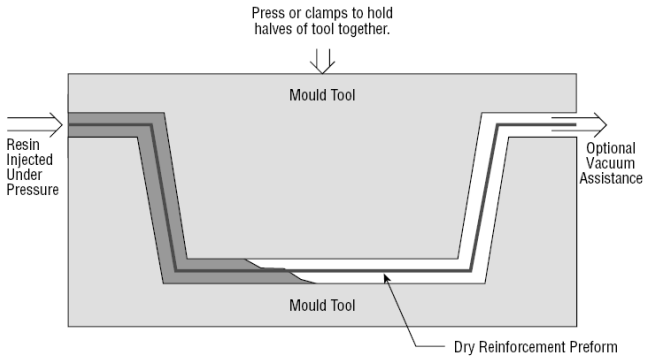

Figure 1.1: Schematic View of Resin Transfer Molding Process [2, 3]

In RTM the dimensions of the component are defined by the separation of the mold faces, whilst in all the other processes examined in this study; the thickness of the part is a function of the pressure history during the process [4].

1.1.2. Vacuum Assisted RTM (VARTM)

The VARTM process has similar advantages to the RTM process. As well as it providing a high fiber to resin ratio and a low void content and reducing the emission of volatiles; this method also requires a less rigid molding tool due to the low pressures involved. As a result, tooling cost is reduced dramatically considering the need for a single sided mold, which does not require high strength. This process allows the production of large pieces [2].

However, there are several disadvantages of the VARTM process. The resin system used should have low viscosity thus affecting the mechanical performance of the final product. Moreover, the final part has a one-sided surface finish due to the single-side mold application. The maximum compaction pressure is 1 atm limiting the maximum achievable fiber volume fraction. Additionally, a pressure gradient develops during infusion, which results in a thickness gradient along the part length between the injection and vent lines. The thickness gradient directly affects the fiber volume fraction variations in the part. It is critical to properly choose the location of the vent to fully wet out the preform, reduce excessive resin bleeding (i.e. minimize waste), and avoid creating resin-starved regions near the vent locations after the inlet is closed [4].

Similar to the RTM process a preform is laid on a mold. Later a peel ply and a sealing plastic bag cover the preform, and the whole system is vacuum bagged to eliminate all the leaks. Following this procedure the resin is allowed to flow into the system therefore impregnating the dry perform (Figure 1.2).

1.1.3. Light RTM (LRTM)

The Light RTM process is basically the hybrid of the RTM and VARTM processes. Two composite molds are used; one of them being relatively more rigid and another being diaphragm like. After laying the preform, the upper and lower molds are clamped using vacuum at the flanges of the diaphragm mold. Later, the resin is injected with the aid of vacuum applied (Figure 1.3).

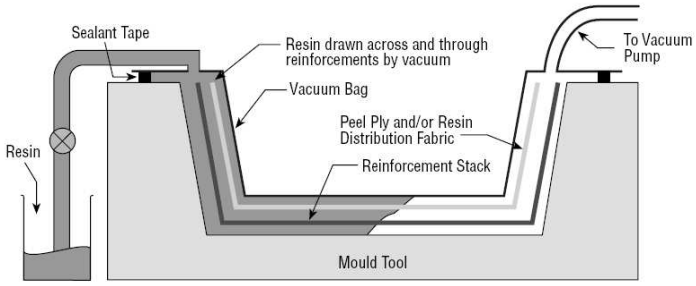

Figure 1.2: Schematic View of Vacuum Assisted Resin Transfer Molding Process [2, 3]

Light RTM process reduces the tooling cost; also the product obtained has low void content, high fiber to resin ratio and good surface quality for both faces. The composite mold can be used for large number of productions therefore reducing the amount of disposable materials used, and once the molds are produced, the manufacturing of products is easier compared to VARTM method. The fabricated products can be larger than those produced with RTM, but are smaller than those of VARTM. However, since the pressure is lower than RTM process, the void content is still greater than that of RTM. Another downside is the mold production, which is complicated and requires highly skilled labor [5].

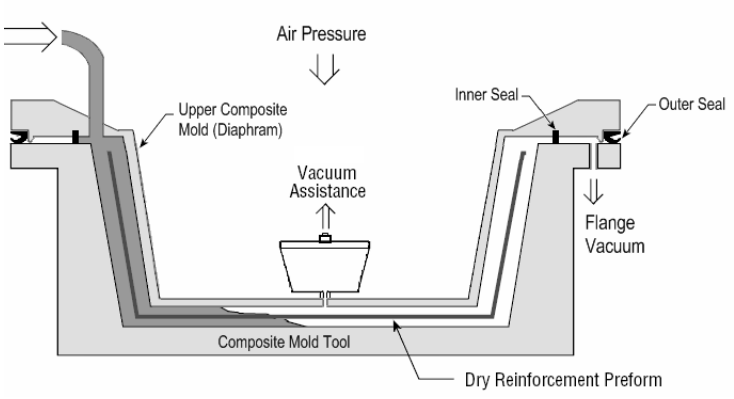

Figure 1.3: Schematic View of Light Resin Transfer Molding Process [2, 3, 5]

1.1.4. Vacuum Packaging (VP)

Vacuum packaging process is an improvement of the conventional hand lay-up process, which improves the uniformity of the distribution of the resin, also regulating the released styrene levels. It can be considered the most primitive and a low performance process used in this study.

Up to the end of impregnation stage, the vacuum packaging process is the same as the hand lay up process. The resin is applied manually to the reinforcement which can be found in the forms of knitted, woven, stitched or bonded fabrics. After the impregnation, a sealing plastic bag is laid over the laminate. Later, the air underneath is extracted using a vacuum pump; thus achieving up to one atmosphere pressure over the laminate. This pressure forces excessive resin to flow in to bleeder, which is removed after curing (Figure 1.4).

Due to the atmospheric pressure involved during curing; higher fiber to resin ratio structures are obtained with this process, when related to hand lay-up process. Also void content, and volatiles emitted are reduced considerably. Because of the resin flow and pressure involved, this process provides a better fiber wetting. On the other hand, this process increases the cost of both labor and disposable materials. Also the resin content

and composition is still affected by operator's skill, therefore the process requires a skilled operator.

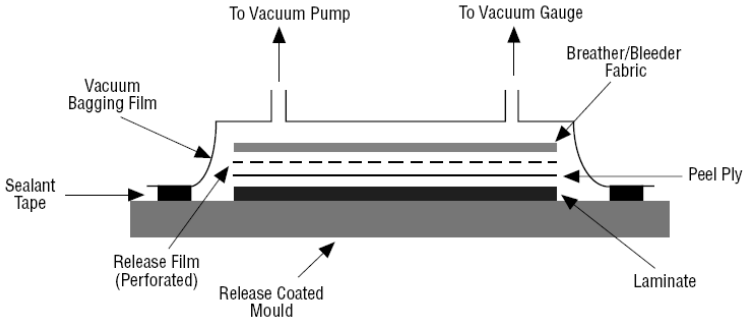

Figure 1.4: Schematic View of Vacuum Packaging Process [2, 3]

1.1.5. Modified Vacuum Packaging (BP)

This process is developed for this study in Barış Elektrik End. A.Ş. to have a different more controlled process relative to vacuum packaging process and no commercial name was found for.

The only difference from the vacuum packaging method is that the resin is applied to the extra bleeder mat which is laid below the preform instead of the fabric itself. Later a peel ply is laid above the wet bleeder following that, the dry fabric is laid above all. Finally the vacuum is applied as performed in the vacuum packaging process (Figure 1.5).

This process is aimed to reduce the void content and to increase the uniformity of the distribution of resin throughout the laminate. The obtained results concerning the mechanical and chemical properties are provided in the test results.

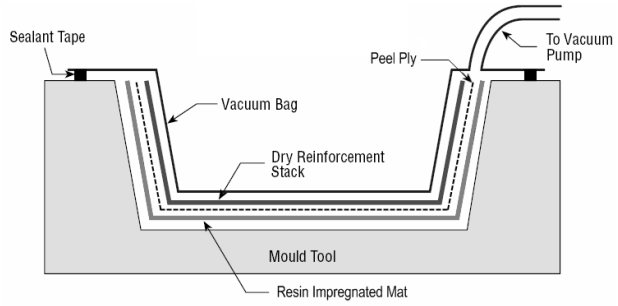

Figure 1.5: Schematic View of Modified Vacuum Packaging Process

1.2. The Scope

The aim of this study is to characterize composite plate products manufactured using the above production methods with the same tooling that is, finding the orthotropic material properties such as E_{xx}, UTS_x, E_{yy}, UTS_y, ν_{xy}, G_{xy} etc. Also Thermo Gravimetric Analysis (TGA) and Differential Scanning Calorimetry (DSC) tests were performed to determine the fiber content and transition temperatures of each specimen respectively. Later these data are compared with micro mechanical calculations and the results are expected to aid in characterizing these processes and enabling the designer to approach further analyses problems more accurately.

RTM, VARTM, LRTM processes were determined to be appropriate for this thesis study. RTM was selected to provide the controlled data, being the most well known and controlled process of all. Many studies were made concerning RTM; thus the obtained data was expected to be more accurate. VARTM was selected because the process is the most fundamental of nearly all impregnation processes. Finally, LRTM was selected to provide some data for processes developed for specific uses.

After the main processes were decided, a simpler process, VP was introduced to provide more data for comparison with a process which is not ideal. This process was determined due to its ease of manufacturing and low cost, but it is still a more controlled

method compared to hand lay-up providing more accurate results. The second simple process, Modified Vacuum Packaging (BP), was introduced by Barış Elektrik End. A.Ş. engineers, as an alternative to VP process, to answer the question if this process could be improved with accessible materials.

A certain number of specimen plates were manufactured using these methods. Later a given number of specimens were extracted from these plates to perform; tensile, compressive and in-plane shear stress tests. The results provided material properties for every manufacturing process. Finally TGA and DSC tests were performed to determine the fiber content and the glass transition temperatures. After determining the material properties, the results were compared with theoretical results obtained using analytical analysis.

These steps are thoroughly explained in the following chapters and the results are compared and findings are discussed in related chapters.

1.3. Literature Survey

1.3.1. Manufacturing Processes

As it was explained in the previous pages, there are various similar resin infusion processes in the market, which aim to increase the performance, reduce the cost and volatile emissions etc. This study focuses on only four of the most common of these processes. This chapter reviews some other common resin infusion methods and some developments promoted for these methods.

The RTM process can be considered as the most fundamental of resin infusion techniques. It provides high quality products and reduces the volatiles emitted during the curing of resin. There have been many developments to better the performance of the process, reduce the cost of both labor and tooling and to reduce the processing time.

For further developing the RTM process; Takashi et al proposed a smart manufacturing technique of RTM integrated with numerical simulation, monitoring, and process control [6]. The preliminary process parameters were determined using numerical simulation; the resin impregnation process was controlled using dielectric sensors, which continuously monitored the progress of the resin-flow front.

For larger parts and lower tooling costs relative to RTM process resin infusion under flexible tooling (RIFT) processes were developed. RIFT can be defined as the class of all similar processes in which one tool face is replaced by a flexible film or a light splash tool. For these processes the flow of resin generally depends only on the vacuum drawn under the film and any gravity effects [1].

A version of RIFT dates back to the 1950s when it was used in the production of boat hulls. A flexible female splash tool was the basis behind this process. During the 1980s, the use of a rubber bag as the flexible tool was investigated and several patents were filed. The process was rediscovered during the 1990s and has been used up to date, particularly in the marine and automotive industries. [7]

RIFT retains many of the environmental advantages of RTM, but at a much lower tooling cost, since half of the conventional rigid closed mold is replaced by a bag. Adapting existing contact molds for the RIFT process may be feasible. RIFT has some disadvantages over the RTM process as it offers limited direct control over the thickness or fiber content of the final composite laminate [7]. However several advancements were promoted during the years to minimize these disadvantages.

Summerscales and Searle have classified the RIFT processes to 4 subgroups; (1) *in-plane flow parallel to the layers of reinforcement*, (2) *through-plane flow from a flow medium or scored core*, (3) *resin film infusion (RFI)* and (4) *infusion with partially pre-impregnated materials* [1]. This study consorts to this classification and the processes are investigated accordingly.

The processes where the flow is in-plane and parallel to the layers of reinforcement can be summarized as follows: The dry fabric preform is positioned on the mold, covered with a vacuum bag and sealed. One set of tubing delivers the resin, whilst a second set allows vacuum. The negative pressure removes air from the dry laminate stack, minimizing trapped air, later the resin inlet is opened to permit resin to move through the laminate from into the preform, impregnating the dry reinforcements. Additionally, the flow front in the reinforcement pushes any residual air towards the vacuum port. Figure 1.6 provides a schematic summary of the process [1].

Figure 1.6: Schematic Presentation of the Flow in In-Plane Flow Process [1]

Two of the processes investigated in this study, LRTM and VARTM are classified in this group. The main research and developments are in the field of bag materials and composite molding techniques, as used in LRTM. Many processes were patented by different companies having little differences in the application procedure.

Vacuum assisted resin injection system (VARI) developed by Lotus cars, employs vacuum (typically 0.34 –0.95 bar) used to pull resin into the preform. The process may additionally use pressure to push resin at the same time [1].

In vacuum infusion molding process (VIMP) [2], resin is fed by vacuum or gravity, and may also use positive pressure. The resin transfer occurs from preform interior within the mold.

Resin injection recirculation molding (RIRM) is a combination of vacuum and pressure infusion in which the resin is circulated until satisfactory wet out is achieved [2].

Co-injection RTM (CIRTM) [2] is developed by the US Army for the injection of more than one resin into soft-sided tooling and vacuum bag mold. The process allows separation of flow between multiple resins through the thickness of the part, hence eliminates the need for secondary bonding. The final product consists of multiple layers that contribute various unique properties (e.g. fire resistance, strength, ballistic protection, etc.).

The Scott Bader 'VacFlo' process [8] involves a lightweight, matched two-part mold. The upper half is usually a lightweight 3-6 mm thick GRP laminate. A double seal arrangement allows the first vacuum source to close and clamp the mold halves while the second vacuum source is used to pull the resin from a peripheral inlet channel to a central outlet port.

The Plastech VM (vacuum molding) adds an injection machine to the equation to control the introduction of resin similarly to the LRTM process investigated in this study. Two different levels of vacuum are employed for VM. The clamping vacuum, used to close the mold and seal around the mold flange and the mold cavity pressures [5].

In the process known most commonly as Seemann Composites Resin Infusion Molding Process (SCRIMP^{TM}) or some VARTM applications; the flow is through plane from a flow medium or scored core [1]. The main difference of these types of processes is the flow medium placed above or within the preform, before positioning the vacuum bag. A schematic representation is show in Figure 1.7.

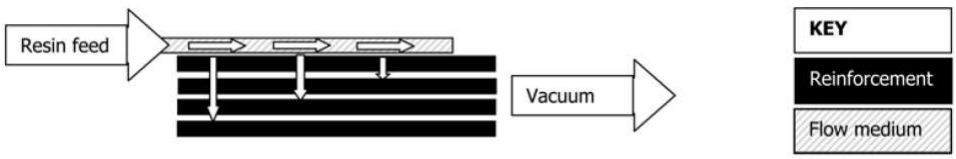

Figure 1.7: Schematic Presentation of the Flow in Through-Plane Flow Process [1]

SCRIMP^{TM} (Seemann Composites Resin Infusion Molding Process) [2] is a patented process involving a vacuum bag with a resin distribution medium. Additionally, the carrier layer may be interleaved with the fabric layers which provides the resin to be distributed quickly across a very large part of the component surface, and then saturates through the preform thickness.

Any feeder material separated from the laminate by peel ply could be used as the flow media to be used either outside the laminate. Additionally several materials have been developed to be used within the laminate; e.g. balsa, Rovicore, Multimat [9] or other materials. Rohacell® also has developed a foam core system that improves the flow of resin [10].

The controlled atmospheric pressure resin infusion (CAPRI) is a process developed by Boeing as a variant of the SCRIMP^{TM} [11]. The process increases the fiber volume fraction of the preform prior to infusion via debulking with several vacuum cycles. Additionally the process minimizes thickness gradients by applying a reduced pressure gradient during infusion.

Vacuum-Assisted Process (VAP) was developed by EADS Deutschland and uses a gas-permeable membrane for uniform vacuum distribution and continuing degassing of the infused resin. Li *et al.* has shown that this improvement results in a more robust VARTM process that minimizes the potential for dry spot formation as well as lower void content and improved dimensional tolerances [4].

The semi-cured resins used in prepregs are available as films. The resin film infusion (RFI) process uses those resin films to be laid within the preforms or over their surfaces. The flow distance is thus limited to the thickness of the component or, if the films are placed within the reinforcements, may be as little as half the ply thickness [1]. Figure 1.8 provides a schematic representation of the flow in RFI process.

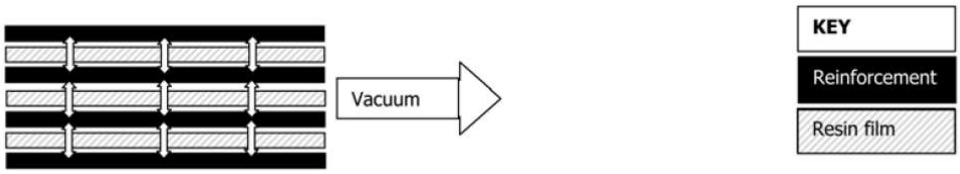

Figure 1.8: Schematic Presentation of the Flow in Resin Film Infusion Process [1]

An innovative process employing resin films is FRTM; a hybrid process, which combines the technical characteristics and respective favorable economics of RFI and RTM. Separate sheets of dry fiber and resin film are placed between elastomeric diaphragms. The fiber and resin are then compacted by drawing a vacuum between the diaphragms, and formed to shape by drawing the diaphragm assembly over hard tooling [12].

The FRTM process eliminates the labor intensity typically associated with preparation of the three-dimensional fibrous preform used in RTM. Another advantage of the FRTM process is the fact that the diaphragm system is deformable, and provides a low cost reconfigurable tooling surface.

In some cases the reinforcement is supplied *partially pre-impregnated* with resin, often referred to as ‘semi-preg’. The semi-preg infusion process is represented in Figure 1.9.

Various commercial systems are available such as; Advanced Composites Group’s ZPREG, Cytec’s Carboform system, SP Systems’ SPRINT® (SP Resin Infusion New Technology) [1, 13].

Frost *et al*. [13] compared the three systems named above to demonstrate that lightweight automotive body panels can be manufactured without using capital intensive equipment, such as autoclave. Panels were lighter, had a better surface finish, and overall cost was lower than for prepreg components. However, the impact resistance was lower when compared to the prepreg panels.

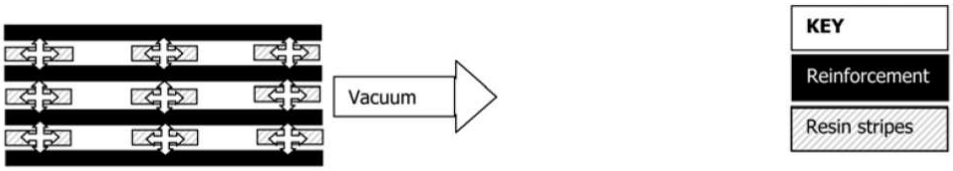

Figure 1.9: Schematic Presentation of the Flow in Partially Pre-Impregnated Infusion Process [1]

In practice, the boundaries between the, afore mentioned, four classifications are not clear. There are various methods that associate different aspects of several approaches. As some of the examples are given above; the many variants of RIFT are known by a wide variety of names, which may not always be used for a specific procedure. Two, most innovative, of such approaches are investigated below.

An optimized resin infusion technology was developed at the DLR Institute of Structural Mechanics in order to manufacture aerospace grade performance composites with good laminate and surface quality that was comparable with autoclave method while reducing the raw material, namely prepreg, costs. To achieve these goals, a combination of dry fiber preforms and autoclave technology named Single Line Injection-RTM (SLI-RTM) was employed [14].

The advantage of this method in comparison to the LRI method is that the resin is injected under pressure and that the laminate can be compacted by the autoclave pressure. The resulting products are virtually void-free and the component quality almost reaches the status of a Class-A surface [14]. A schematic view of SLI method is seen in Figure 1.10.

An additional characteristic of the SLI method is the possibility to directly influence the fiber content. By adjusting the autoclave pressure to similar levels as the inner resin pressure, permeability of the preform is increased allowing easier impregnation [14].

After the preform is completely impregnated, increasing the autoclave pressure while curing provides the desired fiber volume content (Figure 1.11).

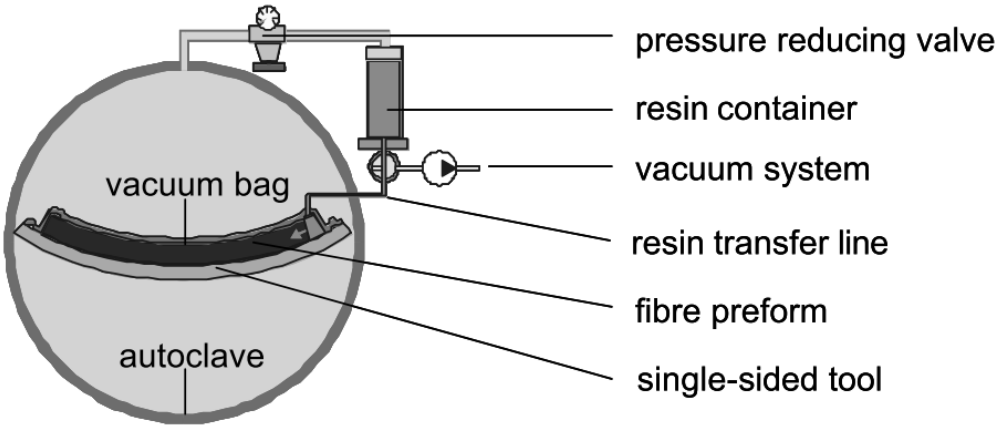

Figure 1.10: Schematic View of SLI Method [14]

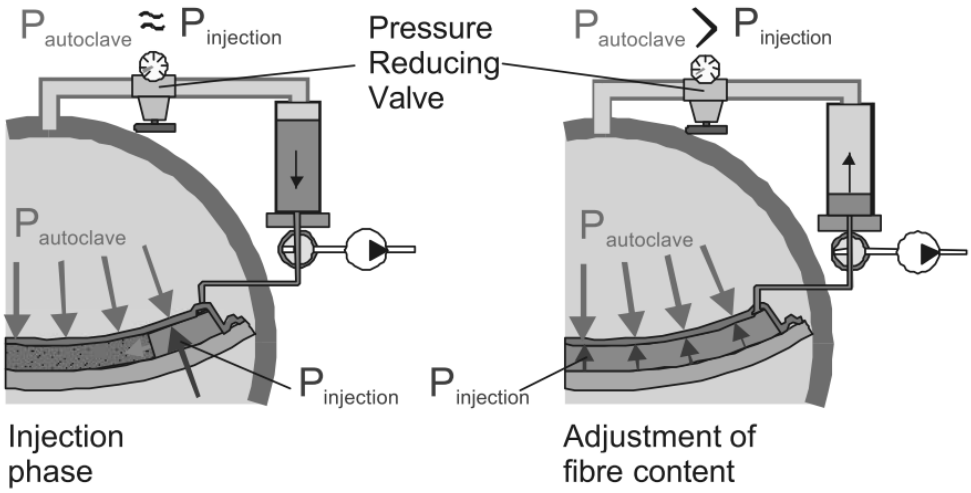

Figure 1.11: Pressure Distribution During Two Phases of SLI [14]

Another process developed deserving further investigation is called Resin infusion between double flexible tooling (RIDFT) and intends to solve problems associated with

other liquid composite molding techniques [7]. These problems include achievable fiber volume, part thickness consistency, manufacturing cycle time and process complexity. Unlike the FRTM process, the RIDFT process does not use dry solid sheets of resin, but the preform is impregnated with a low viscosity thermoset resin similar to RIFT processes. After the preform is fully impregnated, the process is carried on like FRTM process (Figure 1.12).

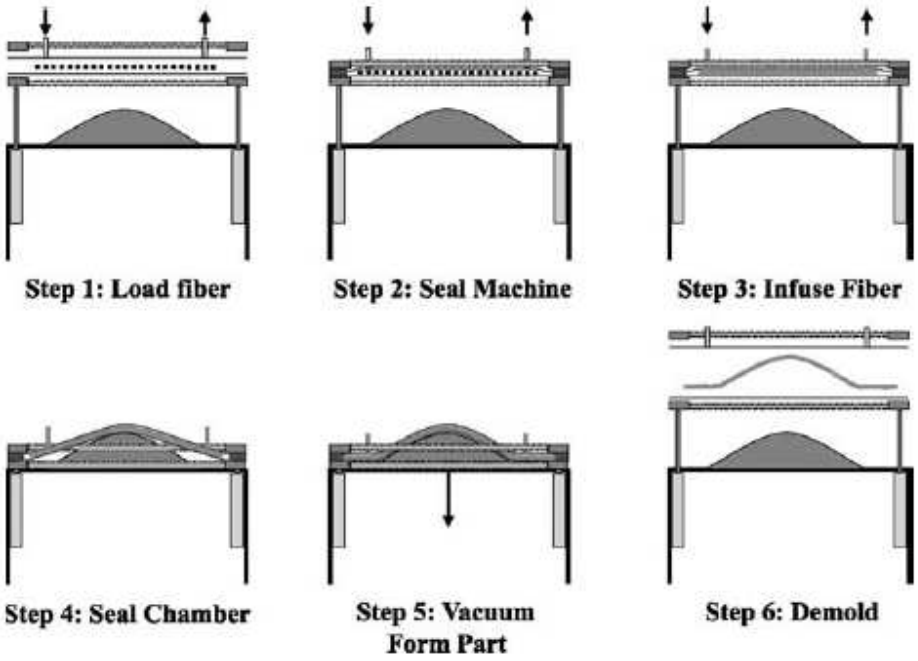

Figure 1.12: Schematic View of RIDFT Process [7]

RIDFT has various advantages over more conventional processes. An advantage of the RIDFT that the flow of resin is two-dimensional eliminating the complexity of the three-dimensional flow front experienced with RTM [18]. An advantage of RIDFT over RIFT is in the use of a second flexible tooling that reduces cleanup and manufacturing preparatory work and the scrap materials are reduced when reusable bagging materials

are employed. Additionally, the low viscosity resin provides better lubrication for reinforcing fibers, thus enhancing formability compared to FRTM.

Thagard [7] has compared the economics of RIDFT process with SCRIMP. It was reported that in almost all the categories examined, the RIDFT process had a cost advantage; especially in categories such as consumable materials, tooling amortization and labor with only a higher cost in equipment area. An overall advantage of 24% was achieved.

In addition, curing methods have been investigated throughout the development of these methods, since cure cycle times also have significant impact on process feasibility. Some of these developments are discussed below.

Microwave curing holds great potential for improving current composite manufacturing techniques, substantially reducing cure cycle times, energy requirements and operational costs. Paparygis and his colleagues have incorporated microwave heating into the resin transfer molding technique, and reported that 50% cure cycle time reduction was achieved through the use of microwave heating [15].

Quickstep is a curing procedure designed for resin infusion; where the tool and uncured component inside the vacuum bag; are placed in a low-pressure liquid filled chamber. Three different temperature levels; low temperature, dwell temperature, and the curing temperature; are delivered by a computer controlled system; and the mold is surrounded by a liquid at hydrostatic pressure so no significant loads are imposed on the tool structure [16].

UV curing is a process which provides several important advantages when combined with RIFT processes. The resin only cures with the presence of intense UV light. This allows for complete forming without the concern of gel times as with most vinyl ester resins. This results in the reduction of process cycle times since UV curing provides for accelerated curing times [7].

1.3.2. Woven Fabrics

The fiber material used in this study was preferred to be woven 3 harness satin textile carbon fabric, due to availability considerations and the fact that textile fabrics are more appropriate for utilizing in the production methods studied in this thesis. The resulting products are described as woven textile composites and this type of composites differ from unidirectional composites in both mechanical characteristics and the methods used in micromechanical analysis of these structures.

Textile composites are determined as composite structures produced by impregnating matrix materials into dry preforms formed by textile fabrics to hold the multidirectional yarns together. The impregnation is generally done by using afore mentioned liquid molding techniques and other commercially used methods given in Table 1.1. In general, classification of textile composites reflects the macro geometry (e.g., shape and dimension of the structure), method of fabric formation/construction, and the resulting structural micro geometry. The micro geometry includes directions of reinforcement, linearity of reinforcement in each direction, continuity of reinforcement, fiber packing density, fiber bundle (or yarn) size in each direction and the geometrical feature of the fiber bundles etc.[17]. However, no simple method to classify textile composites, which meets the above requirements, was found.

Textile composites are generally classified into three basic categories according to the textile manufacturing techniques used for reinforcements [17]. These are; woven, knitted and braided fabrics. Woven fabric textile composites, will be discussed for this study, since the specimens used for this study are produced from this type of fabrics.

Woven fabric textiles are the most commonly used form of textile composites in structural applications. They are mainly woven by the multiple warp weaving method, and generally consist of two sets of interlaced yarn components, warp and weft (or fill) yarns, named according to the yarn orientation[17, 18]. Warp yarns run vertically or lengthwise in woven fabrics, while weft yarns run horizontally or crosswise [18]. Each

yarn is a bundle of fibers and its size is defined by the number of fibers in the yarn [19]. Three-dimensional woven fabrics have additional yarns placed in through the thickness direction [20], and can be generally classified into three types, namely, 3-d, 3-x and interlocks. They have higher delaminating resistance and damage tolerance than 2D woven laminates [21]. The interlacing pattern of the warp and weft yarns is known as weave [22]. Currently, most of the pure and hybrid woven fabrics used in textile composites are simple 2D fundamental weaves, i.e., plain, twill and satin weaves, which are identified by the repeating patterns of the interlaced regions in warp and weft directions [23, 24].

Plain weave is the most basic reinforcement used for woven composites. In a plain weaving structure, one warp yarn is repetitively woven over and under weft yarns as shown in Figure 1.13(a). Twill weave has a looser interlacing and the weave is characterized by a diagonal line. In a twill weave (3-Harness satin) structure (Figure 1.13(b)), each warp yarn floats over two consecutive weft yarns, and under the following one weft yarn. Satin weave fabrics have good drapability, with a smooth surface and minimal thickness. In a satin weave (Figure 1.13(c)), one warp yarn is woven over n_g ($n_g > 2$) successive weft yarns, and then under one weft yarn. This weave structure, with interlaced regions that are not connected, is called ($n_g + 1$)-harness satin weave [17, 23].

Woven fabrics can be classified into open-packing weaves or closed-packing weaves. In an open-packing weave there are gaps between two adjacent yarns, whereas in a closed-packing weave fabrics are tightly woven and no gap occurs between any two adjacent yarns [22]. In addition, woven fabrics can also be classified as balanced and unbalanced weaves [25]. A balanced weave has the same properties and geometric dimensions in both the warp and weft directions, while an unbalanced weave has different properties and/ or different geometric dimensions.

Mechanical properties of woven fabrics are governed by two parameter groups. First; the weave parameters such as weave architecture, yarn size, yarn spacing length (or pitch),

fiber orientation angle, fiber volume fraction; and second; the laminate parameters such as stacking orientation and overall fiber volume fraction [17].

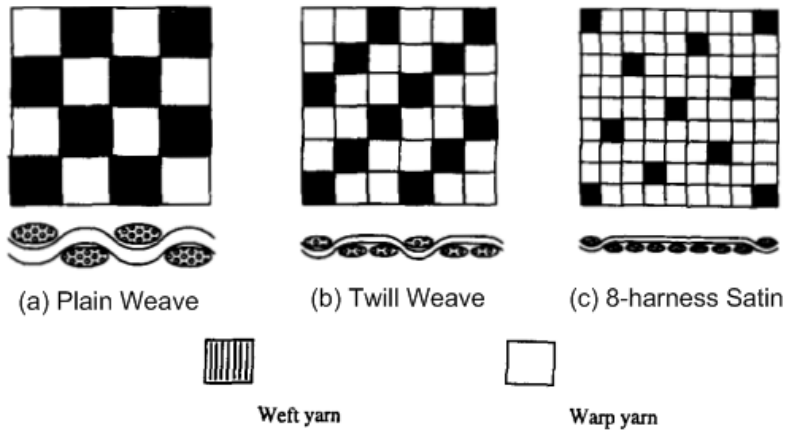

Figure 1.13: Schematic Representations of Common Fabric Weaves [17]

Woven fabrics generally show good dimensional stability in the warp and weft directions and they offer highest cover or yarn packing density. In addition, woven fabrics generally have a very low shear rigidity which gives a very good formability. However, they offer anisotropy, and they are poor in resisting in-plane shear [17, 26].

1.3.3. Experimental Procedures and Results

Due to the complicated structure composites, experimental tests become one of the major approaches for studying mechanical properties of these materials. In this section, some experimental procedures used previously for investigating mechanical properties of textile composites and various process techniques are examined.

Early research was administered to verify the models developed for woven fabrics, and most studies investigated the behavior of woven prepreg materials produced by autoclave or compression molding methods.

Ishikawa *et al.* [27] carried out some experiments to verify the theoretical predictions obtained in their previous work [23]. The materials used were plain weave and 8-harness satin fabric composites of carbon/epoxy prepregs. It was found that for plain weave textile composites, the modulus of elasticity increased with the laminate ply number but leveled out at about 8-ply thickness. The ratio of ply thickness to yarn width (i.e., h/a) was also found to be a very important variable, and affected the elastic moduli of plain weave composites strongly. And for the satin weave fabric composites, the in-plane shear modulus was found to decrease almost linearly with the fiber volume fraction which decreased with n_g thus the effect of thread undulation was concluded to be insignificant as far as in-plane shear modulus is concerned (Figure 1.14). A discrepancy based upon two limiting cases, local warping completely prohibited or allowed, was observed.

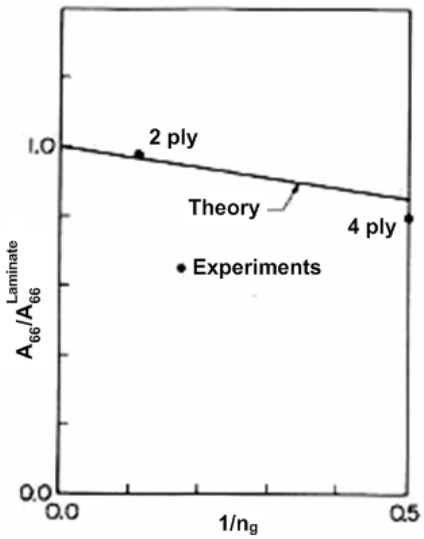

Figure 1.14: Relationship Between In-Plane Shear Modulus in $1/n_g$ [27]

Reifsnider and Mirzadeh [28] studied the compressive strength and failure mode of 8-harness satin Celion 3000/ PMR15 woven prepreg composite materials. It was observed

that the compressive behavior was influenced by the weave geometry, including the crimp size, cross-sectional shape and fiber volume fraction. The nature of the surface and the specimen thickness also influenced the compressive strength. For the unnotched laminate, where compressive stresses are uniform in each ply, fiber kinks occurred in the crimp parts of the yarns; this phenomenon was explained by the presence of out-of-plane shear stresses. The results of this study are summarized in Table 1.2.

Table 1.2: Laminate Geometries and Compressive Strengths [28]

Stacking Sequence	**Unnotched Strength (MPa)**	**Notched Strength (MPa)**	**Notched/ Unnotched**
$(0,45,0,45)_S$	413.68	36.60	0.6131
$(0,45,0,45,0,45)_S$	415.89	39.19	0.6497
$0,45,0,45,0)_3$	453.41	44.35	0.7744
$(0,45,0,-45,0)_4$	462.67	43.19	0.6436
$(0)_{12}$	675.69	46.26	0.4720
$(0)_{22}$	623.42	51.31	0.5674

A total of 400 tension tests were performed by Naik *et a1*. [18] for studying the failure behavior of unnotched and notched specimens. Plain weave fabrics of E-glass and Carbon prepregs manufactured with compression molding were used. The experimental results showed that the mechanical coupling between warp and weft fibers gives rise to higher failure strains in the off-axis unnotched and notched woven fabric composite than the equivalent unidirectional tape laminates.

Naik and Shembekar [29, 30] validated their 2D woven fabric models via measurements of in-plane elastic moduli of three types of plain weave E-glass fabric/ epoxy (named a,b and c) and one type of carbon fabric/ epoxy laminates that were in good agreement with the predicted results (Table 1.3). However, variation tendencies of the elastic constants with the major architecture parameters of textile composites were not mentioned in their

study. Note that the predictions were made using parallel (P), series (S), series-parallel (SP) and parallel series (PS) models which will be discussed further in Section 1.3.4.

Table 1.3: Elastic Moduli Predicted by WF Models in Comparison with Experimental Data (E_x: along fill, E_y: along warp) [30]

		T-300 carbon/epoxy	**E-glass/ epoxy**		
			a	**b**	**c**
Lamina Thickness (mm)		0.16	0.2	0.5	0.15
E_x Experimental Average (GPa)		49.3	-	13.8	14.5
Predicted E_x (GPa)	*P*	54.1	22.1	22.1	21.1
	S	51.5	26.8	26.3	23.1
	PS	45.8	17.1	16.1	14.9
	SP	31.1	16.7	15.7	13.9
E_y Experimental Average (GPa)		60.3	18.1	14.8	14.5
Predicted E_y (GPa)	*P*	67.8	28.6	29.5	21.1
	S	54.7	24.1	24.4	23.1
	PS	58.8	21.5	21.6	14.9
	SP	38.2	18.4	18.4	13.9

An experimental program was conducted by Karayaka and Kurath [31] for investigating the deformation behaviors and failure mechanisms of 5-harness 0/90 weave graphite/ epoxy laminates under tension, compressive, and 3- and 4-point bending loading. The experimental observations indicated that the woven laminates exhibited orientation dependent mechanical properties and strength as expected, and the results were consistent with their predictions.

Naik and Ganesh [32] carried out a total number of about 90 experimental tests. Test specimens for 10° and ±45° off-axis tension tests were prepared according to ASTM D-3039. In 10° and ±45° off-axis tests the weft yarn was 10° and ±45° to the loading direction respectively. The experiment results showed that the deformation for the 10°

test was very much less than those for the ±45° test at ultimate failure. The in-plane shear strength obtained by the 10° and ±45° off-axis tests were nearly the same and the Iosipescu test gave higher in-plane strength. The in-plane shear moduli obtained by the 10° off-axis test were higher than those obtained by the ±45° off-axis test. In addition, it was noted that in the case of the ±45° tension test, the failure was essentially due to the shear.

Fleck et al. [33] investigated the compressive failure mechanisms. The specimens were made from the T800 carbon fiber - 924C epoxy laminates, AS4 carbon fiber - PEEK laminates, 2D woven T800 carbon fiber - 924 epoxy, and 3D woven AS4 carbon fiber - LY564 epoxy. For both 2D and 3D woven composites, the compressive stress - strain response was almost linear to fracture. Compressive fracture of the unnoted woven specimens was found to be dominated by plastic microbuckling of the load-bearing axial stuffers.

The next part investigates the studies that examine various properties of different processes.

Kim *et al.* [34] investigated the mechanical properties of RTM Glass/ Polyester composite panels with various fabrics. The comparison of the mechanical and physical properties is tabulated in Table 1.4. Additionally the dynamic characteristics of composite bus housing panels were compared with steel panels employing impulse frequency response tests. The fundamental natural frequency and damping ratio of the composite panel were found to be 13.22 Hz and 0.0110 respectively. These values were 153% and 244% of those of steel bus panel respectively.

Kaş and Kaynak [35] evaluated the microvoid formation in RTM using an ultrasonic inspection method (C-scan) additionally optical and electron microscopy were used to examine microvoids and failure mechanisms. Woven carbon fabric/ epoxy composite sample plates were produced by RTM with different injection pressures; and three point

bending and Charpy impact test were carried out. C-scan inspection indicated that increasing injection pressure above 2 atm increased the number of microvoids leading to decreased mechanical properties. The mechanical test results have shown that the specimens molded under 2 atm injection pressure had the highest flexural strength, flexural modulus, and impact toughness values. Increasing the injection pressure decreased these mechanical properties due to the increased void formation. The microscopic analysis results were consistent with the C-scan and test results.

Table 1.4: Mechanical Properties of the Composite Specimen [34]

Reinforcement	**Satin**	**Continuous Strand Mat**	**Plain Weave**	**Housing Panel**
Volume Fraction	0.424	0.266	0.285	0.40
Young's Modulus (GPa)	28.2	8.8	13.5	18.0
Tensile Strength (MPa)	471	150	259	342

Pinter *et al*. have investigated the fatigue behavior of Carbon/ Epoxy RTM composites [36]. Tensile and tensile fatigue tests were carried out for uncompacted, compacted and stitched laminates all produced by RTM process. The stiffness values were found to be similar for all specimen classes. The tensile strengths for uncompacted and compacted specimens were found to be equivalent while the stitched specimens were measured to have lower strength. Although it was observed that different preform compaction methods such as binder-coating and stitching had little influence on the tensile fatigue behavior; it was also reported that if the stitching density was to exceed a certain limit, the fatigue behavior was influenced in a negative way.

Beier *et al*. [37] examined the overall performance level of stitched Non Crimped Fiber (NCF) composites produced by RTM. In plane tensile and compressive properties were examined as well as dynamic and in-plane properties such as compression after impact (CAI) and apparent interlaminar shear strength (ILSS) respectively. It was demonstrated

that mechanical properties such as the tensile and compression stiffness and CAI strength were not reduced by the chosen stitching parameters, while the tensile and compression strengths, ILSS and the tensile fatigue behavior were reduced as a result of localized fiber undulations due to stitching. The comparison of tensile and compressive stiffness is given in Figure 1.15. A 5H satin fabric from Hexcel with additional epoxy binder content was used as a reference. In contrast, a 0°/90° non-crimped carbon fabric manufactured by Tenax was used both stitched and non-stitched. Both fabric types had equal contents of high-tensile strength carbon fibers. In all cases the resin medium was epoxy.

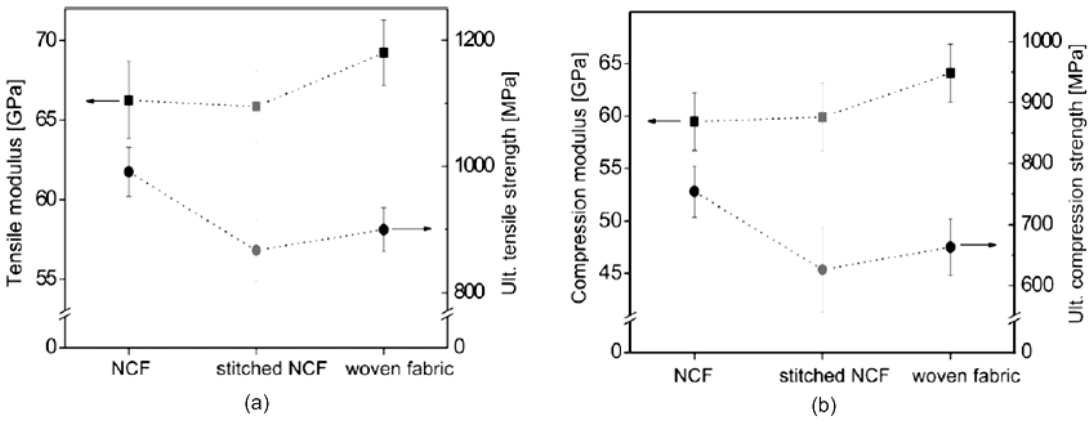

Figure 1.15: Comparative Plot of the Resulting Tensile Properties (a) and Compressive Properties (b) of Various Composites [37]

Kelkar *et al.* [38] studied the tension–compression fatigue performance twill woven S2 glass/C50 vinyl ester and of plain-woven S2 glass/SC-15 epoxy thick composites for composite armored vehicle applications. Additionally stitch-bonded and woven roving E glass/510A-40 vinyl ester composites were investigated under low velocity impact loadings.

It was observed that plain-woven S2 glass/epoxy composites had higher that fatigue life than twill woven S2 glass/ vinyl ester composites. For E glass/vinyl ester composites, the stitch-bonded structures displayed better impact resistance properties and also absorbed more energy than woven roving structures [38].

Niggemann and colleagues [39] experimentally investigated the effect of debulking and reduced pressure gradient on the incoming material parameters, process behavior and final dimensional tolerances. Several E-glass plain weave preforms have been infused with controlled atmospheric pressure resin infusion (CAPRI), later the pressure and thickness data has been recorded and compared to traditional VARTM. It was observed that debulking resulted in a significant reduction in the permeability of both the in-plane and out-of-plane direction and thus increased flow time and lead length during infusion. It was shown that the process decreases thickness gradients to less than 1% while increasing fiber volume fraction by 5% in the composite part (Figure 1.16). In addition, debulking also reduced the overall spring-back effect by almost 40% thus reducing any potential thickness gradient during VARTM processing.

Overall, the CAPRI process produced more uniform thickness components with higher fiber volume fraction and thus product quality and performance approached those of autoclave parts. The trade-off was considered to be the reduced permeability which resulted in increased infusion time and lead length which could provide more challenging processing in particular for thick section or low-permeability parts. In addition, the debulking step and additional vacuum applied to the injection bucket increased the hardware requirement and cycle time of the set-up [39].

Li and colleagues [4] examined the performance improvements of vacuum assisted process (VAP) and compared them to the SCRIMP^{TM} process. The investigated process parameters were fiber volume fraction and void content (Table 1.5). Additionally, the flow characteristics of both processes and thickness variations were evaluated. Two types of VAP panels were produced; VAP_{low} which was fabricated with the infusion

bucket placed below the tool surface (≅ 1.3m) and VAP in which the bucket had the same height with the tool surface. The specimens were produced from 15 layers of E-glass plain weave fabric / epoxy composites.

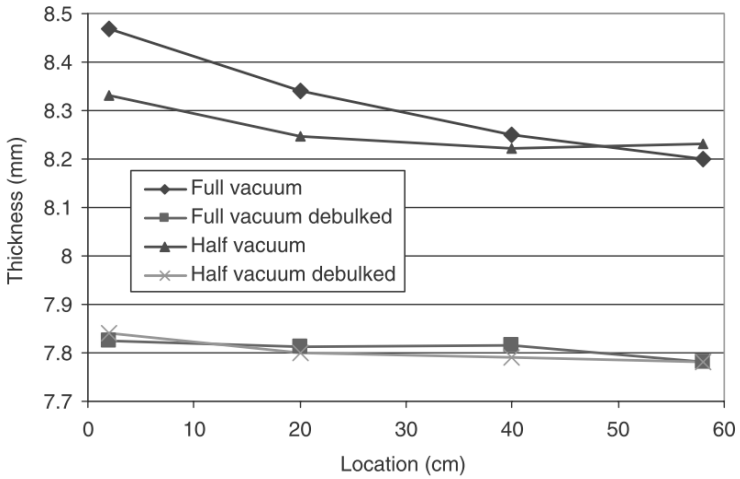

Figure 1.16: Final Thickness Gradients for VARTM and CAPRI after Full Infusion [39]

Table 1.5: Fiber Volume Fraction and Void Content for Panels With no Degassing and Degassing of Resin [4]

	Fiber Volume Fraction (%)/ Standard Deviation (%)		**Void Content (%)/ Standard Deviation (%)**	
	No Degassing	**Degassing**	**No Degassing**	**Degassing**
VAP	50.9/0.5	52.8/0.7	0.37/0.3	0.23/0.2
VAP_{low}	54.0/0.3	n/a	0.6/0.3	n/a
SCRIMP	56.0/1.0	56.12/1.2	1.64/1.2	1.07/0.7

The study illustrated that the selection of the vent location was not critical in VAP compared to SCRIMP processing for complete resin fill showing that the VAP is a more robust filling process which is able to manufacture composite parts with complex geometries with low risk of dry spot formation. The uniform vacuum pressure (VAP)

resulted in uniform thicknesses after infusion. The SCRIMP had a higher fiber content however with greater standard deviation, whereas the VAP shoved lower standard deviation and the fiber content was concluded that it was able to be optimized with ideal resin injection. The void content and thickness distribution was found to be superior in VAP.

Gu [40] investigated the bending and tensile behaviors of two layer E glass/ polyester laminates manufactured by VARI process having various fabric crossing angles of 0°, 30°, 45°, 60°, and 80°, respectively. Three-point bending and tensile strength of the specimens were measured. The results showed that orientation of the fabric layers had a significant effect in both bending character and tensile strength. Additionally parallel lay-ups of the fabric increased the elongation at break greatly. The bending deflection change due to lay up angle was shown in Figure 1.17.

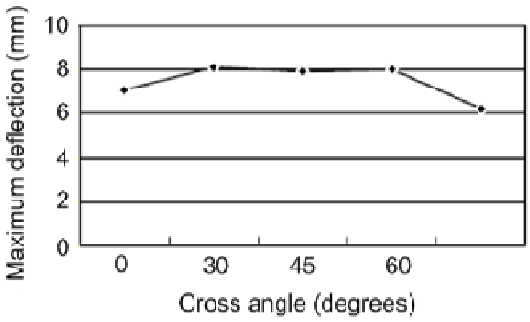

Figure 1.17: Bending Deflection of Laminates Having Different Fiber Cross Angles [40]

Himmel and Bach [41] examined the mechanical behaviors of $[0°]_8$ unidirectional, $[+45°/0°/\pm45°/90°]_S$ quasi-isotropic and $[+45°/\pm45°]_{3S}$ angle-ply laminates produced by RTM or vacuum assisted resin infusion (VARI) produced from unidirectional carbon fiber reinforcement and various vinylester (VE) resin systems. The study included the determination of ultimate in-plane tension, compression and shear properties as well as the characterization of the cyclic fatigue behavior under stepwise increasing and

constant amplitude loading. The results showed a better fatigue performance of an epoxy-terminated butadiene-nitrile rubber modified VE resin system. Furthermore, the cyclic strength of the composites produced by VARI was lower compared to RTM composites (Table 1.6).

Wu and Hahn [42] investigated the bearing properties of mechanically fastened E glass/ vinylester composite joints via double-lap joint bearing tests. Two composite structures, M3 and M4 were produced with VARTM method. M3 consisted of quasi-isotropic plain weave 0.45 whereas M4 consisted of quasi-isotropic chopped mat with a fiber ratio of

Table 1.6: Quasi-Static Properties of RTM Manufactured VE Resin Composites with Carbon Fiber Fabric Reinforcement

Property	**Laminate**	**Sample Mean ±1 . σ Standard Deviation**		
		CF/VE: Al-EP	**CF/VE: Cal-EP**	**CF/VEUH: ETBN**
Ultimate tensile strength $X_{1,t}$ (MPa)	$[0°]_8$	1561±159	1856±93	1477±164
Young's modulus (tension) $E_{1,t}$ (MPa)	$[0°]_8$	133.446±8791	142.378±7456	122.991±10.650
Ultimate compressive strength $X_{1,c}$ (MPa)	$[0°]_8$	651±100	576±18	622±56
Ultimate shear strength $X_{S,t}$ (tension) (MPa)	$[+45°/-45°]_{3S}$	67±2.3	67±7.8	74±6.2
Shear modulus $G_{12,t}$ (tension) (MPa)	$[+45°/-45°]_{3S}$	3256±456	3520±275	4346±205
Ultimate shear strength $X_{S,c}$ (compression) (MPa)	$[+45°/-45°]_{3S}$	74±4.8	69±3.3	75±2.5

0.382. The effect of edge distance ratio (e/d) and width ratio (w/d) was investigated. It was found that the ultimate bearing strength increased with increasing thickness and e/d ratio. For M3 specimens with thickness smaller than 2.4 mm; that ultimate bearing strength increased when width was increased. The results show that the quasi-isotropic weave had higher bearing strength than chopped fiber mat structure.

Papargyris *et al.* [15] incorporated microwave heating into the resin transfer molding technique and showed that a 50% cure cycle time reduction was achievable. The specimens were manufactured from carbon fiber/epoxy composites mechanical and physical properties were compared to those manufactured by conventional curing.

Mechanical testing showed similar values of flexural moduli and flexural strength for the two test groups. A 9% increase of the interlaminar shear strength (ILSS) was observed for the microwave cured composites. This enhancement in ILSS was attributed to a lowering of resin viscosity in the initial stage of the curing process providing better wetting. This was also confirmed via scanning electron microscopy which indicated improved fiber wetting and less fiber pullout. Both types of composites yielded minimal void content (<2%) and the thermal analysis revealed comparable glass transition temperatures for both methods.

It was reported that the average panel thickness of the microwave cured composite panels was slightly higher due to small dimensional differences of the mold cavity attained at machining which resulted the microwave cured samples to exhibit slightly lower fiber volume fraction. Given the same number of carbon fiber layers used to manufacture composites with both methods a common fiber volume fraction was normalized [15].

The results indicated the microwave heating was capable of improving composite processing and manufacture. Despite the half cure cycle time employed, the mechanical and physical properties of the microwave cured composites were found to be similar and, in some cases, superior [15].

1.3.4. Theoretical Analyses

Both numerical and analytical analysis methods are used for predicting the mechanical behavior of composite materials. When applied to characterize textile composites, FEM visualizes them as an assemblage of unit cells interconnected at a discrete number of nodal points. The unit cell is a periodic square array of fibers embedded regularly in the matrix. Hence, if the force - displacement relationship for an individual unit cell is known, it is possible, by using various well-known theories and techniques of elasticity theory to evaluate its mechanical property and study the mechanical behavior of the assembled composite structure. The ability of a FEA model for predicting mechanical

properties depends upon the accuracy of the modeling of the fiber geometry in a unit cell. Analytical models for elastic properties of composites are generally developed based on classical laminate theory and rule of mixture, and a similar unit cell concept is governed [17].

Earlier research in modeling of woven fabric reinforced structures was carried out by Ishikawa and Chou [43]. They developed a '*mosaic model*' for analyzing elastic behavior of woven hybrid composites. In this model, a fabric composite was simply defined as an assemblage of pieces of asymmetrical cross-ply laminates (Figure 1.18).

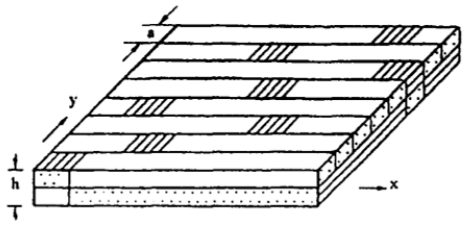

Figure 1.18: 'Mosaic Model' for an 8-Harness Satin Fabric Composite [44]

The model neglected the shear deformation in the thickness direction. Also the two-dimensional (2D) extent of a lamina was simplified to two one-dimensional (1D) models namely parallel model and series model depending on the arrangement of cross-ply laminates [24]. The parallel model gave upper bounds while the series model results in lower bounds of in-plane stiffness constants [30]. By inverting the upper and lower bounds of stiffness constants respectively, the relevant lower and upper bounds of in-plane compliance constants can be obtained. This model used the lamination plate theory to calculate the mechanical stiffness and compliances of the cross-plied laminate units with the assumption of constant stress or strain. This gave upper and lower bound solutions for the effective elastic constants of the structure. These upper and lower bounds differ for plain woven composites [17]. However, fiber continuity and non-

uniform stresses and strains in the interlaced region were not considered in this model [22, 24] although a good agreement between predictions and experimental results was reported.

Following that, a 1D crimp model named as '*fiber undulation model*' was proposed [24], which took into account the fiber continuity and waviness which was omitted in the 'mosaic model'. The relevant unit cell was divided into three regions; i.e., straight cross-ply region, undulated cross-ply region and pure matrix region as shown in Figure 1.19 (b). For the straight regions, analysis of the previous mosaic model was carried out while for the undulated region, the classical laminated plate theory was taken to be applicable to each infinitesimal slice of the threadwise strip along the x-axis; then these infinitesimal pieces could be integrated along warp (loading) direction. In this model, the undulation in the weft yarns running perpendicular to the loading direction was neglected. Later, solutions based on assumption of uniform stress for the infinitesimal

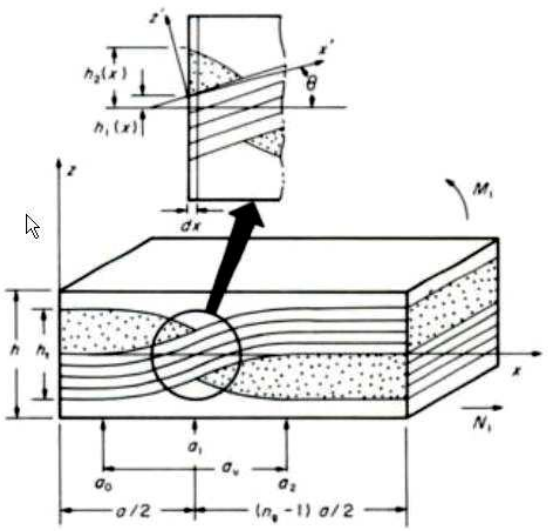

Figure 1.19: Unit Cell in 'Fiber Crimp Model' [24]

pieces in the straight and the wavy regions were assembled, and the elastic constant could be calculated from compliance elements. Hence, this model is an extension of the series model and is particularly suited for fabrics with low n_g values [17].

Chou and Ko [26] predicted the relationship between the in-plane stiffness C_{11} and n_g by governing both mosaic model and fiber undulation model. Figure 1.20(a) shows that the reduction in C_{11} was most severe in plain woven and least in cross-ply laminates. In addition, the effect of fiber undulation shapes on the in-plane compliance S_{11} was examined by fiber undulation model (Figure 1.20(b)). It was shown that S_{11} was affected by the undulation shape, particularly at smaller n_g values. The highest S_{11} value (i.e., the lowest in-plane stiffness) was obtained at around $a_u/h = 1$; where a_u is the undulation length and h is the overall thickness of the unit cell.

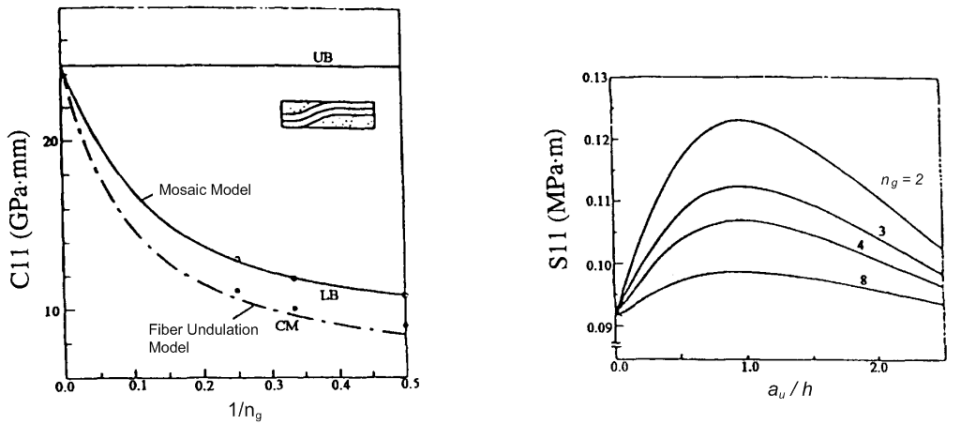

(a) C_{11} against $1/n_g$ for the graphite/epoxy composite, V_f=60%.

(b) Relationship between average in-plane compliance and undulation length

Figure 1.20: C_{11} and S_{11} Variation Trends for Woven Fabrics [26]

In summary, both the mosaic model and the fiber undulation model were useful for understanding the basic aspects of mechanical properties for woven fabrics, even though they only considered a 1D strip of a fabric and therefore, were inadequate for simulating

the behavior of satin composites where interlaced regions are not connected [45, 46]. In order to develop a model suited for high n_g value satin fabrics, a '*bridging model*' was proposed which takes the load transfer mechanisms into better consideration. Hence, this model was a combination of series and parallel models and only valid for the satin weaves where $n_g \geq 4$ [26].

In the bridging model, interactions between an undulated region and its surrounding regions with straight threads were considered. The hexagonal shape defined as the repeating unit in a satin weave was first modified as a square shape of the same area for simplicity of calculations. A schematic representation of the bridging model is shown in Figure 1.21, which illustrates the division of the repeating region into subregions for studying the local transfers occurring due to applied force in the x direction. The four regions denoted by A, B, D, and E consist of straight threads, and hence are regarded as pieces of cross-ply laminates. Region C has an interlaced structure where only the weft yarn is assumed to be undulated, because the effect of the undulation and continuity in the warp yarns was expected to be small since the applied load was in weft (or fill) direction.

Ishikawa and Chou have shown [23] that the stiffness of the undulated region C, where $n_g = 2$, was lower than that of the surrounding regions (A, B, D, and E) which had straight threads. Assuming uniform mid-plane strain and uniform curvature in region B, C, and D, the regions B and D are regarded to carry more load than region C thus, play the role of load transferring '*bridges*' between adjacent regions A and E. By this model, the characteristics of load distribution and transferring could be simulated for the satin fabric composites. It was also assumed that same averaged mid-plane strain and curvature were the same for regions B, C and D. Then the overall elastic properties of the unit cell can be obtained from an averaging technique.

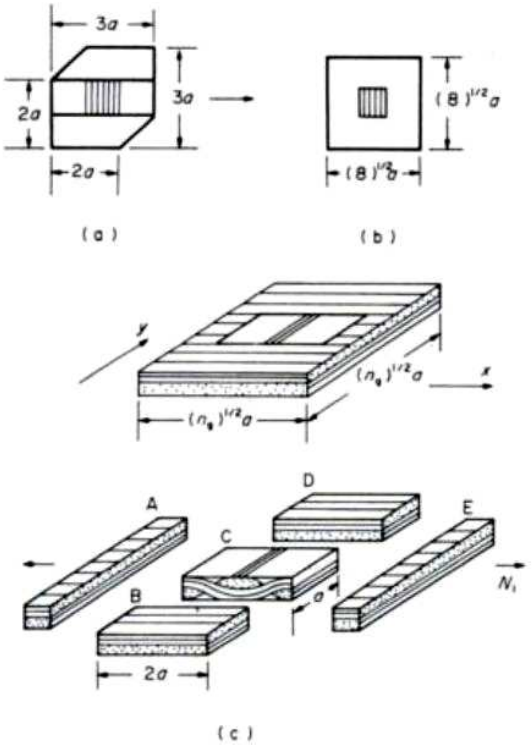

Figure 1.21: 'Bridging Model' for an 8-Harness Satin Fabric Composite: (a) Shape of Repeating unit, (b) Modified Shape for Repeating Unit, (c) Idealization for the Bridging Model [44]

Ishikawa and Chou [23] applied the bridging model to investigate the linear elastic properties of woven fabrics and non-linear behavior due to the initial failure of the fabrics. It was reported that the elastic stiffness in satin weave composites were higher than those in plain weave composites due to the presence of bridging regions in the weaving pattern. The experimental results of in-plane stiffness (A_{11}) as functions of $1/n_g$ are presented in Figure 1.22 along with the analytical predictions. Note that the stiffness values are normalized by the corresponding cross-ply laminate stiffness. The analytical models shown in the figure are the upper bound (UB) and (LB) predictions of the mosaic model, fiber undulation model (CM) and bridging model (BM). *Local Warping Allowed* (LWA) and *Local Warping Constrained* (LWC) are two cases in which the local

warping, that is local out-of-plane deformation due to the in plane tensile force, is assumed not to be restricted and to be constrained respectively, and it is reported that both LWA and LWC are limiting cases. Note that all prediction models are governed in the n_g intervals where they are most suited.

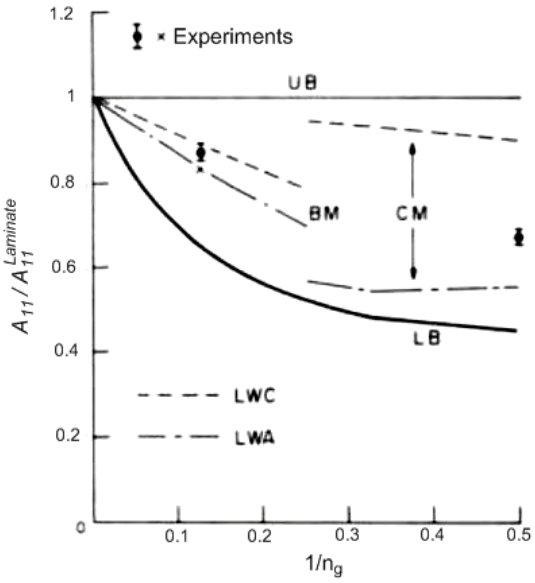

Figure 1.22: Relationship Between in Non-Dimensional In-Plane Stiffness vs. the Inverse of Harness Number ($1/n_g$) and the Experimental Data [27]

Ishikawa and Chou; later applied the fiber undulation model and bridging model to analyze the non-linear elastic behavior of fabric composites [46], with the non-linear constitutive relation developed by Hahn and Tsai [47]. These models solely cover the undulation and continuity of yarns along the loading direction and the yarn undulation in the transverse direction and its actual cross-sectional geometry were not considered.

Whitney and Chou [48] developed a new model to predict the in-plane elastic properties of composites reinforced with 3D angle-interlock textile preforms. In this model, micro-

cells were introduced by dividing the unit cell into a number of structural regions. The fibers in the micro-cells were presumed to form a series of inclined plates. The results showed that stiffer yarn systems generally exhibited greater ranges of variability in in-plane properties. The plain weaves generally had higher transverse moduli and lower Poisson's ratio than the satin weaves. However, it was mentioned that the preliminary experimental results from the literature showed less agreement with satin weave predictions. The shear modulus was in general unaffected by inclination angle. The in-plane properties were shown to be highly sensitive to fiber volume fraction as expected.

Zhang and Harding [49] have used the strain energy equivalence principle with the aid of the finite element method for micromechanics analysis of the elastic constants for a plain weave fabric lamina in the undulation direction. The strain energies of the constituent phases were evaluated using ABAQUS finite element package. The effect of the undulation ratio on the in-plane elastic constants; modulus of elasticity (E_l) and Poisson's Ratios (ν_{12} and ν_{13}) were studied and it was shown that increasing the undulation ratio decreases E_l and slightly increases both ν_{12} and ν_{13}. The plain weave fabric lamina was modeled by assuming the undulation in one direction only. Hence, Cox and Dadkhah suggested [50] that this method should be extended to the case of a 2D undulation model.

Based on the 1D and 2D woven fabric models, Naik and Shembekar conducted an extensive numerical study and proposed a 2D crimp model for the elastic analysis of a 2D plain weave [29, 30, 51]. This model was an extension of the 1D '*crimp model*' and incorporated the fiber undulation and continuity in both warp and weft directions and possible presence of gaps between adjacent yarns and actual cross-sectional geometry of yarns. In this model the unit cell is divided into the sections which are parallel to the z-y and z-x planes as shown in Figure 1.23, and then the '*series-parallel*' (SP) and '*parallel-series*' (PS) models were used to estimate the lower and upper bounds of the elastic constants. The experimental results have shown consistency with in-plane elastic moduli predicted by this method.

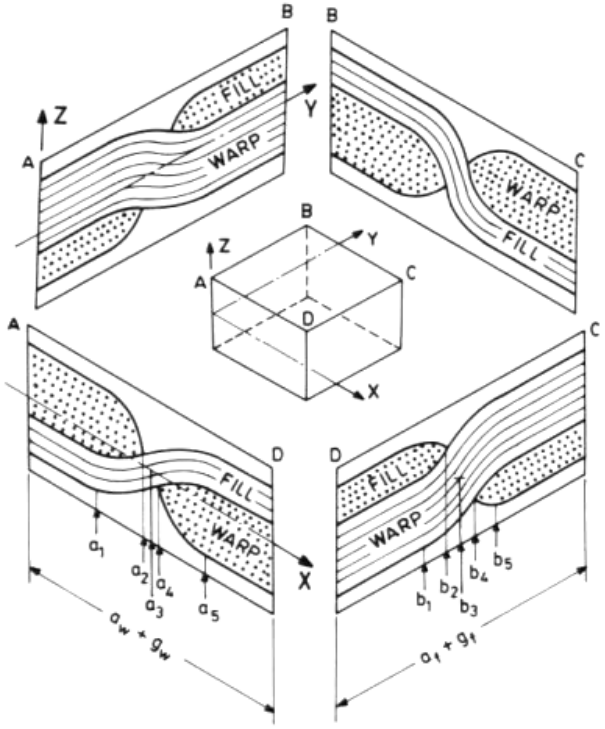

Figure 1.23: Unit Cell of a Plain Weave Fabric Lamina [30]

Naik and Shembekar found that the elastic moduli and shear modulus increased with the undulated length. The calculated results for elastic moduli are shown in Figure 1.24(a). However, the predicted values of Poisson's ratio proved inconsistent between the 1D woven fabric parallel and 1D woven series and 2D woven fabric models. The former model predicted; with the increase in undulation, Poisson's ratio initially increased and then decreased, whereas the latter two models predicted that the values initially decreased and then increased. Also with increasing lamina thickness, the Poisson's ratio increased but the elastic shear modulus remained constant. However, with the increase in lamina thickness, elastic moduli predicted by 1D woven fabric series model and 2D woven fabric model reduced and those predicted by the 1D woven fabric parallel model remained unchanged (Figure 1.24(b)). Additionally the findings have shown an increase in elastic moduli with the increase in overall fiber volume fraction.

In addition, for smaller undulation to yarn width ratios (u/a), the effects of change in the lamina thickness to yarn width ratio (h/a) on the elastic moduli was found to be insignificant. For a given ratio of u/a, higher elastic moduli can be obtained with a small h/a. It has shown that the increase in gap, results in a decrease in V_f^o ρ_c E_x, E_y and G_{xy} but leads to an increase in ν_{xy}.

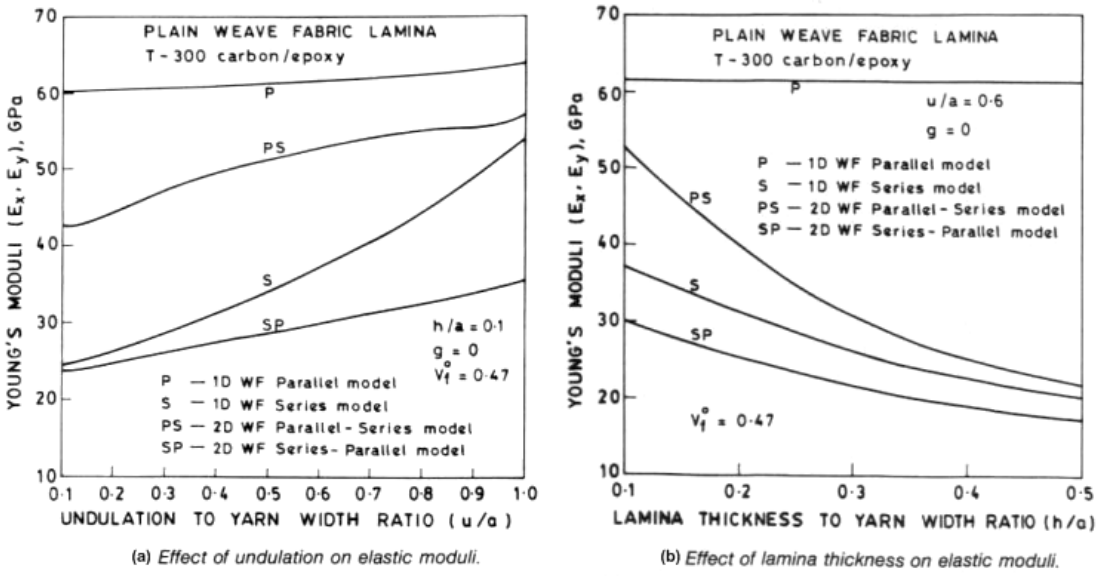

(a) *Effect of undulation on elastic moduli.* (b) *Effect of lamina thickness on elastic moduli.*

Figure 1.24: Effect of Fiber Undulation and Lamina Thickness on Elastic Moduli [30]

Two refined models, known as '*slice array model*' (SAM) and '*element array model*' (EAM) were presented by Naik and Ganesh [22]. In the slice array model, the unit cell was sliced along the loading direction. In element array model, the unit cell was sliced either along or across the loading direction and these slices were separated into elements. Later the elastic constants of the slices were estimated by assembling the elements and those of the unit cell were evaluated by assembling the slices either in series or parallel.

This SAM and EAM approach was also implemented for prediction of the on-axes thermal expansion coefficients of plain weave composites; for which, Naik and Ganesh proposed three 2D plain weave fabric composite analysis models [52]. The first two models were SAM and EAM. In the third model, the representative unit cell was idealized as a cross ply laminate. It was reported that the predicted results were in good agreement with the experimental values. The study was followed by a 2D model for predicting the in-plane shear strength of 2D plain weave fabric laminates under in-plane shear loading [32], and an analytical method for predicting the on-axis linear thermal expansion coefficient [53]. Naik and Ganesh used these models to predict the shear moduli and thermal expansion coefficient for three idealized laminate configurations. A good correlation was observed between the predicted and experimental results for both models.

Ganesh and Naik [54] investigated the effects of some geometrical parameters on the in-plane shear strength and in-plane shear modulus of 2D plain weave fabric laminates under in-plane shear loading. This investigation was carried out using a 2D woven fabric shear strength model [32] for in-plane shear strength predictions and a 2D stiffness model [22] for in-plane shear modulus predictions. The geometrical parameters included the yarn width, yarn thickness, inter-yarn gap and the corresponding fiber volume fractions. It was noticed that the fabric geometry could affect the shear strength and shear modulus significantly. A good correlation was observed between the predicted and experimental results (Figure 1.25).

In a more recent study, Naik and Ganesh developed a 2D woven fabric composite strength model for predicting the failure strength of 2D plain weave fabric laminates under on-axis uniaxial static tensile loading [55]. This model was developed on the basis of the geometry defined by mathematical expressions derived by Ganesh and Naik [56]. This model was governed to investigate; the ultimate tensile strength, stresses at different stages of failure, the stress-strain history of 2D plain weave fabric laminates

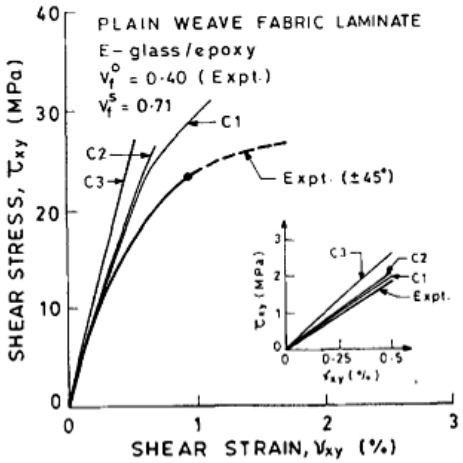

Figure 1.25: Predicted and Experimental Shear Stress vs. Shear Strain Behavior for E-Glass/Epoxy Laminate [54]

under on-axis uniaxial static tensile loading and finally the effect of fabric geometry on the failure behavior [56, 57]. All these studies were carried out for the three idealized laminated configurations. In the first configuration (C1), each layer is exactly stacked over the next layer; in the second configuration (C2), the adjacent layers are shifted with respect to each other by a distance in both weft and warp directions. The final configuration (C3) is formed by giving maximum possible shift to the layers in the C2 laminate in z-direction (thickness direction) so that the peaks of one layer fit the valley of the adjacent layers. The symmetric stacking for these configurations is schematized in Figure 1.26.

The studies of Ganesh and Naik have shown that an increase in the overall fiber volume fraction increased the strength (Figure 1.27). Additionally, a large crimp of yarn resulted in a higher strain concentration and thus led to a lower strength. It was also shown that different failure modes could be predicted using the analytical model, even though all the failure modes were not observed in the experimental results for all the laminates. Plain weave fabric laminates with optimum gap, which depends on the fabric structure and material system used, gave ultimate failure strength higher than those with any other

gap. The closed weave fabric had higher strength in certain cases. Overall, a good correlation was observed between the predicted and experimental results [58-60].

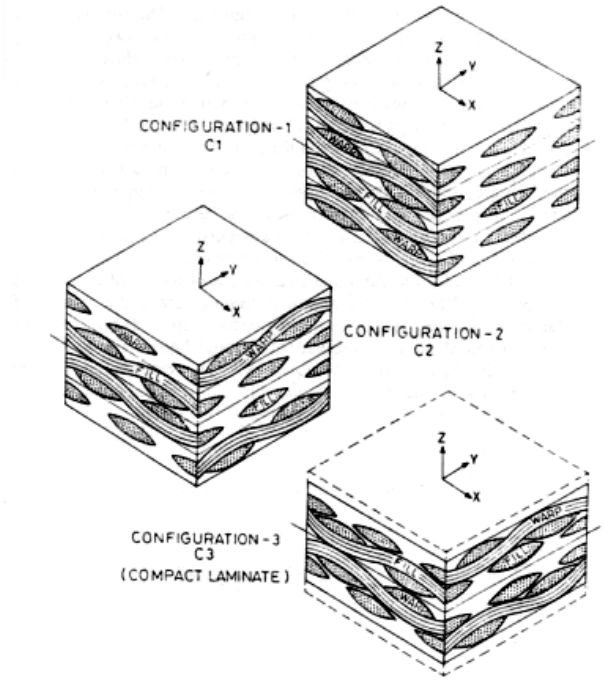

Figure 1.26: Symmetric stacking of layers [58]

Sankar and Marrey proposed a unit cell model for predicting stiffness properties of textile composite beams [59]. In this model; in macroscopic scale the structure was assumed to be subjected to a uniform state of strain, and in microscopic scale all unit cells were considered to have identical displacement, strain and stress field. It was suggested that on opposite faces of a unit cell, tractions were equal in magnitude and opposite in direction at the corresponding points, defined as traction boundary condition; and the displacements were different only by a constant, defined as periodic displacement boundary condition. That is, the displacements and tractions were continuous across opposite faces of the unit cell. In addition, three linearly independent deformations; pure extension, pure bending and pure shear, were applied to the unit cell.

These deformations were assumed to be homogeneous in the macroscopic scale. Hence, the relevant average forces required to create such deformations could be computed from the finite element model of the unit cell, in which the unit cell was modeled by using eight-node isoparametric plane strain element. This analytical method has been verified by applying the isotropic and bimaterial beams, and a good agreement has been achieved between the predicted results and those obtained from both beam and lamination theories.

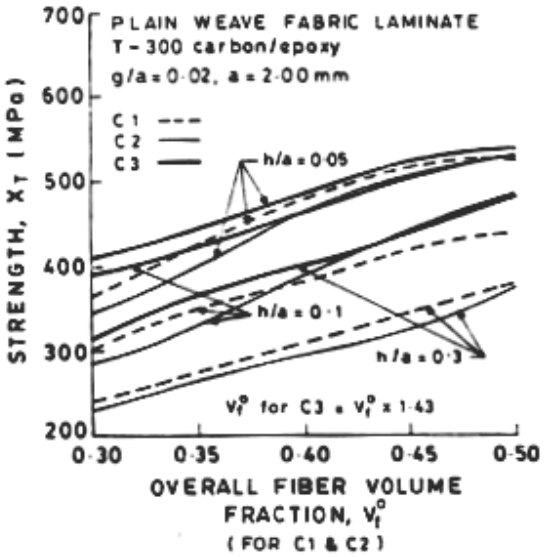

Figure 1.27: Effect of V_f^0 on Strength for T-300 Carbon/Epoxy [60]

Under the light of the above information; it was concluded that theoretical analysis methods become one of the powerful tools for studying the mechanical properties of textile composites. The microstructure of textile composites is very complex due to their nature and there are various parameters controlling the mechanical properties. Therefore it is difficult to model the textile composite architecture in detail using theoretical methods or FEA methods. In addition to numerous theoretical analysis models; various finite element techniques and assumptions were proposed to simplify modeling and

analysis procedures. However in the survey study a completed standard for optimum textile composite architectures for practical application was not found and the relevant database of mechanical properties was found to be incomplete. It is found to be necessary to further develop theoretical approaches in order to obtain reasonable predictions of the mechanical properties with major parameters of textile composites. Afterwards, the predicted results may be used to establish a reliable database, which will be important in practical design and manufacturing of textile preform structures.

CHAPTER 2

MATERIALS AND PRODUCTION

2.1. Introduction

Within the large family of composites, this study concentrates on polymer matrix continuous fiber composites. There are many alternatives for the resin system used as well as for the fiber material. These alternatives differ from each other by mechanical, chemical, thermal properties and some other characteristics like; flammability, conduction chemical resistance, etc.

An epoxy resin system suitable for RTM process was selected for this study due to its extended use in advanced applications, good chemical properties, low shrinkage and reliable mechanical properties. As fiber reinforcement an aerospace grade carbon fiber was preferred because of reliable mechanical properties. These properties are briefly explained in this chapter.

With the determined materials the plate specimens were fabricated using the Resin Transfer Molding (RTM), Light RTM (LRTM), Vacuum Assisted RTM (VARTM), Vacuum Packaging (VP) and Modified Vacuum Packaging (BP) methods. The specimens having appropriate properties for the tests performed were then cut out from the plates with a laser cutting machine. The production steps and parameters are thoroughly explained in this chapter.

2.2. Materials

This part involves the materials used in manufacturing the specimens. The properties of the constituent carbon fabric and epoxy resin system, are briefly covered and the numerical properties provided by the manufacturers, HUNTSMAN and HEXCEL are given.

2.2.1. Epoxy Resin System

Epoxy resins have been the major matrix material of polymer-matrix composites, especially for aircraft and defense industry applications where low cost is not as needed as high performance. They are thermosetting and inert resin systems which provide high mechanical properties, while rendering moderately easy manufacturing. They can be used for relatively high service temperatures. They also have high resistance to common solvents, oils, and chemicals [61].

In this study, a HUNTSMAN product, Araldite® LY5052 (Epoxy Resin)/ Aradur® 5052 (Hardener) system was used. It is a hot-curing, low viscosity resin system that exhibits good wetting properties and is easy to process. It has good chemical resistance, especially to acids at temperatures up to about 110°C. It is a suitable resin system for production of composites with filament winding, wet lay-up, pressure molding and RTM processes.

2.2.2. Carbon Fiber Reinforcement

Carbon fibers have found a widespread area of employment especially in high technology applications thanks to their superior mechanical properties and very low weight. They have high temperature and chemical resistance, and a very low thermal expansion ratio.

Two layers of woven carbon fabric, HEXCEL product named CARBON TISSU INJECTEX GF-630-E04-100 with properties shown in Table 2.2 is used for this study

Table 2.1: Properties of HUNTSMAN Araldite® LY5052/ Aradur® 5052 Resin System

Property	Units	Value		
Tensile Strength	(MPa)		80 – 86	
Tensile Modulus	(MPa)		3300 – 3550	
Elongation at break	(%)		3 – 5.9	
Cured Density	g/cm^3		1.17	
Glass Transition Temperature	(°C)	114 – 122 (cured at 80 °C)	120 – 134 (cured at 100 °C)	120 – 132 (cured at 130 °C)
Viscosity	(mPa.s)	1150 – 1350 (at 18 C°)	500 – 700 (at 25 C°)	250 – 200 (at 40 C°)
Thermal Exp. Coeff.	$(10^{-6}/K)$		71-97	
Poisson's Ratio			0.35	
Nom. Curing Schedule	(h/ °C)		24/ 23+ 4/ 100	

Table 2.2: Properties of HEXCEL CARBON TISSU INJECTEX GF-630-E04-100

Property	Units	Value or Description
Weave Style		3H Satin
Weight Rate	(Warp/Weft)	50 / 50
Area Density of Fabric	(g/m^2)	630
Area Density of Powder Binder	(g/m^2)	30
Fiber Count	(Picks/cm)	7.4
Type of fiber		Carbon T300J 6k
Tensile Strength of fiber	(MPa)	4210
Tensile Modulus of fiber	(GPa)	230
Poisson’s Ratio of Fiber		0.2
Elongation at break	(%)	1.9
Density	(g/cm^3)	1.79

2.3. Specimen Production

Seven plates were manufactured for each of the five processes, using aforementioned resin system and two layers of woven carbon fabric. After the plates were produced, test specimens for tensile, compressive and in-plane shear tests were cut using a 3-axis laser cutting machine. The plate geometries produced by VARTM, VP, and BP processes were identical and the specimens were cut as shown in Figure 3.1. As for RTM and LRTM processes smaller plates were fabricated to keep the mold costs low.

In all the processes, the initial temperature of resin is 75°C. Similar cure cycles were performed to keep the process parameters similar as much as the process itself allowed. For the LTRM process however, the resin was cured at lower temperatures due to mold properties.

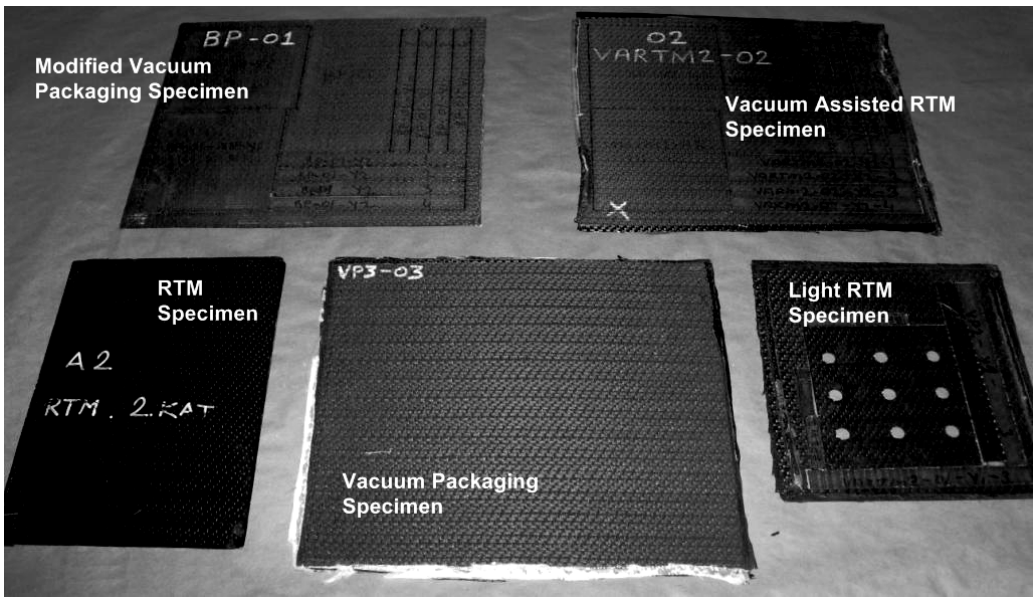

Figure 2.1: Plate Specimens Produced

2.3.1. RTM Production

Of all the processes performed in this study RTM process is the least labor intensive. First, a preform is laid inside a closed metal mold with ports for the resin to be injected and to be taken out after the mold is completely filled. (Figure 2.2).

The resin system is then mixed in a vacuumed container connected to a control system which takes out any air or gas bubbles that are formed during mixing of resin. When the resin system is ready the mold with the preform is connected to the resin reservoir with flexible plastic tubes, and inserted to an oven. The RTM machine and the oven are shown in Figure 2.3 and 2.4. After the cloth is fully wetted the mold is left for curing.

After the first set of RTM plates were produced, it was seen that the fiber content of the specimens were lower when compared to the other processes. It was implied to be a result of a larger mold cavity which allows more resin introduction hence resulting in greater resin to fiber ratio. To avert this problem with the most cost efficient way possible, a 0.5mm thick copper plate was attached inside the mold cavity with high temperature resistant silicon adhesive. Although the resulting surface quality was not as good as the original mold surface, the resulting products had very little thickness gradient and a good surface quality.

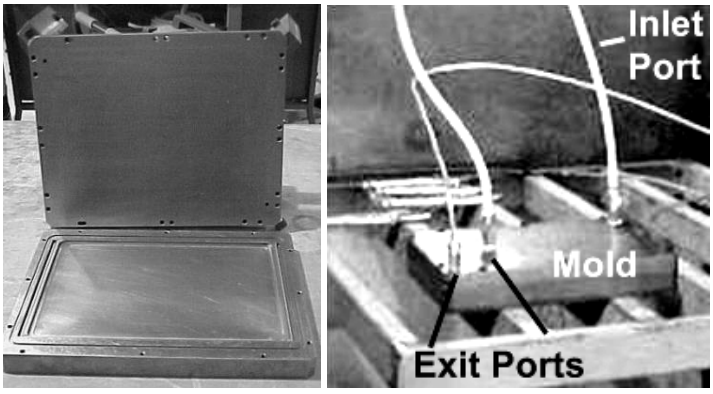

Figure 2.2: RTM Mold

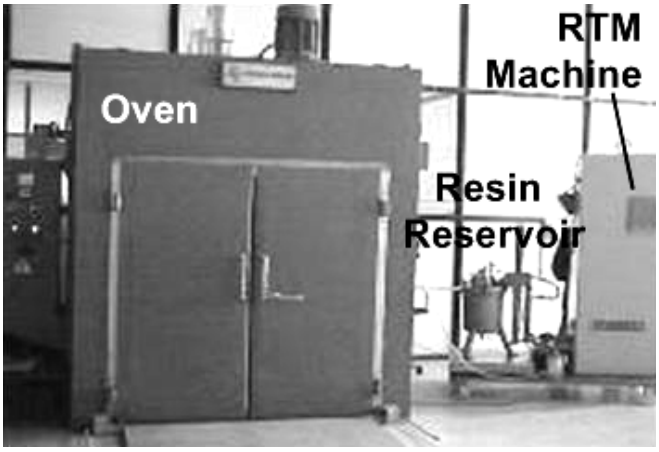

Figure 2.3: Oven Connected to RTM Machine

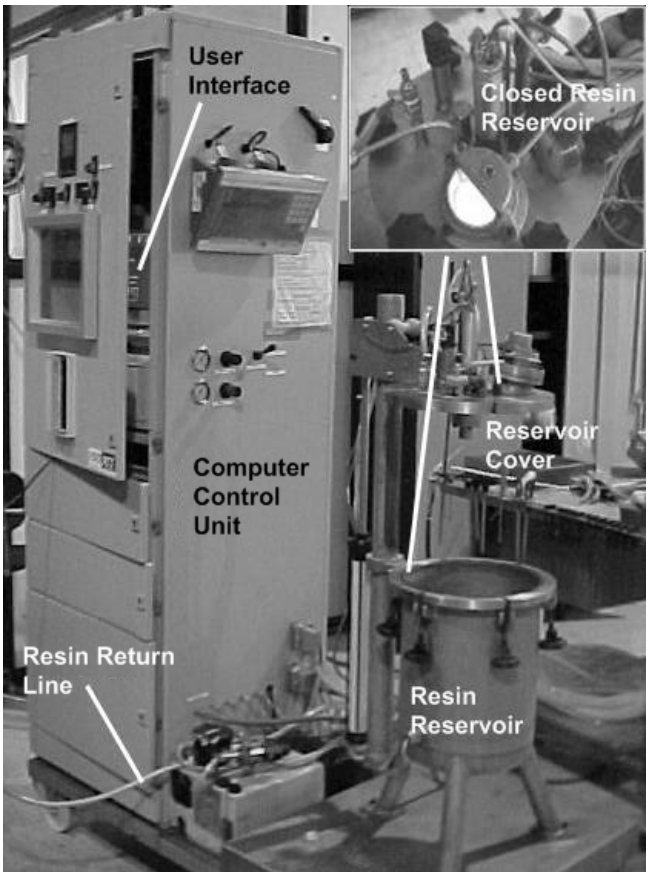

Figure 2.4: RTM Machine and Reservoir

2.3.2. VARTM Production

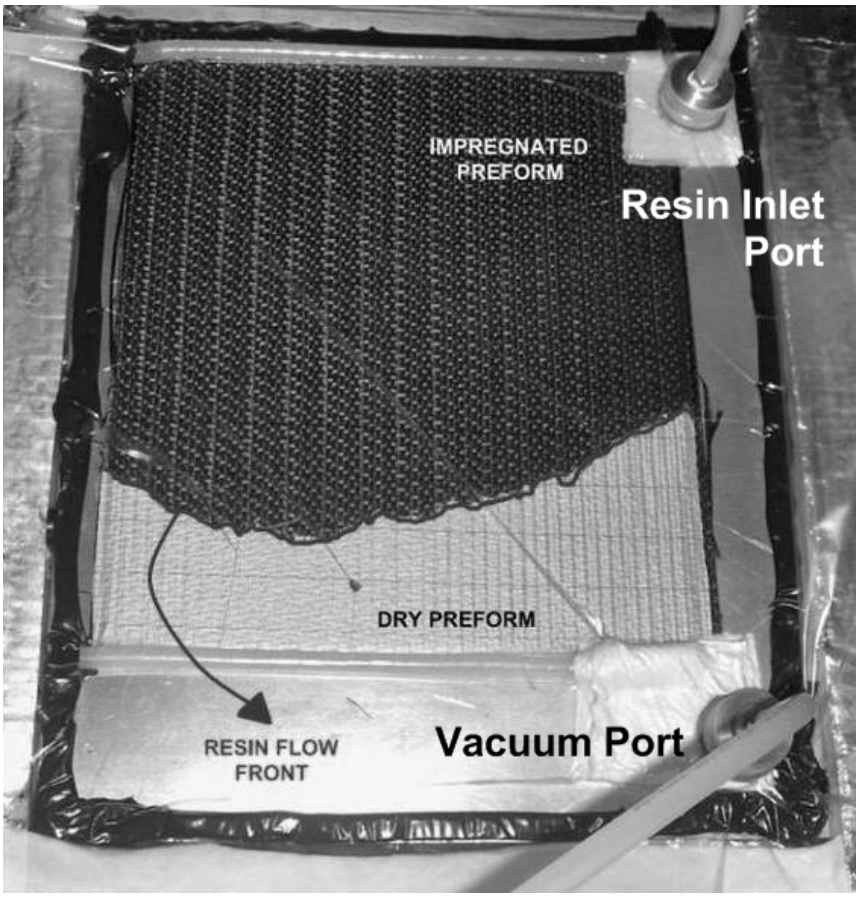

Figure 2.5: VARTM Process

As stated before, the VARTM process requires a single mold. Since the products were meant to be plates; a flat metal surface was used as a mold. The peel ply and bleeder fabric were laid on top of the preform, after it was placed on the mold surface. Then the vacuum ports were placed over some thicker bleeder fabric considering most of the excess resin was going to be accumulated in those areas. Later, the sealant tape and the vacuum bag were employed. After these preparations were complete, one of the vacuum ports were connected to the resin reservoir with a flexible tube, whereas the other

vacuum port was connected to the vacuum pump with another tube. Figure 2.5 shows the wetting of the fabric in the VARTM process. After whole preform was wetted with the resin, the appropriate cure cycle was performed under vacuum.

2.3.3. LRTM Production

Before manufacturing a product with LRTM process, a mold should be produced. In this study, the base mold is fabricated from a clay-like material specifically developed for mold applications. This material is resistant to high temperatures and at the same time provides good conduction. The clay-like material is mixed with a high quality epoxy resin and before the system started curing; a copper tubing was laid in the mold for cooling. During manufacturing of plates, hot water would circulate through this tubing; heat the mold and therefore the resin system to desired temperatures. A gel coat is applied on the inner surface of the mold to provide good surface finish. A metal plate having the same planar geometry with the final product is laid above the surface of the mold to have geometrical accuracy while curing. Finally when the mold material was cured, it was wrapped with insulating material to prevent heat loss during manufacturing of specimens.

Following the production of base mold, the diaphragm of the upper mold is prepared. This port of the mold was made from very fine glass fabric- epoxy composite material. The key here is to produce the thinnest mold possible, which is air tight at the same time. First a plate simulating the plate for specimens is laid above the prepared base mold. Then, the composite mold was fabricated using vacuum packaging technique. Another important point is to make a stronger frame for the mold, by employing a thicker fabric. The vacuum ports were embedded to the mold prior to curing. A set of vacuum ports was used for stabilizing the mold under air pressure, while two other become the resin intake port, and the vacuum port for excess resin.

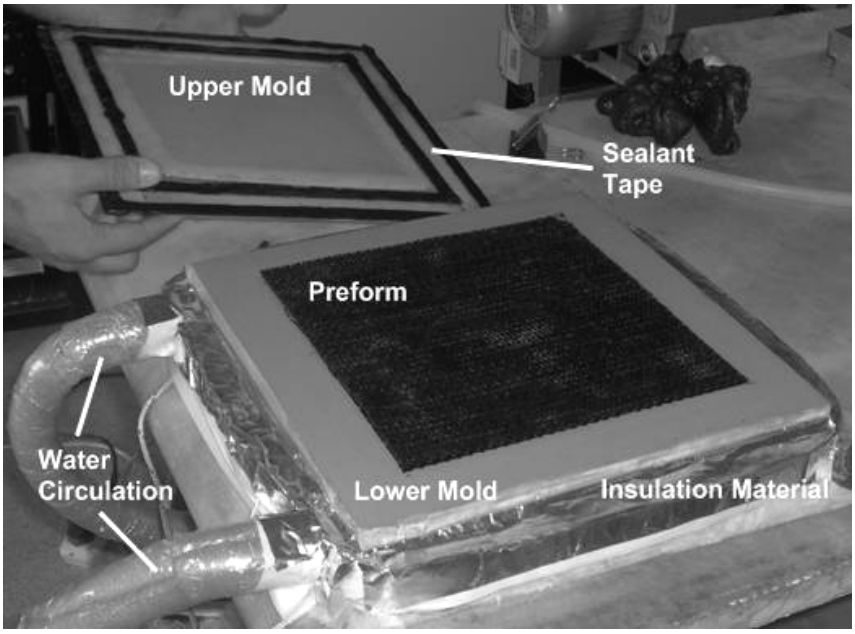

Figure 2.6: LRTM, The Upper and Lower Mold

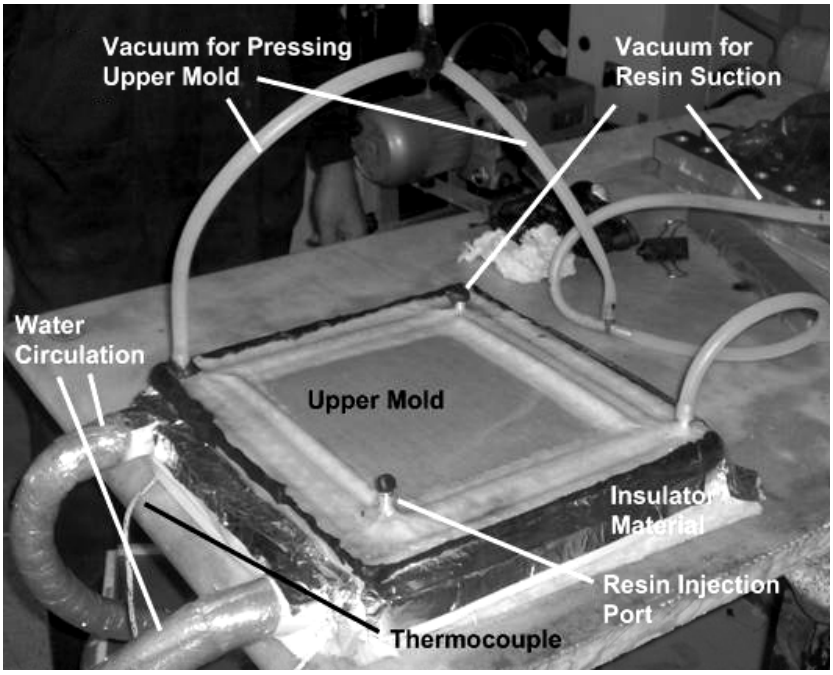

Figure 2.7: LRTM Process

After the molds were prepared, plates for specimens were manufactured in a very similar way with VARTM. While the resin intake and vacuum ports were used exactly the way explained in Section 2.3.2, the other set of ports were used to vacuum the air below the strengthened frame providing the atmospheric pressure to press the upper mold over the lower mold.

The mold preparation requires considerable amount of time and labor, after that; the production of parts were much faster and easier, compared to VARTM process.

2.3.4. VP and BP Production

Very much like the VARTM process a flat metal plate was used as mold for the production of plates using both VP and BP. Unlike VARTM, while employing VP there was no preform. Instead, the fabric were wetted manually while being laid, using rollers. Metal rollers were used on every ply laid to provide an even and thorough wetting. Then the peel ply and bleeder fabric were laid followed by vacuum bag and vacuum ports sealed with a sealant tape. The vacuum pump was kept connected while curing continued in the curing oven.

Different from VP, the fabric was not wetted in BP process. Instead, a bleeder fabric was laid below the preform, and this bleeder fabric was wetted with resin again by using metal rollers to mechanically extract any air bubbles that may have formed. Following this step, the preform and upper bleeder fabric was laid. Finally similar to VP, vacuum bag and vacuum ports were applied and the system was sealed with a sealant tape. When the vacuum pump was connected, the atmospheric pressure caused the preform to be wetted with the resin applied below. As stated below, this process was expected to reduce the voids and provide a better thickness distribution.

CHAPTER 3

EXPERIMENTS AND THEROETICAL CALCULATIONS

3.1. Introduction

Due to the complicated structure and anisotropic behavior of advanced composite materials, the test procedures used to determine their mechanical characteristics are different than those of conventional materials such as metals. Among these differences the specimen selection, specimen geometry and nature of calculations performed after acquiring the data are a few worth to mention.

Five different tests were performed for specimens cut out from the plates produced. All the tests are performed according to appropriate ASTM standards. In this chapter, the information about these standards and the tests is provided.

Thicknesses of specimens vary due to the nature of the processes. However, the thickness in RTM is controlled with the mold cavity geometry. Thus as explained in Section 2.3.1, RTM specimens had two different thicknesses and the specimens were named $RTM_{(Thick)}$ and RTM accordingly.

Mechanical characterization tests were performed by INSTRON 4206 universal test machine at ambient conditions. Test specimens are cut out from the plates according to Figures 3.1-3. Note that for all specimens the *x*-axis is called as the longitudinal direction and the fabrics were laid to have the warp direction along this axis; similarly the *y*-axis is called the transverse axis and weft direction.

The specimen nomenclature consisted of the process abbreviation, the plate number, the specimen direction and the specimen number, e.g. VARTM523 is the 3rd specimen from the y-direction of 5th VARTM plate. Similarly the shear test specimens were designated with an ‘S’ instead of the specimen number, e.g. VP31S. This nomenclature defines the x-axis as ‘1’ and the y-axis as‘2’ (Figures 3.1-3).

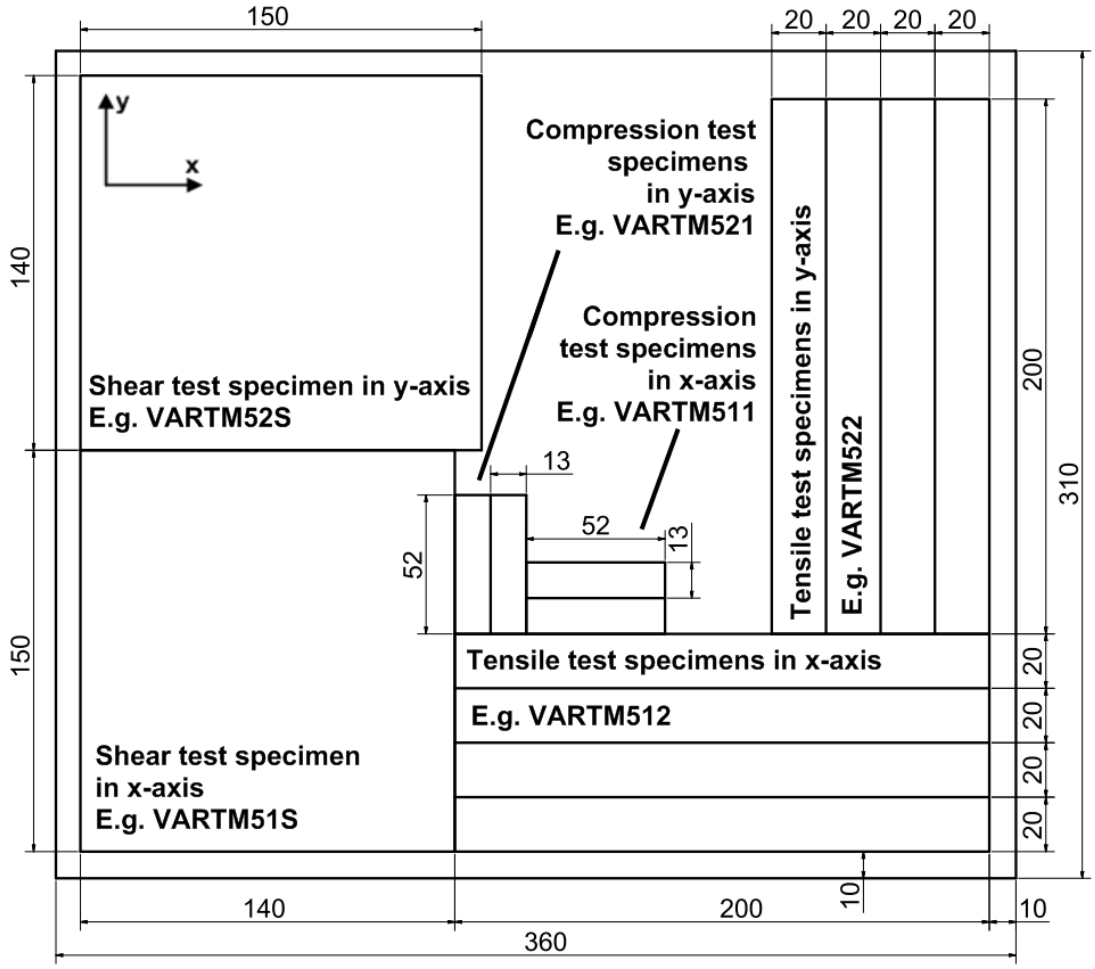

Figure 3.1: Geometry of Specimens Cut from Plates Made by VARTM, VP and BP

Four types of strain gages were used for tensile tests. Properties of these gages are given in Table 3.1. Note that the TML-UFRA type strain gage can measure strains in three directions, e.g. 0°, 45° and 90°; while TML-FCT type measures in two, 0° and 90° and TML YFLA and HBM-6 type gages measure only in longitudinal direction.

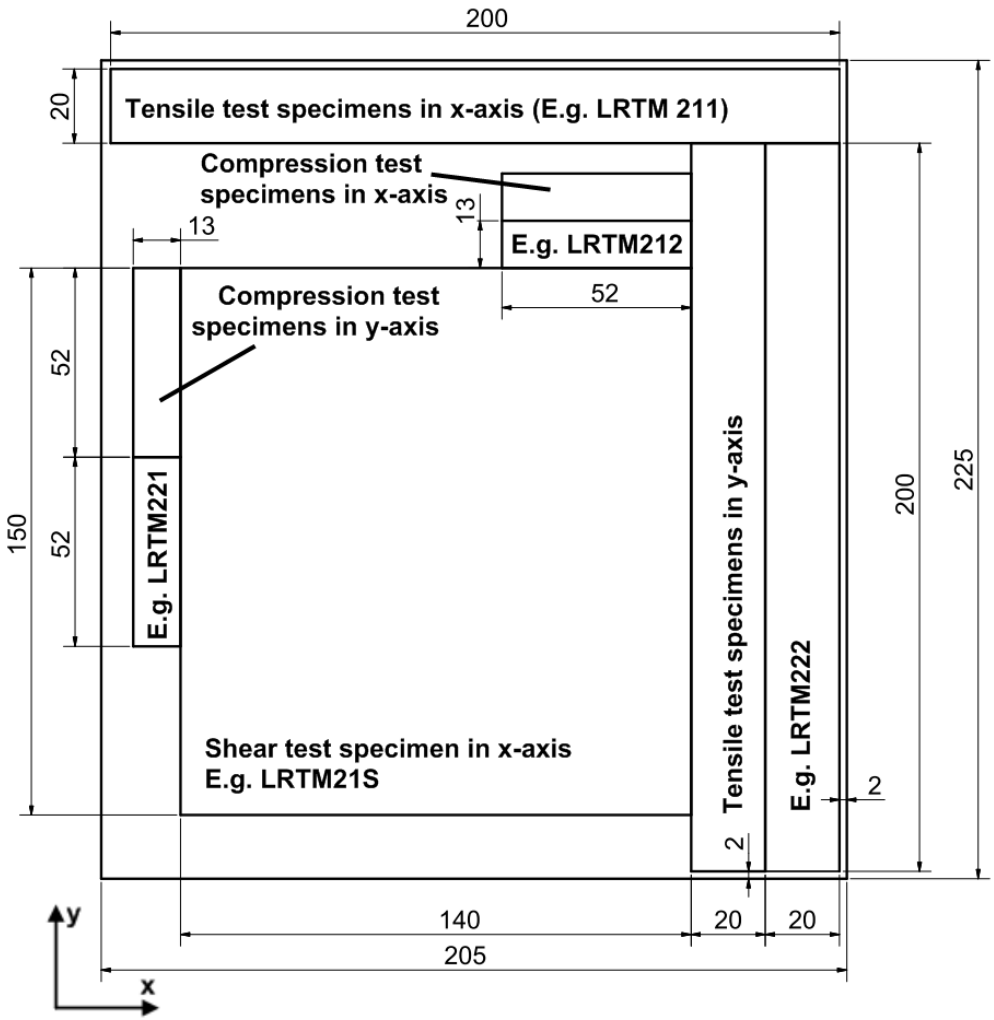

Figure 3.2: Geometry of Specimens Cut from L-RTM Plates

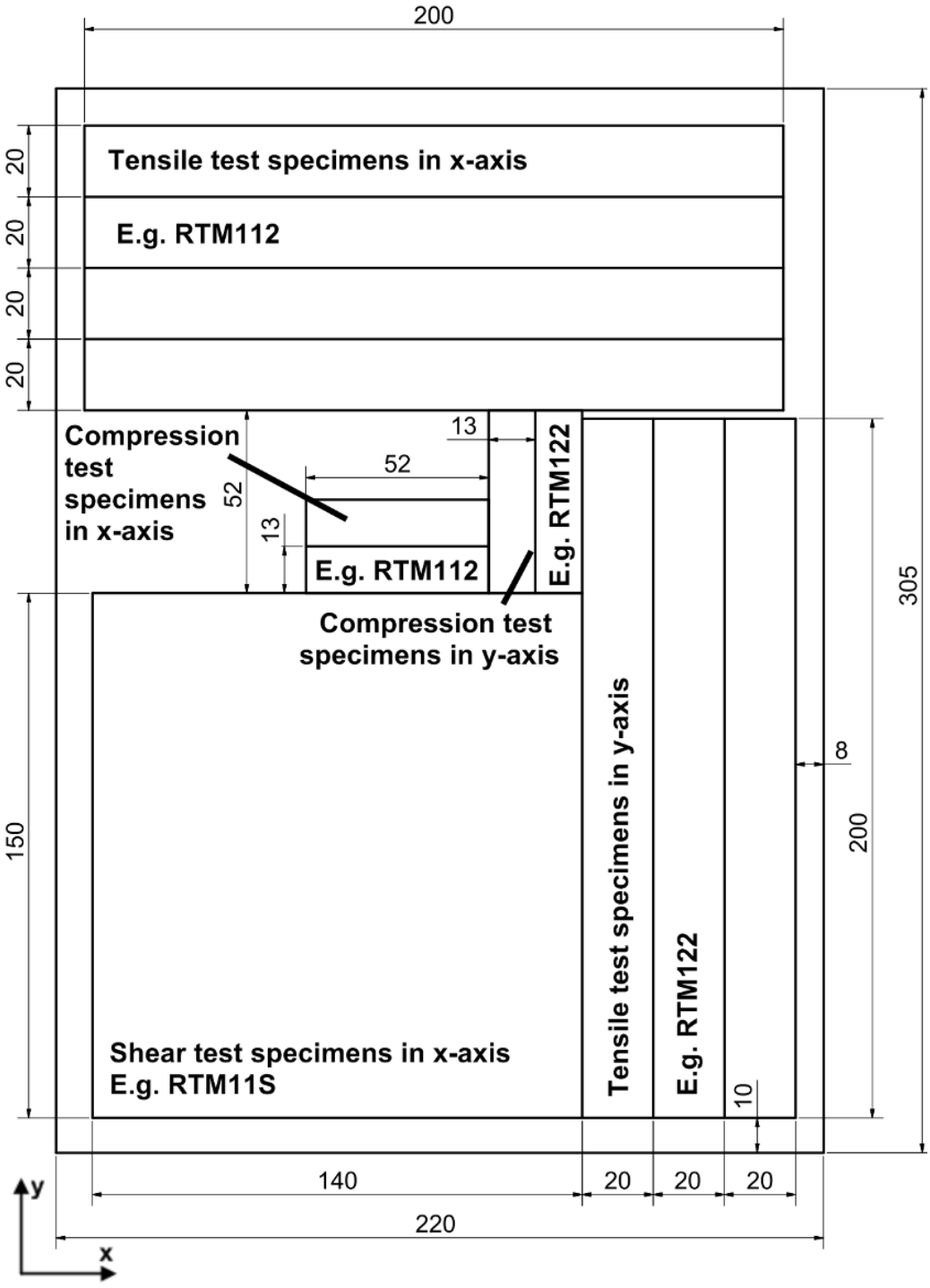

Figure 3.3: Geometry of Specimens Cut from RTM Plates

Table 3.1: Properties of the Strain Gages, Used in Tensile Tests

Strain Gage	HBM-6/120LD20	TML-UFRA-5-350-23	TML-FCT-2.350-11	TML-YFLA-5
Gage Resistance	120 ± 0.6 Ω	350 ± 1 Ω	305 ± 1 Ω	120 ± 3 Ω
Gage Factor	2.05 ± 1%	2.15 ± 1%	2.09	2.12 ± 2%
Gage Length	5mm	5mm	2mm	5mm
Transverse Sensitivity	0.0 %	0 %	-	0.2 %

3.2. Tensile Tests

The objective is to determine the tensile strengths (UTS_x, UTS_y), moduli of elasticity (E_{xx}, E_{yy}) and Poisson's ratios (ν_{xy}, ν_{xy}) in-plane directions. Tests were performed according to ASTM D3039/ D3039M-00, 'Standard Test Method for Tensile Properties of Polymer Matrix Composite Materials' [62]. It covers the determination of the in-plane tensile properties of polymer matrix composite materials reinforced by high-modulus fibers.

Tests were performed for in-plane directions. 4 specimens were cut for each directions from plates produced with VARTM, VP and BP whereas from RTM plates, 4 specimens in longitudinal and 3 specimens in transverse directions were cut. Finally, the amount of specimens cut from LRTM plates in longitudinal and transverse directions were 2 and 1 respectively. All specimens tested were used to determine the ultimate tensile strength (UTS). In addition, strain gages were attached to one specimen in each planar direction in the longitudinal direction, of the specimen, to determine the modulus of elasticity. Also another pair of specimens was attached in longitudinal and transverse strain gages directions to determine the modulus of elasticity and Poisson's ratio.

3.2.1. Specimen Geometry

According to ASTM D3039/ D3039M-00; recommended dimensions for a balanced symmetric composite material are 250×25×2.5mm. However, they are allowed to be

varied according to the needs. In this study, 250×20mm specimens with their thicknesses varying depending on the process were used, to cut out the maximum number of specimens from each plate. Also E-glass polymer composite tabs were attached on the tensile test specimens to ensure there was no stress concentration at the grip areas. The geometry of tabs was given according to the standard. The specimen geometry is given in Figure 3.4.

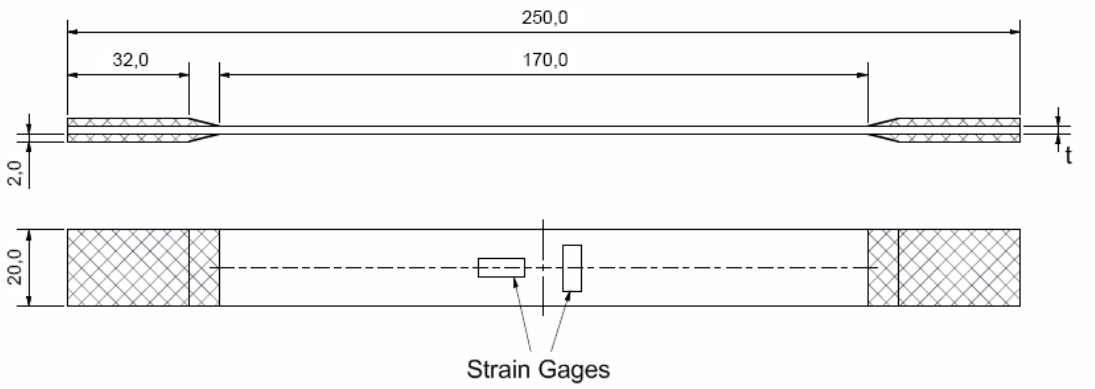

Figure 3.4: Geometry of Tensile Test Specimens

3.2.2. Test Setup and Equipment

The specimen was fixed using standard mechanical clamps of INSTRON testing machine (Figure 3.5) and the strain gages were connected to a data acquisition system.

The universal testing machine INSTRON 4206, is used for testing metallic and composite materials in either tension or compression, has a testing capacity of 150 kN, a crosshead speed range of 0.005 to 500 mm/min with an accuracy of 0.2% over 100 mm, and its operating temperatures are at –150 to 300 °C. Other equipment used was; digital calipers, strain gages, type TML-YFLA – 5, HBM-6/120LD20 or TML-UFRA-5-350-23 and data acquisition system

3.2.3. Procedure

The test procedure was carried on in accordance with ASTM D3039/ D3039M-00. Additionally, to determine the strain response; the strain gages were attached to the specimen with an adhesive. Also with the same adhesive, the tabs were attached. Speed of testing (velocity of separation of the two members of the testing machine) is set to a constant speed and the test was started. Load and strain data were recorded until the failure of the specimen.

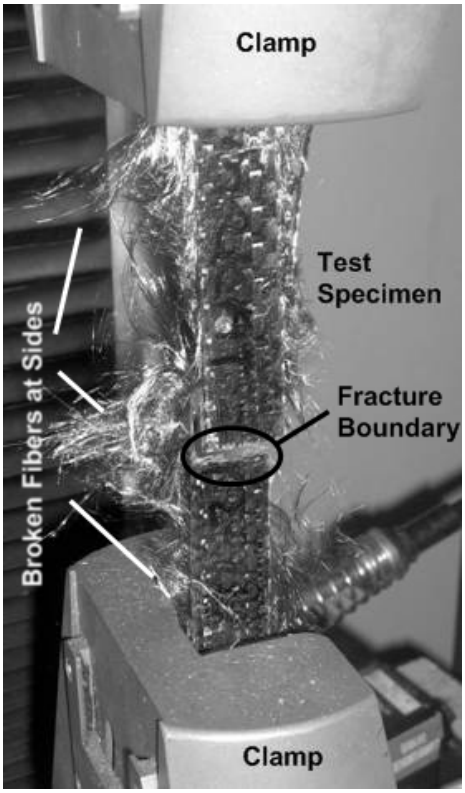

Figure 3.5: A Tensile Test Specimen.

3.2.4. Calculations

The ultimate tensile strength is calculated as follows.

$$\sigma_t = \frac{P_{max}}{A} \qquad (3.1)$$

where

σ_t : Ultimate Tensile Strength (UTS), MPa

P_{max} : Maximum Load at Failure, N

A : Cross Sectional Area, mm^2

The testing machine provides the load value while the data acquisition system acquires strain data every one third of a second. Therefore to obtain the modulus of elasticity and the Poisson's ratio the data acquired from test machine and strain gages have to be synchronized. With that data obtained, the stress vs. strain graphs are plotted as shown in Figure 3.6. Then slope of the linear portion of the graphs were determined, by fitting a straight line to the linear portion of the graphs, with the least square method to obtain the modulus of elasticity. Therefore:

$$E = \frac{d\sigma}{d\varepsilon} \qquad (3.2)$$

where

E : Modulus of Elasticity, GPa.

$d\sigma/d\varepsilon$: Slope of the stress-strain curve.

The Poisson's ratio is calculated with three data points within the elastic region of the plot and the arithmetic mean of these results were considered as the final result.

$$\nu^i = -\frac{\varepsilon_T^i}{\varepsilon_L^i} \qquad (3.3)$$

where

ν^i : Poisson's ratio at i^{th} instant

$\varepsilon_T{}^i$: Transverse strain at i^{th} instant

$\varepsilon_L{}^i$: Longitudinal axial strain at i^{th} instant

The Poisson's ratio is found as $\nu = \frac{1}{n}.\left(\sum_{i=1}^{n} \nu^i\right)$.

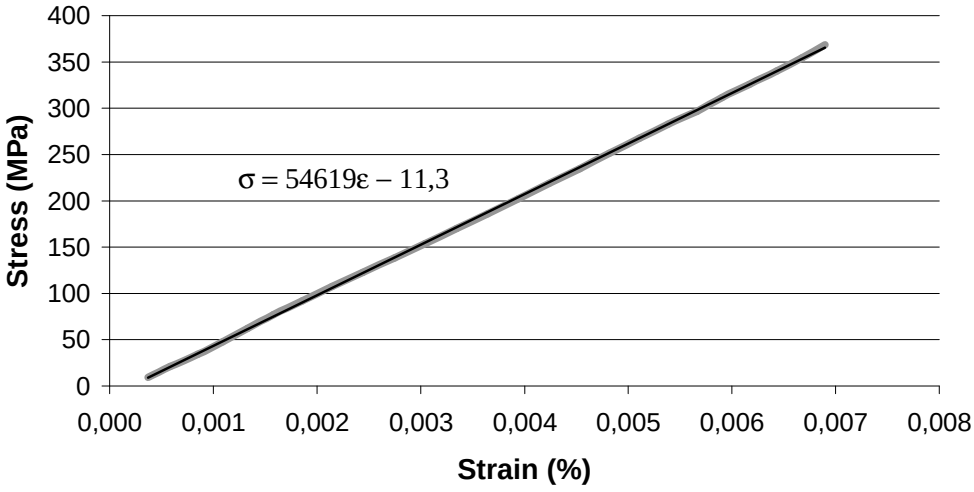

Figure 3.6: A Typical Stress-Strain Graph of Tensile Test

3.3. Compression Tests

The objective of this test is to determine the compressive strengths in both planar directions (UCS_x, UCS_y). The tests were performed according to ASTM D 695-02a, 'Standard Test Method for Compressive Properties of Rigid Plastics' [63]. The standard covers the determination of the mechanical properties of non-reinforced and reinforced rigid plastics, including high-modulus composites, when loaded in compression at relatively low uniform rates of straining or loading.

Tests were performed for both planar directions of the specimen plates. 2 specimens were cut out for each direction of each plate except thin RTM plates. All specimens tested were used to determine the ultimate compressive strength.

3.3.1. Specimen Geometry

The specimens were cut in the geometry shown in Figure 3.7.

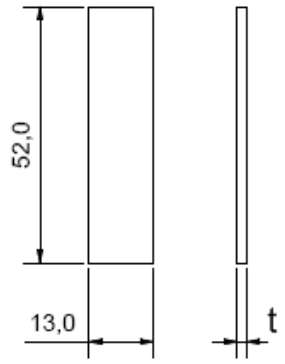

Figure 3.7: Compressive Test Specimen Geometry

3.3.2. Test Setup, Equipment and Procedure

The specimen was fixed using a compressive test fixture according to ASTM D695-02a to the INSTRON testing machine. The test fixture involves a half cylinder component with a disk-shaped base on which the specimen rests. The face in contact with the specimen is serrated in a way that allows downward motion but restricts upward motion. Another smaller half cylinder part is fastened to the larger base using two bolts, therefore compressing the specimen to aforementioned serrated face. A final part is used for compressing and is basically a cylinder, which presses the specimen from above. An illustration of the fixture is given in Figure 3.8. Universal Testing Machine, INSTRON 4206, was used with the compressive test fixture for the tests. The test procedure was carried on in accordance with ASTM D 695-02a.

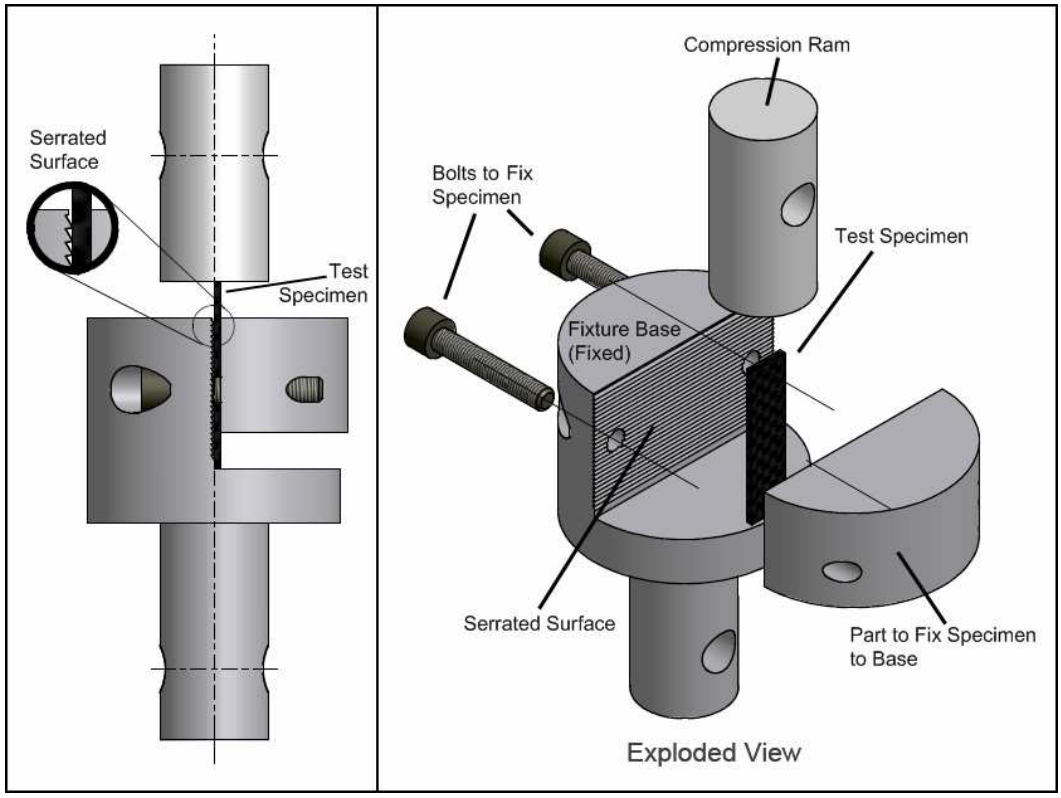

Figure 3.8: 3D Model of Compressive Test Fixture.

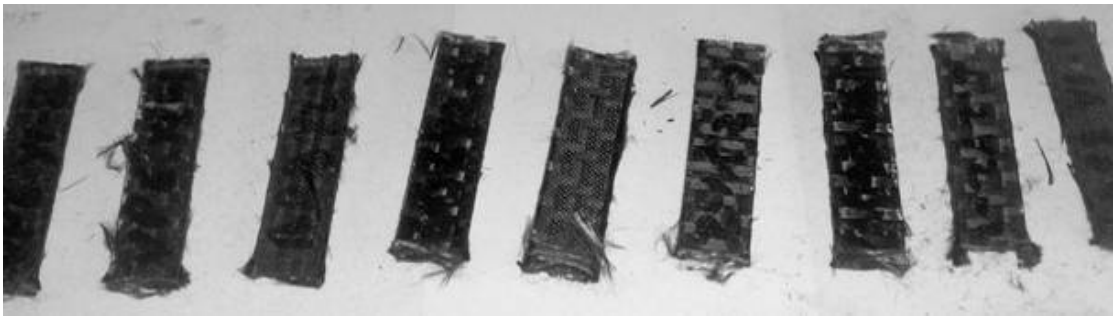

Figure 3.9: Compression Test Specimens after Tests

3.3.3. Calculations

The ultimate compressive strength is calculated as follows.

$$\sigma_c = \frac{P_{\max}}{A} \qquad (3.4)$$

where

σ_c : Ultimate Compressive Strength, MPa

P_{max} : Maximum Load before Failure, N

A : Cross Sectional Area, mm^2

3.4. In Plane Shear Tests

The objective of this test is to determine the in-plane shear strength (USS_{xy}, USS_{yx}) and moduli (G_{xy}, G_{yx}). They were performed according to ASTM D4255/ D4255M-01, 'Standard Test Method for In-Plane Shear Properties of Polymer Matrix Composite Materials by the Rail Shear Method' [64]. It covers the determination of in-plane shear properties of high-modulus fiber-reinforced composite materials by either of two procedures, Procedure A or B. In Procedure A, laminates clamped between two pairs of loading rails are tested. When loaded in tension, the rails introduce shear forces in the

specimen. In Procedure B, laminates clamped on opposite edges with a tensile or compressive load applied to a third pair of rails in the center are tested. In this study Procedure B was determined to be the testing method.

The tests were performed for both planar directions of the RTM, $RTM_{(Thick)}$, VARTM, VP and BP specimen plates. A specimen was cut out for each direction from these plates. However, due to geometric constraints only, one specimen could be cut from LRTM plates, as a result only the specimens in longitudinal direction were used for these plates. All specimens tested were used to determine the in-plane shear strength and modulus of each plate. To calculate the in-plane shear strain modulus, strain gages were attached to the specimens aligned in 45 degrees.

3.4.1. Specimen Geometry

The specimen geometry is determined according to ASTM D4255/ 4255M-01 as in Figure 3.11.

3.4.2. Test Setup and Equipment

The specimen was fixed using a three rail shear test fixture according to Procedure B of ASTM D4255/ D4255M-01 (Figure 3.12) and the strain gages were connected to a data acquisition system. In the cases where one directional strain gages are employed, two of them were used symmetrically, to verify the accuracy of the data. Note that in Figure 3.11, the schematic of two different strain gage attachment cases were given.

The fixture shown in Figure 3.12 consists of four different parts. First part is the base which has two perpendicular rails that are fixed to provide a frame for the specimen. The coupling part of the base also has symmetric rails which are fastened to the rails using six bolts. The moving center rail consists of two parts which are fastened together using three bolts to secure the specimen. The moving rail couple is used to compress the middle part of the specimen thus simulating in-plane shear.

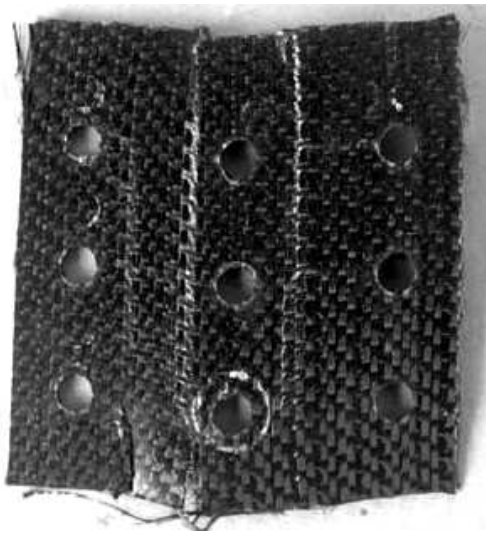

Figure 3.10: Sample Shear Test Specimen after Test

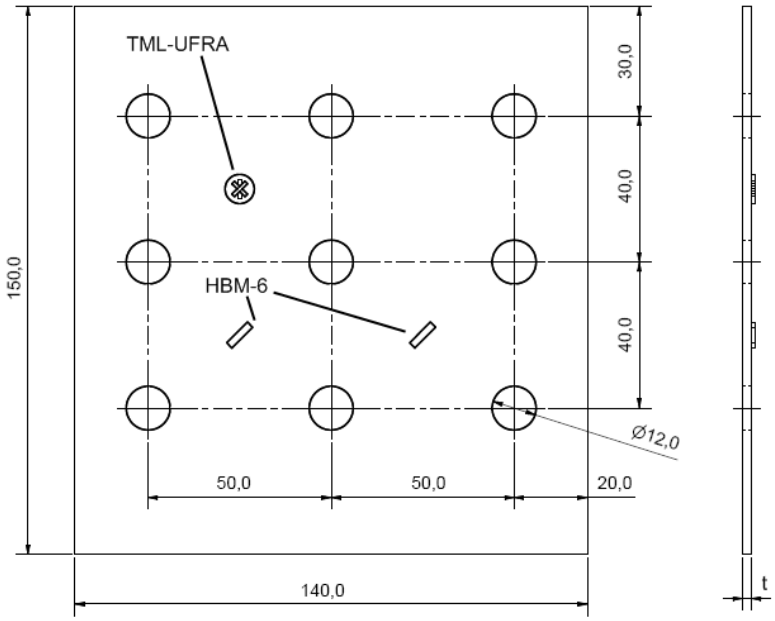

Figure 3.11: Shear Test Specimen Geometry

Universal Testing Instrument, INSTRON 4206 with three-rail shear test fixture was used along with digital calipers, strain gages, type HBM-6/120LD20 or TML-UFRA-5-350-23 and data acquisition system.

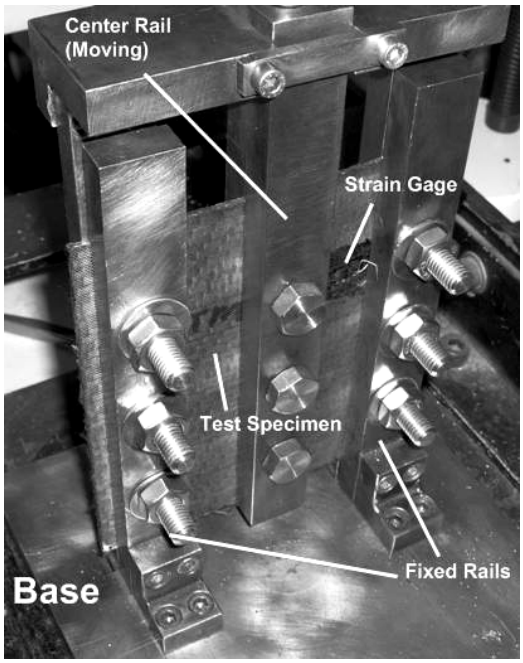

Figure 3.12: Shear Test Specimen Assembled to the Testing Machine.

3.4.3. Procedure

The test procedure was carried on in accordance with ASTM D4255/ 4255M-01. Additionally, to determine the strain response; the strain gages were attached to the specimen with an adhesive. The specimens were placed in the fixture, and nuts were tightened with a specific torque (60kN was found to be the most appropriate torque). Load and strain data were recorded until the failure of the specimen.

3.4.4. Calculations

The shear strength is calculated as follows.

$$\tau = \frac{P_{max}}{2A} \qquad (3.5)$$

where

τ : Ultimate Tensile Strength (UTS), MPa

P_{max} : Maximum Load before Failure, N

A : cross-sectional area at test section calculated as the product of the average length, l, and thickness, t; mm^2

Similar to the tensile test calculations; the data acquired from the test machine and strain gages have to be synchronized, to obtain the modulus of elasticity. With that data obtained, the stress vs. strain graphs are plotted for the data taken from both strain gages as shown in Figure 3.13. When the strain gages are placed asymmetrically they obtain the strain data in opposite signs, in those cases absolute values are considered instead of the negative values. Following the plotting of graphs, slope of the graphs were determined, by fitting a straight line to the linear portion of the graphs, with the least square method to obtain the in-plane shear modulus then calculating the arithmetic average of these slopes. Therefore:

$$G = \frac{d\tau}{d\gamma} \qquad (3.6)$$

where

G : In-plane Shear Modulus, GPa.

$d\tau/d\gamma$: Slope of the stress vs. strain curve.

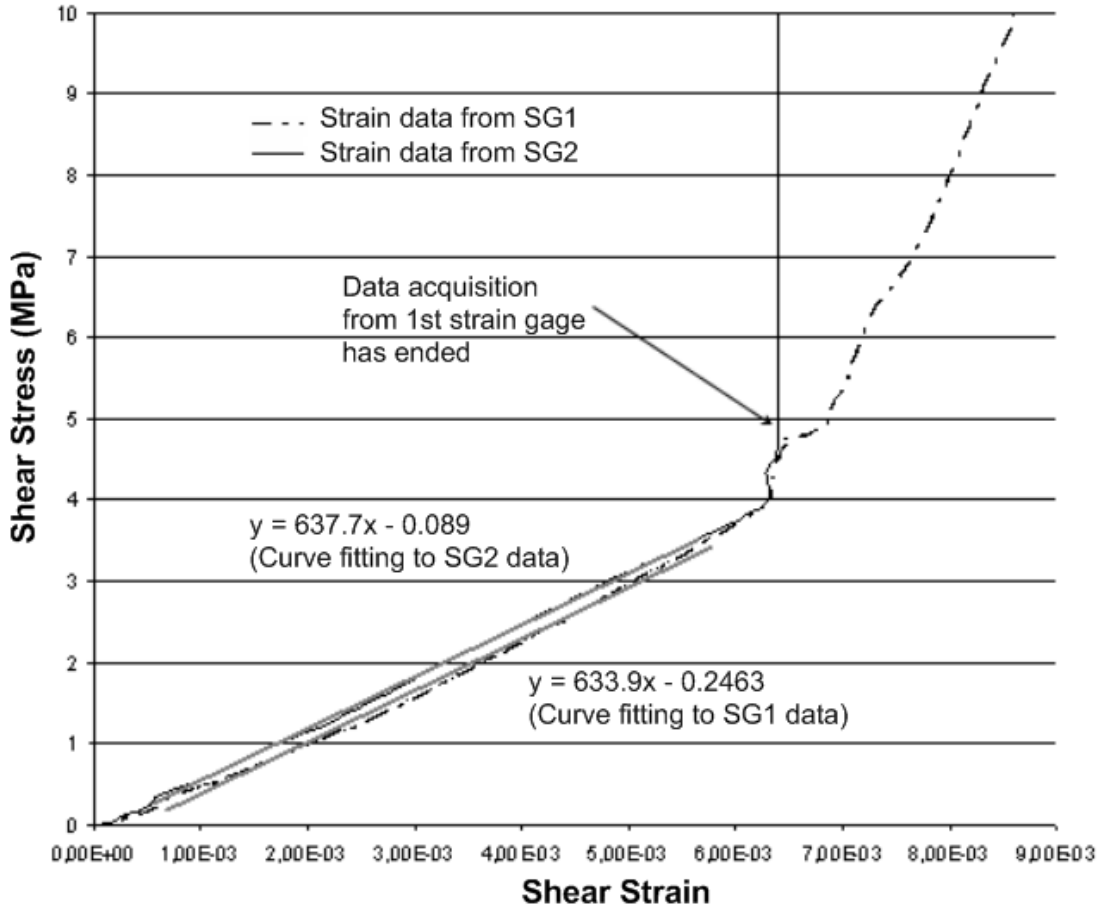

Figure 3.13: A Typical Stress-Strain Graph of In-Plane Shear Test

3.5. Differential Scanning Calorimtery (DSC) Tests

The objective of this test is to determine the glass transition temperatures of the materials. The tests were performed according to ASTM E 1356 - 91, 'Standard Test Method for Glass Transition Temperatures by Differential Scanning Calorimetry or Differential Thermal Analysis' [65]. It covers the determination of the glass transition temperatures (T_g) of amorphous or partially crystalline materials containing amorphous regions that are stable and do not undergo decomposition or sublimation in T_g; using DSC or DTA.

This test method monitors the difference of heat flow between the test material and a reference material when they are heated or cooled at a controlled rate [65]. The resulting data is a Heat Flow vs. Temperature graph, which is then analyzed for its extrema and slopes.

The tests were performed on two randomly selected specimen plates for every process. The specimen needed is about 20mg. The aim was to determine the T_g of the products. This material property is not directly related to the process but rather the thermal process parameters such as cure cycle. These tests were performed to prove the polymer matrix was cured appropriately.

3.5.1. Test Setup, Equipment and Procedure

The specimen was placed inside the heating chamber of the DSC testing machine; in an aluminum pan along with the reference pan, which is empty.

Polymer Laboratories PL-DSC 12000 DSC testing Device with the specifications; temperature range of -150 to 770°C, heating rate range of 0.1 to 60 K/min, measuring range of ±100 mW with a precision: ±1% of the change in enthalpy and a baseline stability of 1 mW between RT and 600°C was used for these tests

The test procedure was carried on in accordance with ASTM E 1356 - 91. The heat rate was set to 10°C /min and the test was started at 25°C and heat flow and temperature data were taken until the temperature rises to 500°C.

3.5.2. Calculations

To calculate the glass transition temperature, T_g, the first derivative of the graph (Figure 3.14) should be determined. After the Onset Temperature of Transition, T_{os} and End Temperature of Transition, T_e points are determined; the built-in software of the DSC testing machine calculates the required result as follows.

$$T_g = \frac{T_{OS} + T_E}{2} \qquad (3.7)$$

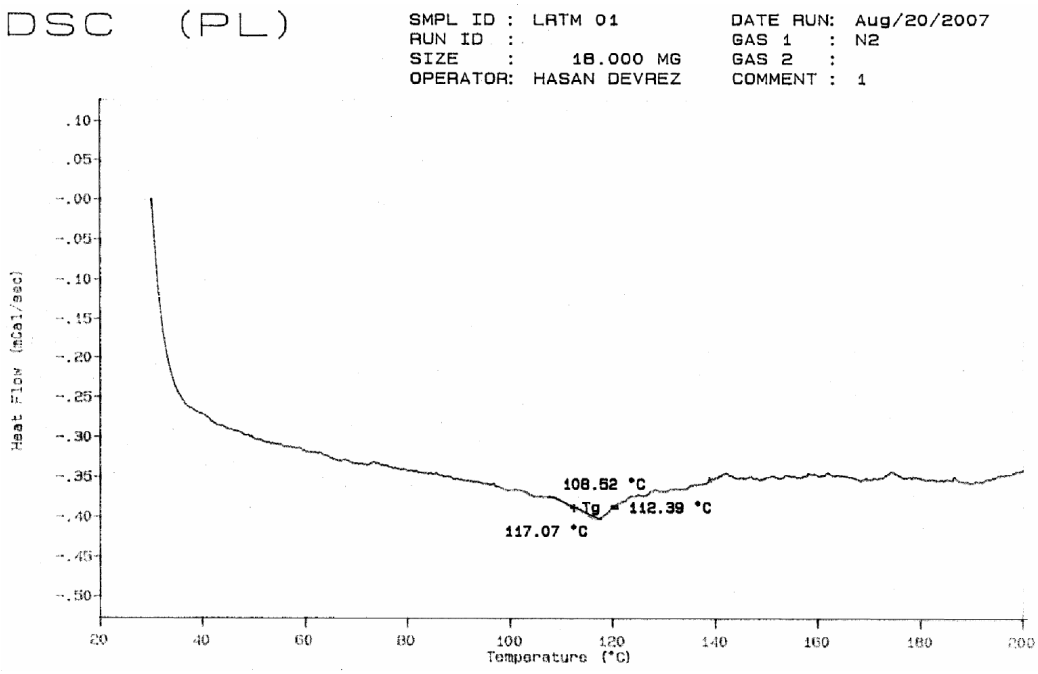

Figure 3.14: Sample DSC Test Result for a LRTM Specimen.

where

T_g : Glass Transition Temperature

T_{OS} : Onset Temperature of Transition, the temperature where the transition begins

T_E : End Temperature of Transition, the temperature where the transition ends

3.6. Thermogravimetric Analyses (TGA)

The objective of the test is to determine the fiber-to-resin mass ratio of the plates. The tests were performed according to ASTM E 1131- 86, ‘Standard Test Method for

Compositional Analysis by Thermogravimetry' [66]. The mass of a substance is heated in a controlled rate in an appropriate environment and is recorded as a function of temperature. The mass loss over specific temperatures and specific atmosphere provide a compositional analysis of the substance.

The idea emerges from the differences in the characteristics of resin and fiber. The resin is considered to have medium volatile matter characteristics, whereas the fiber possesses combustible matter characteristics. The medium volatile matters degrade between 200 to 550°C for thermoset polymers, while combustible materials degrade above 750°C.

The tests were performed on two randomly selected specimen plates for every process. The aim was to determine the fiber/resin mass ratio of the products.

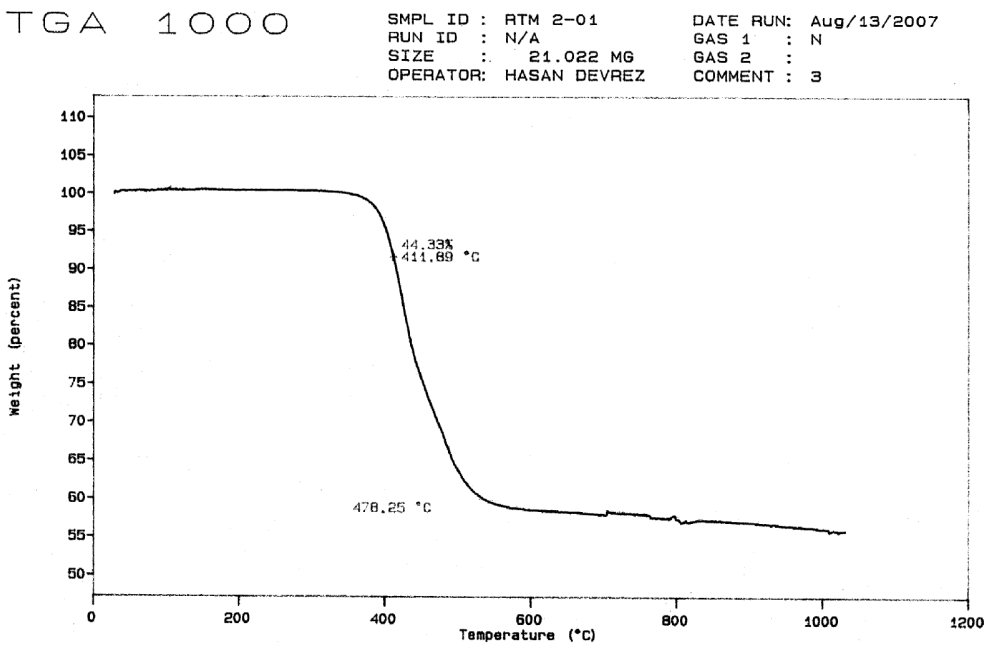

Figure 3.15: Sample TGA Test Result for a RTM Specimen.

3.6.1. Test Setup, Equipment and Procedure

The specimen was placed over a scale inside the heating chamber of the TGA testing machine. Polymer Laboratories PL-TGA 100 TGA testing device was used in TGA tests

The test procedure was carried on in accordance with ASTM E 1131- 86. The heat rate was set to 10°C /min and the test was started at 20°C and mass and temperature data were taken until the temperature rises to 1000°C.

3.6.2. Calculations

The percent fiber content ratio is determined with the following equation.

$$m_f = \left(1 - \frac{W - F}{W}\right) \times 100 \qquad (3.8)$$

where

m_f : Fiber mass fraction, %

W : Initial mass, mg

F : Final mass, mg

The volumetric fiber ratio is calculated as follows:

$$v_f = \frac{d_r m_f}{d_r m_f + d_f (1 - m_f)} \qquad (3.9)$$

where

v_f : Volumetric Fiber Ratio, %

m_f : Fiber mass fraction, %

d_f : Density of Fiber, g/cm^3

d_r : Density of Resin, g/cm^3

Density Calculations

The volumetric ratios and area densities of the plates were also calculated with geometric and mass measurements taken from specimens. The objective was to compare the findings with the TGA measurements. First the area densities of composite specimens (ρ_A) were calculated dividing the measured specimen mass to measured specimen area.

The densities of resin and fabric were obtained from the manufacturer data and the areas and masses of the composite were measured. Later the masses of fabric layers were calculated as shown.

$$m_f = 2A \cdot \rho_{A_f} \qquad (3.10)$$

where

m_f : Mass of Total Layers, g

A : Area of Specimen, cm^2

ρ_{Af} : Area Density of a Single Fabric Layer, g/cm^2

After obtaining the fiber mass; the resin mass is simply the difference between total mass and fiber mass. The volumes of resin and fiber were calculated individually by dividing the calculated masses to known densities. Since the thickness was variable throughout the specimen for most processes, the composite volume was calculated by adding the volumes of resin and fiber; instead of measuring the dimensions. Later the volumetric fiber ratio was obtained as given below.

$$v_f = \frac{V_f}{V_c} = \frac{V_f}{V_f + V_r} \qquad (3.11)$$

where

v_f : Volumetric Fiber Ratio

V_f : Fiber Volume, cm^3

Vc : Composite Volume, cm^3

V_r : Resin Volume, cm^3

3.7. Theoretical Analysis

As stated in Section 1.3.4 there are various analytical solutions for woven fabric parameters. It was shown that for 3-Harness satin (twill) weave fabric composites; the available models were mosaic model and fiber undulation (crimp) model. However, it was seen that although the crimp model was much more complicated than the mosaic model, the improvement it provides is not as much (Figure 1.22). Therefore the mosaic model proposed by Ishikawa [67] will be used in this study. There are two solutions in this model, which result in an upper bound (UB) and lower bound (LB) values for elastic properties. The UB approach simply governs the parallel model while the LB approach solves the problem via the series model. Note that this solution is one dimensional and it is assumed that the loads and shear values are uniform within a cell. While the UB solution is relatively simple, the LB approach is rather complex. Analyzing the performances using the LB approach would expand the study to a great extent. Thus only the UB approach was solved to provide a general comparison with the experimental results.

3.7.1. Upper Bound Solution

As stated in the previous chapter the parallel model is governed in this approach, where the strains are uniform throughout the unit cell (Figure 3.16). Ishikawa's solution states that the extensional stiffness matrix [*A*] for the satin weave is equal to that of the part

from 0 to *t*. Therefore to find the UB solution one should simply calculate [*A*] and calculate the laminate elastic parameters accordingly.

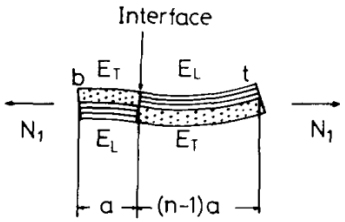

Figure 3.16: 1D Unit Cell for Mosaic Model [67]

At the beginning of the problem, the ply parameters should be found via classic micromechanics:

$$E_L = E_f v_f + E_m(1-v_f) \qquad (3.12)$$

$$E_T = \frac{E_f E_m}{E_f(1-v_f)+E_m v_f} \qquad (3.13)$$

$$\nu_L = \nu_f v_f + (1-v_f)\nu_f \qquad (3.14)$$

$$\nu_T = \frac{E_T}{E_L}\nu_L \qquad (3.15)$$

where, E_L and the E_T are the moduli of elasticity and ν_T and ν_L are the Poisson's ratio in longitudinal and transverse directions respectively, and v_f is the fiber ratio. E_f, E_m, ν_f and ν_m are the fiber and matrix parameters provided by the manufacturer. Assuming fiber and the matrix to be isotropic, the shear modulus becomes;

$$G_{LT} = \frac{G_f G_m}{G_f(1-v_f)+G_m v_f} \qquad (3.16)$$

where; $G_f = \frac{E_f}{2(1+\nu_f)}$ and $G_m = \frac{E_m}{2(1+\nu_m)}$.

Next, the ply stiffness matrix [Q] is calculated:

$$[Q] = \begin{bmatrix} Q_{11} & Q_{12} & 0 \\ Q_{21} & Q_{22} & 0 \\ 0 & 0 & Q_{66} \end{bmatrix} \tag{3.17}$$

$$Q_{11} = \frac{E_L}{1 - \nu_L \nu_T} \tag{3.18}$$

$$Q_{22} = \frac{E_T}{1 - \nu_L \nu_T} \tag{3.19}$$

$$Q_{12} = Q_{21} = \frac{\nu_L E_T}{1 - \nu_L \nu_T} \tag{3.20}$$

$$Q_{66} = G_{LT} \tag{3.21}$$

Since the laminates investigated in this study consist of two layers, applying the appropriate simplifications, the laminate shape could be shown as in Figure 3.17. Note that the whole thickness of the laminate is measured from the specimen plates, and the '*h*' values are calculated from those measurements (e.g. $h_0 = -t/2$, $h_3 = t/4$ etc.)

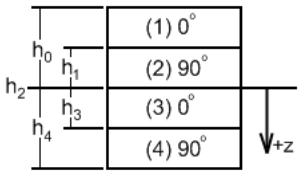

Figure 3.17: Laminate geometry after simplification.

Then the elements of [A] matrix are simply calculated as:

$$[A] = \begin{bmatrix} A_{11} & A_{12} & A_{16} \\ A_{21} & A_{22} & A_{26} \\ A_{61} & A_{62} & A_{66} \end{bmatrix} \quad (3.22)$$

$$A_{mn} = \sum_{j=1}^{N} (Q_{mn})^{j} \left(h_j - h_{j-1} \right) \quad (3.23)$$

Once all the elements of extensional stiffness matrix are calculated, the elastic parameters of the laminate are calculated as:

$$E_{xx} = \frac{A_{11}A_{22} - A_{12}^{\ 2}}{tA_{22}} \quad (3.24)$$

$$E_{yy} = \frac{A_{11}A_{22} - A_{12}^{\ 2}}{tA_{11}} \quad (3.25)$$

$$\nu_{xy} = \frac{A_{12}}{A_{22}} \quad (3.26)$$

$$\nu_{xy} = \frac{A_{12}}{A_{11}} \quad (3.27)$$

$$G_{xy} = \frac{A_{66}}{t} \quad (3.28)$$

CHAPTER 4

RESULTS AND DISCUSSIONS

This chapter involves the results and discussion of experimental studies performed and the comparison between these results and micromechanical analyses performed under the scope of the thesis. In the next section, tabulated results of experimental work will be presented. Comprehensive discussions of these results will be given in the following section.

4.1. Experimental Results

Various specimens were tested from the number of plates produced. The methodology of the productions and tests are explained in the previous chapters. The following section will provide graphs and tables explaining the results of these tests.

4.1.1. Tensile Test Results

The load and strain data were taken until the failure of the specimens in correlation with ASTM Standard D3039/D3039M-00. These data were used to calculate the ultimate tensile strength of the specimens, and at the same time, converted into stress vs. strain graphs, as stated in Section 3.2.4. These graphs were then used in determination of the moduli of elasticity of the specimens. For this purpose, the slope of the elastic region of these curves was determined by fitting a straight line, with the least-square method. These graphs were plotted in MS Excel Software. Also the Poisson's Ratio was determined by using Equation 3.3. Later the arithmetic mean of the tensile strength and

tensile modulus, standard deviation, and percent coefficient of variation were calculated for each testing group.

In Table 4.1 and Table 4.2, the tabulated strength results of tensile test specimens for both weft and warp directions are presented. In the second and third columns of the tables, the specimen designations are given. Fourth to sixth columns involve the geometric dimensions of the specimens. The seventh column, show the resulting ultimate tensile strengths. Finally the arithmetic mean of the results, their standard deviation and their percent coefficient of variation are tabulated respectively for each testing group.

Table 4.1: Ultimate Tensile Stress Test Results in Warp Direction and the Related Statistical Results

#	Plate Type	Specimen No.	*w* (mm)	*t* (mm)	*l* (mm)	UTS_x (MPa)	Average (MPa)	Standard Deviation (MPa)	CV (%)
1	VARTM	111	20.27	1.45	147.6	428.58	449.77	30.97	6.89
2		112	20.19	1.49	145.6	429.82			
3		611	20.24	1.44	147.9	436.91			
4		612	20.22	1.48	140.1	499.28			
5		211	20.12	1.46	155.7	426.30			
6		713	20.18	1.45	145.6	477.70			
7	VP	112	20.24	1.32	147.8	490.22	541.96	36.93	6.81
8		114	20.21	1.35	138.8	580.63			
9		611	20.27	1.30	148.0	556.22			
10		612	20.36	1.27	145.6	522.08			
11		213	20.03	1.33	145.79	581.90			
12		713	20.27	1.31	143.72	520.70			

Table 4.1 (continued)

#	Plate Type	Specimen No.	*w* (mm)	*t* (mm)	*l* (mm)	UTS_x (MPa)	Average (MPa)	Standard Deviation (MPa)	CV (%)
13	BP	311	20.24	1.44	147.4	463.18	449.60	21.82	4.85
14		312	20.22	1.52	139.9	421.99			
15		411	20.14	1.49	149.5	470.45			
16		412	20.25	1.51	144.5	442.77			
17	RTM	111	20.07	1.41	200.2	547.70	537.92	11.05	2.05
18		112	20.92	1.39	200.3	550.30			
19		211	19.84	1.61	200.2	535.40			
20		212	20.02	1.68	200.1	523.60			
21		311	20.05	1.45	200.4	532.6			
22	RTM (Thick)	111	20.15	1.75	143.9	461.56	464.55	26.20	5.64
23		112	20.25	1.70	140.5	482.19			
24		213	20.20	1.71	141.0	420.04			
25		311	20.15	1.75	143.2	477.54			
26		312	20.21	1.69	142.9	508.69			
27	LRTM	111	20.31	1.37	146.1	489.38	510.85	33.08	6.48
28		112	20.31	1.41	144.8	560.81			
29		211	20.30	1.34	143.3	469.93			
30		212	20.22	1.39	144.8	532.30			
31		311	20.29	1.39	144.8	519.34			
32		312	20.30	1.35	143.8	493.30			

As seen in Figure 3.6, the stress vs. strain graph is simplified for every specimen and the obtained curve was fitted to a line using the least square method. A simplified stress vs. strain graph is given in Figure 4.1 to illustrate the work done for each test result. Also the Poisson's Ratio was determined for the specimens examining three data points (Figure 4.1 circled points) and taking the average of these results.

Table 4.2: Ultimate Tensile Stress Test Results in Weft Direction and the Related Statistical Results

#	Plate Type	Specimen No.	*w* (mm)	*t* (mm)	*l* (mm)	UTS_y (MPa)	Average (MPa)	Standard Deviation (MPa)	CV (%)
1	VARTM	123	20.17	1.43	141.8	479.66	502.82	34.15	6.79
2		124	20.31	1.39	141.7	457.33			
3		621	20.20	1.46	147.1	534.57			
4		622	20.22	1.49	142.2	483.08			
5		224	20.26	1.44	139.7	520.60			
6		723	20.17	1.46	141.8	541.70			
7	VP	123	20.21	1.38	148.8	563.87	597.09	48.05	8.05
8		124	20.21	1.38	153.6	569.51			
9		621	20.18	1.30	145.7	671.64			
10		622	20.28	1.30	143.4	643.40			
11		221	20.02	1.34	145.47	576.40			
12		723	20.32	1.31	144.8	557.70			
13	BP	321	20.15	1.43	145.6	444.65	441.05	17.28	3.92
14		322	20.23	1.46	140.0	418.85			
15		421	20.19	1.49	144.5	439.92			
16		422	20.19	1.43	145.1	460.77			
17	RTM	121	20.05	1.41	200.2	534.50	547.85	18.88	3.45
18		221	20.10	1.39	199.0	561.20			
19	RTM (Thick)	121	20.26	1.70	140.6	466.008	462.603	31.112	6.73
20		122	20.27	1.83	145.5	425.013			
21		222	20.31	1.56	146.8	496.917			
22		321	20.24	1.69	144.3	482.707			
23		322	20.20	1.66	145.4	442.372			
24	LRTM	221	20.31	1.41	144.8	560.813	501.565	83.789	16.71
25		321	20.32	1.61	144.3	442.318			

In Table 4.3 and 4.4, the calculated moduli of elasticity and Poisson's ratios of tensile test specimens for both weft and warp directions are presented. In the second and third columns of the tables, the specimen designations are given. In the fourth column, the quantity of strain gages used for that test is given. In the columns from fifth to eight, the resulting moduli of elasticity, the arithmetic mean of the results, their standard deviation and their percent coefficient of variation are tabulated respectively for each testing group. The last four columns consist of the Poisson's ratio results, the arithmetic mean of the results, their standard deviation and their percent coefficient of variation for the tests in which two strain gages are used, in both axes.

Table 4.3: Modulus of Elasticity and Poisson's Ratio in Warp Direction and Statistical Results

#	Plate Type	Specimen No.	SG Quantity	E_{xx} (GPa)	Average (GPa)	Standard Deviation (GPa)	CV (%)	ν_{xy}	Average	Standard Deviation	CV (%)
1	VARTM	111	2	51.54	50.72	3.01	5.93	0.249	0.31	0.05	17.06
2		112	1	47.85							
3		611	2	46.83				0.295			
4		612	1	50.85							
5		211	2	55.09				0.317			
6		713	2	52.15				0.376			
7	VP	112	2	61.27	63.09	4.87	7.73	0.332	0.35	0.03	8.67
8		114	1	64.83							
9		611	2	57.73							
10		612	1	57.93				0.310			
11		213	2	69.08				0.370			
12		713	2	67.68				0.371			

Table 4.3 (continued)

#	Plate Type	Specimen No.	SG Quantity	E_{xx} (GPa)	Average (GPa)	Standard Deviation (GPa)	CV (%)	ν_{xy}	Average	Standard Deviation	CV (%)
13	BP	311	2	46.02	46.37	1.91	4.12		0.29	-	-
14		312	1	49.13							
15		411	2	44.77				0.290			
16		412	1	45.58							
17	RTM	111	2	50.90	54.30	2.36	4.34	0.033	0.04	0.00	9.52
18		112	2	53.04				0.038			
19		211	2	56.30				0.041			
20		212	2	56.49				0.035			
		311	1	54.8							
21	RTM (Thick)	111	2	46.01	50.06	3.70	7.40	0.125	0.11	0.01	10.66
22		112	1	47.79				0.106			
23		213	2	55.37				0.110			
24		311	2	52.09				0.097			
25		312	1	49.04							
26	LRTM	111	2	49.43	54.39	4.56	8.38	0.035	0.03	0.00	6.19
27		112	2	56.65							
28		211	2	60.31				0.030			
29		212	1	50.04							
30		311	2	51.82				0.032			
31		312	1	58.09				0.033			

Table 4.4: Modulus of Elasticity and Poisson's Ratio in Weft Direction and Statistical Results

#	Plate Type	Specimen No.	SG Quantity	E_{yy} (GPa)	Average (GPa)	Standard Deviation (GPa)	CV (%)	ν_{yx}	Average	Standard Deviation	CV (%)
1	VARTM	123	2	60.04	57.55	5.00	8.69	0.347	0.33	0.03	8.15
2		124	1	55.80							
3		621	2	52.20				0.299			
4		622	1	51.83							
5		224	2	61.90				0.359			
6		723	2	63.50				0.320			
7	VP	123	2	56.05	58.78	3.82	6.50	0.324	0.34	0.03	8.99
8		124	1	54.88							
9		621	2	60.47				0.306			
10		622	1	59.93							
11		221	2	65.09				0.349			
12		723	2	56.27				0.376			
13	BP	321	2	48.33	47.78	0.86	1.80	0.359	0.34	0.03	7.45
14		322	1	46.63							
15		421	2	47.64				0.323			
16		422	1	48.54							
17	RTM	121	2	56.67	57.51	1.19	2.06	0.033	0.03	0.00	4.16
18		221	2	58.35				0.035			
19	RTM (Thick)	121	2	45.60	51.45	4.09	7.95	0.043	0.04	0.00	9.53
20		122	2	49.94				0.042			
21		222	2	55.94				0.037			
22		321	2	51.15				0.047			
23		322	1	54.62							
24	LRTM	221	2	56.65	56.43	0.30	0.54		0.05	-	-
25		321	2	56.22				0.054			

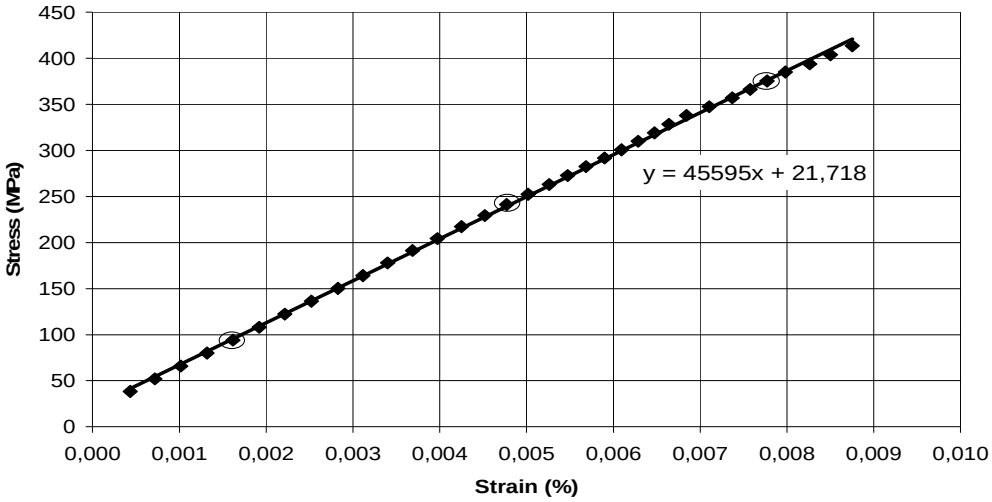

Figure 4.1: Stress-Strain Graph of Tensile Test

4.1.2. Compressive Test Results

While performing the tests, the maximum compressive load the specimens are subjected were noted. Afterwards the averages of these values were calculated along with the standard deviations and percent coefficients to analyze the results accuracy. In Table 4.5 and 4.6, the tabulated strength results of the test specimens for both weft and warp directions are presented. In the second and third columns of the tables, the specimen designations are given. Fourth to sixth columns involve the geometric dimensions of the specimens. The seventh column, show the test results. Finally the arithmetic mean of the results, their standard deviation and their percent coefficient of variation are tabulated respectively for each testing group.

4.1.3. In-Plane Shear Stress Test Results

The load and strain data were taken until the failure of the specimens in correlation with ASTM D3039/ D3039M-00. The data was used to calculate the shear strength of the specimens, and at the same time, converted into stress-strain graphs, as stated in Section

3.4.4. These graphs were then used in determination of the shear moduli of the specimens. For this purpose, the slope of the elastic region of these curves was determined by fitting a straight line, with the least-square method. These graphs were plotted in MS Excel Software. Later the arithmetic mean of the shear strength and shear modulus, standard deviation, and percent coefficient of variation were calculated for each testing group.

Table 4.5: Compressive Test Results in Warp Direction and Statistical Results

#	Plate Type	Specimen No.	*w* (mm)	*t* (mm)	*l* (mm)	UCS_x (MPa)	Average (MPa)	Standard Deviation (MPa)	CV (%)
1	VARTM	111	12.96	1.52	51.94	59.96	60.926	3.580	5.876
2		112	12.94	1.49	51.96	58.21			
3		611	12.92	1.53	51.96	59.35			
4		612	12.88	1.45	51.92	66.18			
5	VP	112	12.97	1.42	51.92	55.13	55.259	4.173	7.552
6		114	12.93	1.41	51.99	49.41			
7		611	12.84	1.41	51.92	58.03			
8		612	12.84	1.41	51.97	58.47			
9	BP	311	12.94	1.43	51.92	45.05	45.036	3.435	7.627
10		321	12.96	1.44	51.9	42.55			
11		411	12.87	1.43	51.9	49.89			
12		412	12.92	1.44	51.93	42.66			
13	RTM (Thick)	111	12.93	1.83	51.98	92.99	92.360	4.824	5.223
14		112	12.9	1.85	51.98	94.83			
15		213	12.97	1.62	51.89	85.40			
16		212	12.89	1.65	51.89	96.22			
17	LRTM	111	12.91	1.41	51.93	58.15	64.720	7.065	10.917
18		112	12.96	1.41	51.86	73.71			
19		211	12.93	1.42	51.96	66.89			
20		212	12.95	1.45	51.89	60.13			

Table 4.6: Compressive Test Results in Weft Direction and Statistical Results

#	Plate Type	Specimen No.	*w* (mm)	*t* (mm)	*l* (mm)	UCS_y (MPa)	Average (MPa)	Standard Deviation (MPa)	CV (%)
1	VARTM	123	12.96	1.51	51.97	68.23	67.154	4.422	6.584
2		124	12.94	1.52	51.92	60.65			
3		621	12.93	1.52	51.92	70.33			
4		622	12.92	1.48	51.93	69.41			
5	VP	123	12.94	1.4	51.91	55.83	59.185	2.807	4.743
6		124	12.97	1.42	51.9	62.43			
7		621	12.93	1.4	51.94	60.21			
8		622	12.93	1.41	51.84	58.27			
9	BP	321	12.86	1.46	51.92	54.70	55.756	6.641	11.911
10		322	12.93	1.43	51.93	62.73			
11		421	12.84	1.43	51.94	58.50			
12		422	12.87	1.46	51.98	47.09			
13	LRTM	121	12.97	1.48	51.9	69.15	74.287	6.216	8.368
14		122	12.91	1.46	51.95	79.01			
15		221	12.94	1.44	51.96	68.70			
16		222	12.97	1.43	51.97	80.29			

In Table 4.7 and 4.8, the tabulated strength results of shear test specimens for both weft and warp directions are presented. In the second and third columns of the tables, the specimen designations are given. Fourth and fifth columns involve the geometric dimensions of the specimens. The seventh column, show the resulting compression strengths. Finally the arithmetic mean of the results, their standard deviation and their percent coefficient of variation are tabulated respectively for each testing group.

As seen in Figure 3.13, the stress-strain graph is simplified for every specimen and the obtained curve was fitted to a line using the least square method. However a very small amount of results was obtained from the strain gages whereas for most of the time, data could not be read due to some complications. Thus no average or standard deviation

could be calculated for the processes except LRTM in weft direction. In Table 4.9, the calculated in-plane shear moduli for both weft and warp directions are presented. In the second column the direction of the test specimen is given, third and fourth columns of the tables provide the specimen designations. In the columns from fifth to eight, the resulting moduli of elasticity, the arithmetic mean of the results, their standard deviation and their percent coefficient of variation, if calculated, are tabulated respectively for each testing group.

Table 4.7: In-Plane Shear Stress Test Results in Weft Direction and Statistical Results

#	Plate Type	Specimen No.	*w* (mm)	*t* (mm)	USS_x (MPa)	Average (MPa)	Standard Deviation (MPa)	CV (%)
1	VARTM	11S	150.30	1.43	58.95	59.83	4.37	7.30
2		61S	150.21	1.46	55.97			
3		71S	150.36	1.36	64.57			
4	VP	11S	150.18	1.32	54.43	58.41	2.71	4.64
5		41S	150.21	1.33	59.97			
6		61S	150.28	1.34	58.99			
7		51S	150.13	1.23	60.26			
8	RTM	21S	150.32	1.40	65.19	66.78	2.24	3.36
9		41S	150.25	1.38	68.36			
10	RTM (Thick)	11S	150.28	1.75	57.02	59.47	3.46	5.82
11		21S	150.03	1.54	61.91			
12	LRTM	11S	150.41	1.54	57.42	58.97	2.57	4.36
13		21S	150.41	1.42	57.54			
14		31S	150.43	1.34	61.94			

Table 4.8: In-Plane Shear Test Results in Warp Direction and Statistical Results

#	Plate Type	Specimen No.	*w* (mm)	*t* (mm)	USS_y (MPa)	Average (MPa)	Standard Deviation (MPa)	CV (%)
1	VARTM	12S	149.44	1.53	55.57	60.60	4.39	7.24
2		62S	150.10	1.44	62.67			
3		32S	150.39	1.39	63.58			
4	VP	12S	149.42	1.42	55.15	57.63	4.45	7.71
5		62S	149.51	1.35	54.97			
6		72S	150.42	1.23	62.76			
7	RTM	12S	150.16	1.34	65.80	67.10	1.84	2.75
8		32S	150.25	1.33	68.41			

Table 4.9: Shear Moduli in Both Directions and the Related Statistical Results

#	Direction	Plate Type	Specimen No.	G (GPa)	Average (GPa)	Standard Deviation (GPa)	CV (%)
1	Warp	VARTM	71S	1.81	-	-	-
2		VP	51S	1.25	-	-	-
3		RTM	21S	2.40	-	-	-
4		LRTM	11S	1.48	1.26	0.32	25.35
5			21S	1.03			
6	Weft	VARTM	32S	0.64	-	-	-
7		VP	72S	0.84	-	-	-
8		RTM	12S	2.15	-	-	-

4.1.4. DSC Test Results

The DSC tests were performed as explained in Section 3.5. The obtained data is provided in Table 4.10.

Table 4.10: DSC Test Results of Plates

	***Tg* (°C)**
VARTM	129
VP	123
BP	124
RTM	125
$RTM_{(Thick)}$	122
LRTM	112

4.1.5. TGA Test Results and Volumetric Ratio Calculations

After the mass fraction data was obtained from the TGA tests, the mass ratio is calculated again using the information of carbon fabric mass used. Afterwards the volumetric fiber ratio is calculated as shown in Section 3.6.2, for both values. While performing these calculations the area density of the plates were also calculated. These results are given in Table 4.11.

4.1.6. Theoretical Analyses

The elastic parameters of all processes were calculated as explained in 3.7. The fiber volumes and thicknesses were taken from the test and measurement results. These results are tabulated in Table 4.12.

Table 4.11: Mass Ratios, Volumetric Ratios and Area Densities of Plates

	Area Density (kg/m^2)	TGA Data		Calculated Data	
		m_f/m_c	V_f/V_C	m_f/m_c	V_f/V_C
VARTM	1.89	65.74	54.11	63.44	51.60
VP	1.72	70.90	59.96	70.00	58.91
BP	1.68	75.80	65.81	71.46	60.61
$RTM_{(Thick)}$	2.27	55.67	43.56	52.83	40.77
RTM	1.97	63.44	51.61	60.94	48.95
LRTM	1.85	66.86	55.35	64.81	53.09

Table 4.12: Theoretical Results of Elastic Parameters for the Processes

	E_{xx} (GPa)	E_{yy} (GPa)	v_{xy}	v_{yx}	G_{xy} (GPa)
VARTM	133.36	133.36	0.0249	0.0249	5.25
VP	147.64	147.64	0.0252	0.0252	5.99
BP	162.28	162.28	0.0262	0.0262	6.98
$RTM_{(Thick)}$	108.10	108.10	0.0260	0.0260	4.29
RTM	127.31	127.31	0.0250	0.0250	4.98
LRTM	136.37	136.37	0.0249	0.0249	5.39

4.2. Discussion and Comparison of Results

This section includes the discussion of the results obtained throughout the study by comparing processes according to all the tests performed, starting with fiber fraction and area density measurements. Mechanical test results were then examined in the light of these results. Afterwards these results are compared with micromechanic calculations, finally the nature of the processes such as environmental conditions, or initial cost is to be discussed.

It is seen that the fiber to resin ratios varied considerably for each process. Since the mechanical characteristics of composite materials are directly affected by the fiber ratios; the comparison of the processes boils down to be the comparison of composite structures with different fiber ratios. It should be noted that the variation in the fiber ratios are mainly caused by the differences between the natures of each process. It is not possible to control the fiber ratio for VP and BP process. Whereas it is only partially possible to control the fiber content in VARTM and LRTM processes and controlling the fiber ratio requires extensive study for these processes. The only process in this study which provides full control in fiber ratio is RTM. Therefore it can be said that; although the ranking of the performances are directly dependent on the fiber ratios, the resulting fiber ratios are directly controlled by the character of the processes, thus the comparison is made between the processes.

4.2.1. TGA Tests and Volumetric Ratio Calculations

By using TGA results, the fiber volume fraction is calculated for each specimen as shown in Section 3.6.2. These values were also calculated using the manufacturer's data and measurement results. In Figure 4.2, calculated and measured volumetric fiber ratios for each method are given.

The TGA results show that the $RTM_{(Thick)}$ specimens have the lowest fiber fraction, followed by RTM. The VARTM and LRTM specimens followed RTM and have similar values. VP specimens have higher values and finally the BP process has the highest fiber ratio. The calculated results are very similar to the measured values and all processes yield slightly lower calculated values. However, the differences between calculated and experimentally obtained data are within 5% for all specimens.

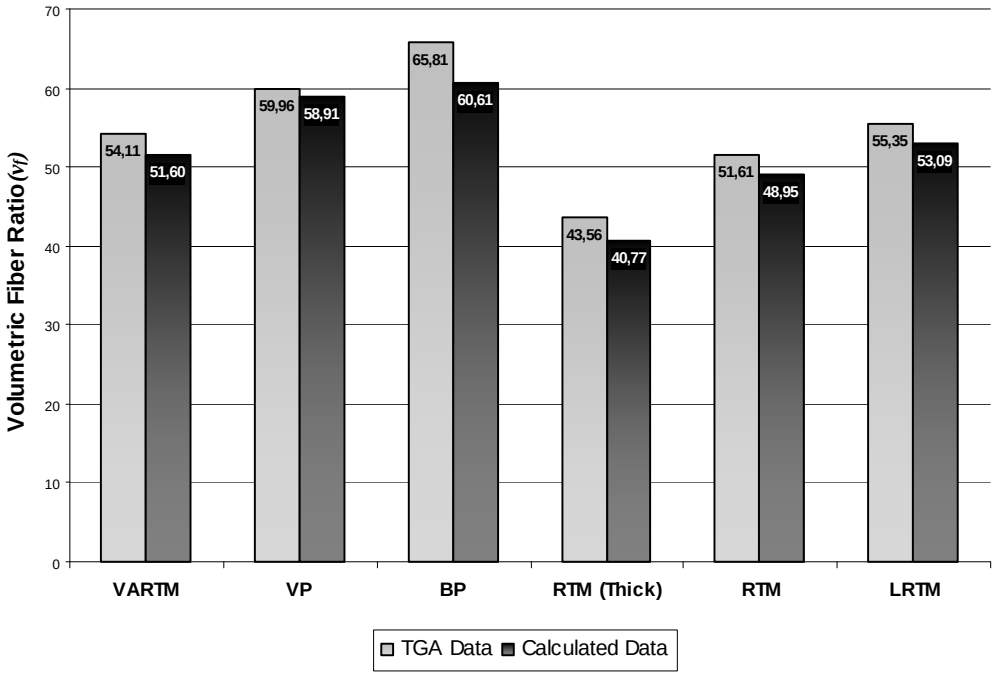

Figure 4.2: Calculated and Measured Volumetric Fiber Ratios

The reason RTM, which is the most advanced and robust process of all, had the least amount of fiber to resin ratio. This can be explained by the mold cavity being large relative to the amount of fabric layers used in the manufacturing process. As stated in Sections 1.1.1 and 2.3.1, the fiber ratio of the specimen produced by RTM is effected by mold cavity. Higher fiber ratios can be achieved by RTM using more layers for the same mold cavity or decreasing mold cavity for the same amount of layers. In this study, a second group of specimens were produced with a smaller mold cavity, by placing a 0.5-mm-thick copper plate inside the mold cavity. Although this modification highly improved the fiber content of RTM process, it was still not enough to achieve the values observed in other processes. Placing a thicker plate would have improved the fiber content even more.

The LRTM and VARTM processes use flexible tooling; therefore the mold cavity does not have a fixed volume. However, the performances of these processes are significantly labor-sensitive. Low fiber ratio values are interpreted as; the low amount of layers could not aid to compensate the labor errors which may have caused some excess resin. It should be noted that the technicians who manufactured the specimens had a better experience especially in hand lay-up and vacuum packaging methods, which may have lead to a more efficient resin usage.

The BP method uses two bleeder layers in each face of the structure, which could take away the excess resin from both surfaces, thereby enabling the specimens to have the largest fiber ratios.

Area densities of specimens were calculated along with the volumetric ratios. Densities are mainly determined by constituents and the fiber/resin ratio. Figure 4.3 shows the calculated area densities of the specimens.

The lowest area density is obtained in the BP method while RTM specimen has the highest. When the area densities are put in an order from highest to lowest; it is the same order for fiber ratio values. This is an expected result since the density is inversely related the amount of fiber used. Therefore, it is seen that the density results agree with the fiber ratio results.

As stated in this section and Section 0, the fiber to resin ratio depends on the character of the examined process. The RTM process was modified increasing the fiber ratio to provide more comparable results. The following sections should be examined within the light of this information.

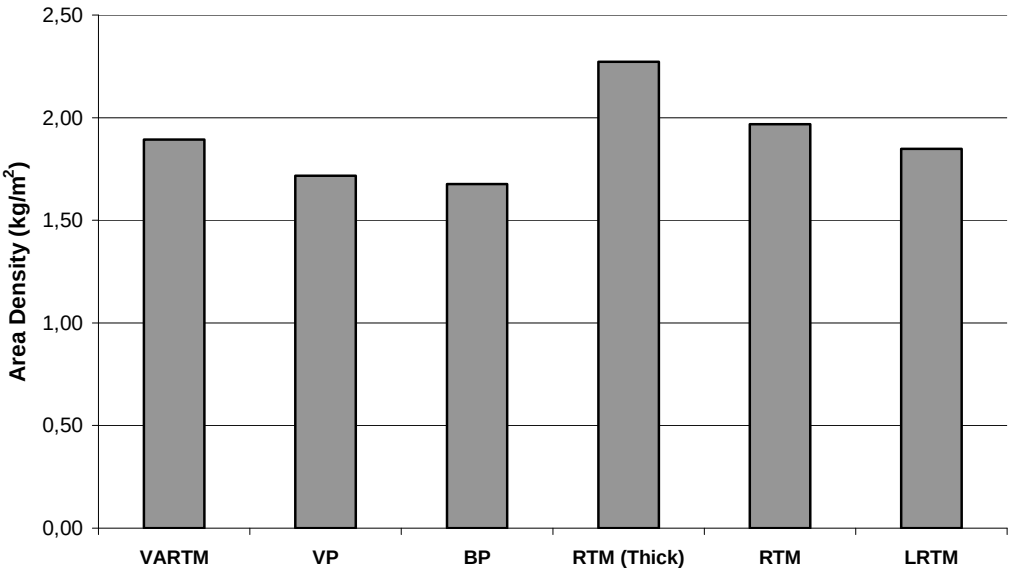

Figure 4.3: Area Densities of Specimens

4.2.2. Tensile Tests

In this part, the ultimate tensile strength and modulus of elasticity values in both directions obtained in tensile tests performed for each production technique are compared.

In Figure 4.4 and 4.5, a comparison of tensile strengths and moduli for all processes in both directions is given respectively. The error bars provided in the graphs symbolize the standard deviations.

The tensile strength results in weft direction are found to be somewhat higher than those obtained for the warp direction. The resulting order in performances in warp direction are; VP, RTM, LRTM, $RTM_{(Thick)}$, followed by close VARTM and BP results. The reason of thick RTM specimens showing a relatively lower performance was their low fiber volume fraction. It is possible to reach higher volume fractions with a decreasing

mold cavity volume for the same number of fabric layers which resulted in thin RTM specimens. This modification provided a considerable improvement in the performance of RTM specimens. Although the RTM specimens did not have the highest fiber fraction, the performance was promising, and it is concluded that it is possible to achieve even higher performance by using a smaller mold cavity.

Similarly, the VARTM and LRTM specimens exhibited a lower performance than relatively simpler method VP. This can be explained with the nature of the resin used. Although the resin was suitable for the RTM process, which is under relatively high pressure and enables the resin to be injected in higher temperatures, and hand lay-up, it could not wet the fabric thoroughly in lower temperatures and lower pressures. This claim is backed up when the specimens were examined visually it was seen that the void content of the VARTM and LRTM plates were slightly larger than VP products.

The low performance of the BP plates despite having the highest fiber ratio was interpreted as the effect of using bleeder as the resin medium. The bleeder being a material which attracts and stores resin, resulted in a less wetted fabric therefore reduced the tensile properties of the plates.

The ordering of the results in the weft direction was similar to that of warp direction. The values were higher except for the $RTM_{(Thick)}$ products, and the performances in decreasing order were; VP, RTM, VARTM, closely followed by LRTM, $RTM_{(Thick)}$ and BP. The increase of strengths compared to warp direction was especially significant for VARTM and VP products. However both RTM and BP processes performances were reduced in weft direction, the resulting values were similar to warp results.

There was a considerable increase in the standard deviations of the moduli measurements and the scatter was even more significant for the results in longitudinal direction. For the average moduli at weft direction were very close for LRTM and RTM plates and the decreasing order was VP, LRTM, RTM, VARTM, $RTM_{(Thick)}$ and BP.

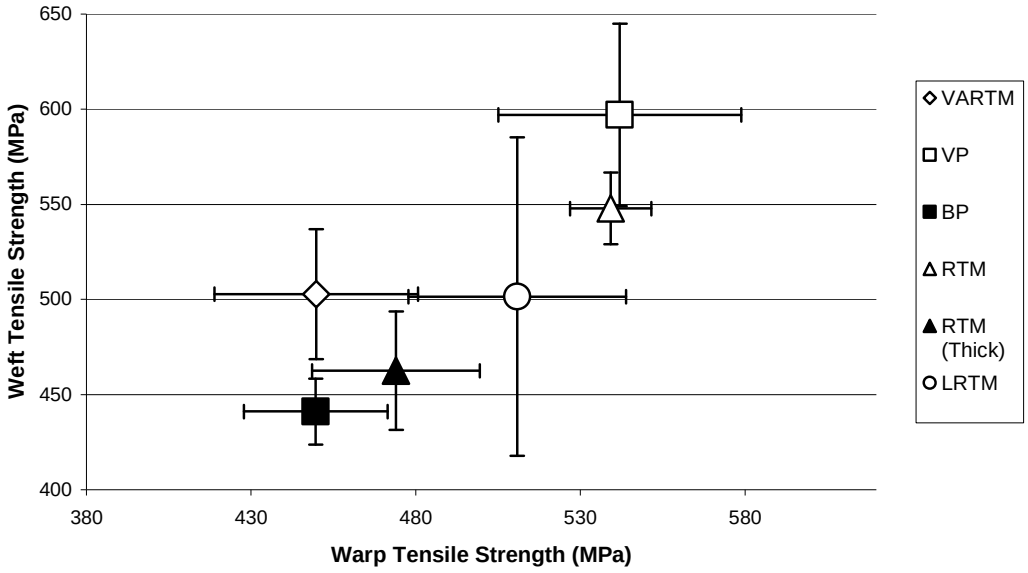

Figure 4.4: Weft Tensile Strength vs. Warp Tensile Strength

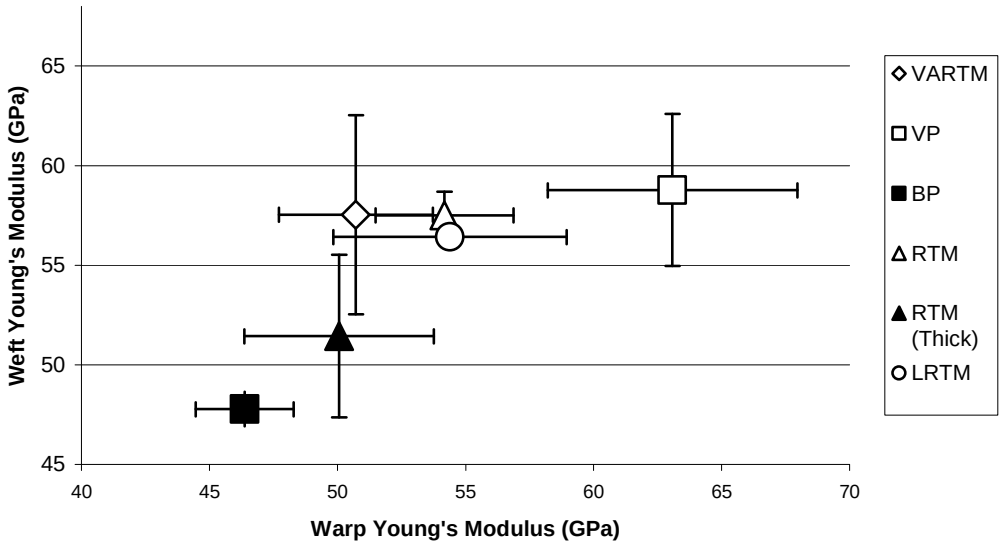

Figure 4.5: Warp Modulus vs. Weft Modulus

Results for VARTM, RTM and LRTM were almost identical in the warp direction, VARTM being the higher. These results consorted with the arguments provided in the previous paragraphs. However it was noted that, very little number of test were carried out for RTM and LRTM processes due to specimen plates' geometric constraints.

As shown in Table 4.3 and Table 4.4 the Poisson's Ratio results were significantly inconsistent. One reason was interpreted as the strain gages' sensitivity. To overcome this issue rosette type strain gages were implemented, this seemed to solve the issue and the VARTM, VP and BP results became more consistent and were found to be closer to the results of different studies which examined unidirectional prepreg composites [68, 69]. However for both RTM classes and LRTM the values were much lower and approached to unidirectional cross-ply prepreg results encountered in previous studies [68] which can be interpreted as more reliable results for the two directional fabric composites used. No solid explanation was found for this issue; as majority of the results had a relatively low standard deviation, but it is obvious that the results were expected to at least be similar to those of RTM, LRTM and the previous studies about cross-ply prepreg composites.

4.2.3. Compressive Tests

In this part, the compressive test results in both directions for each production technique are compared. In Figure 4.6, the graph of results in warp direction vs. the results in weft direction was given. It should be noted that RTM specimens in transverse direction could not be tested; therefore the warp values in the graph also represent the weft direction values. The error bars provided in the graph symbolize the standard deviations thus showing the diversity of data within the test group as well as within other production methods.

Due to the nature of the testing apparatus (see 3.3.2) the failure mode was not appropriate to determine the ultimate compressive strength. Nearly all the specimens failed at the boundary where the specimen was in contact with the pressing tool of the

test apparatus and the failure shapes were observed to be crushed at this boundary. As a result the values were far lower than ultimate compressive strength values encountered in the literature where the values are close to the ultimate tensile strength values [68]. Meanwhile the measurements were close to the interlaminar shear stress (ILSS) values; however no solid link could be established between ILSS and the results [68]. Thus the results should be examined as mere measurements provided to give some idea.

The BP and VP specimens' failure boundary were more crushed while the Thick RTM specimens had somewhat more meaningful failures. This was an expected observation since the thick RTM specimens were expected to bear the greatest load while excessive resin on outer surfaces supports fibers which are placed at the outer surface of the plates, decreasing buckling of these fibers locally. On the contrary, BP specimens' lack of excess resin at both outer surfaces leading to lower values. This was linked to the use bleeder as a resin medium thus all the excess resin in both surfaces is trapped in the bleeder fabric. The compressive test results were similar in both directions; however the results in weft direction were higher than that of warp direction. The order of strength values was; RTM, LRTM, VARTM, VP, BP, where the values of LRTM and VARTM processes were very close and the RTM specimens have significantly higher values than any other process. It should be noted that the compressive tests were implemented for thick RTM specimens only.

While VARTM has comparable strength to that of LRTM specimen in warp direction, the LRTM specimens in the weft direction have significantly higher strength values than VARTM specimens. The results can be explained by the dominant effect of void content as the specimen size is small as defined by related ASTM standards.

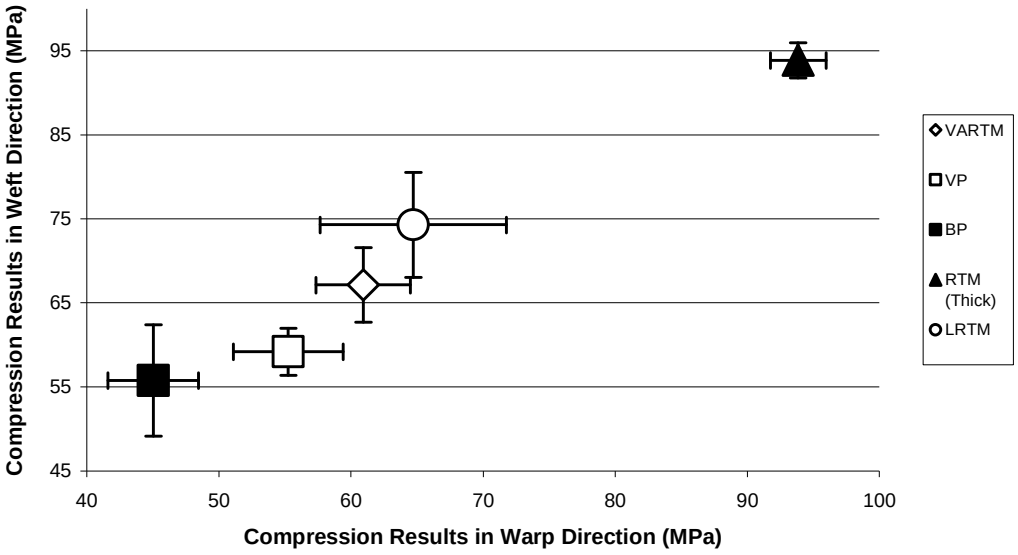

Figure 4.6: Compressive Test results in Both Directions

4.2.4. In-Plane Shear Tests

In this part the shear strength and moduli results in both directions are compared for each process.

In Figure 4.8, the comparison of the processes' shear strengths in both directions were given respectively. $RTM_{(Thick)}$ and LRTM specimens in transverse direction could not be tested; therefore weft values in the graph also represent the warp direction values. The error bars provided in the graphs symbolize the standard deviations thus showing the diversity of data within the test group as well as within other production methods.

In majority of tests, the failure modes were a combination of bearing and shear (Figure 4.7) due to the nature of the testing apparatus (Figure 3.12). To overcome this issue; different torque values were experimented to fasten the bolts of the apparatus and the most appropriate values were found to be between 60-65 Nm. When the bolts were

fastened at these torque values the bearing failure was minimized; however it was not possible to completely eliminate this problem, for when higher torques were implemented the specimens were mangled under the compression effect. Thus, although the measurements were close to the results of earlier studies [69], it is not possible to definitely link the results to shear strengths.

The results had similar values in either direction. In both directions the highest performance was observed at RTM specimens. Following specimens had rather close values in both directions, ranking in decreasing order; VARTM, $RTM_{(Thick)}$, LRTM and VP. Note that due to the low performance of BP specimens this process was not examined for its shear properties. The failure of RTM specimens especially was observed to be as shear failure hence yielded the highest performance.

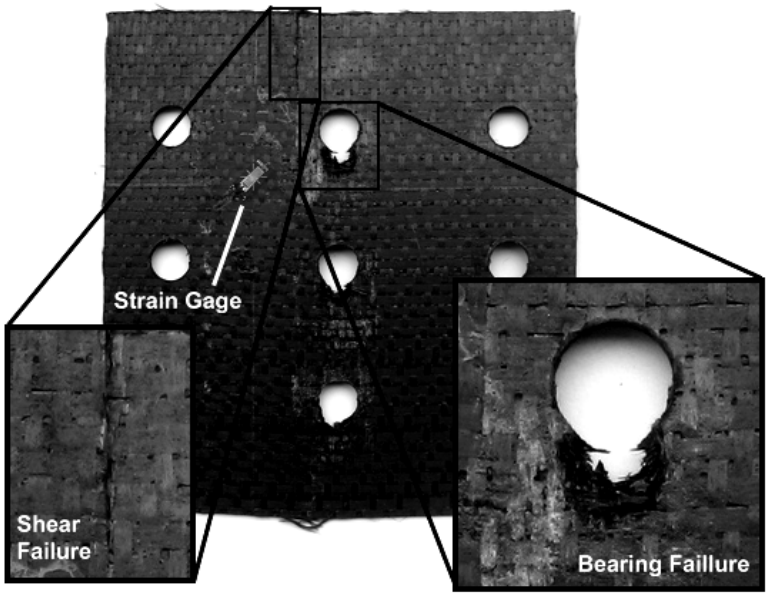

Figure 4.7: Failure Modes Observed in Shear Tests

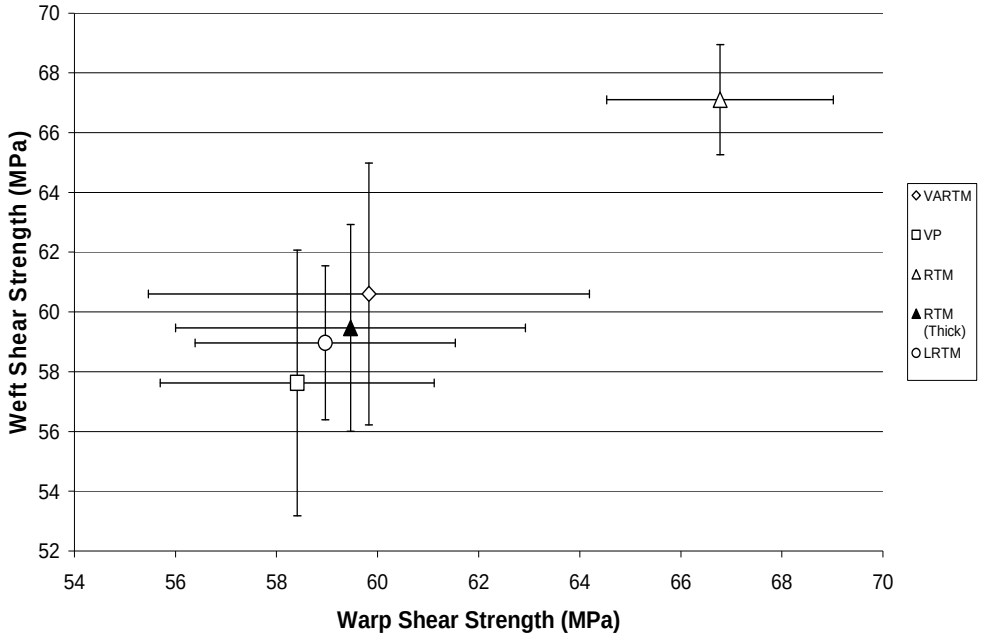

Figure 4.8: Shear Strengths in Weft and Warp Directions

Since all the other specimens additionally had bearing failure characteristics, it was expected for VP to show the least performance as the process resulted in products which had the most variation in thickness and resin content. Recalling the compression test results and failure modes' similarity to bearing, the results were rather expected.

The standard deviations were a considerably high for the shear tests. This was connected to the variations of the failure modes.

The calculated modulus results were not thoroughly investigated as very little data was obtained and no statistical analysis could be made. The examined strain gage data showed different modulus values at various times of the test. This condition was also interpreted as a result of the failure modes rather than strain gage failure; for the data obtained from both strain gages from all tests were consistent with each other. The calculations were given in Table 4.9 and these values were rather low when compared

with previous studies [68, 69]. Additionally the $RTM_{(Thick)}$ and LRTM plates were not examined in weft direction due to the geometrical constraints of the plate geometry

4.2.5. DSC Tests

As stated in the previous sections the DSC tests were performed to prove the cure cycles were performed appropriately and the results were consistent with the specifications provided by the manufacturer. When curing cycles are considered, the T_g values obtained by DSC for each specimen is in agreement with resin manufacturer data. The T_g values are between 122-129°C for VARTM, VP, BP and both RTM specimens which were cured at 120°C. The T_g value for LRTM specimen is 112°C, which was cured at 79°C.

4.2.6. Theoretical Analyses Results

As explained in Section 3.7, the theoretical solution applied provides the upper bound results of the laminates. From the previous work of Ishikawa and Chou, it is known that for 3-harness satin fabric composites; the lower bound values are about one third of the upper bound values [24, 44, 67].

The stiffness results for all the processes excluding BP was observed to be about 40% of the UB values, and both RTM groups provided the highest percentage. BP measurements were about 30 percent of the predicted UB values.

The inconsistencies of Poisson's ratios continued with the calculated values. While the RTM and LRTM measurements were somewhat closer to the predictions; all other measurements were about 10 times their corresponding predictions. This inconsistency between the results of previous studies, measurements and predictions is rather puzzling.

The shear stiffness calculations and measurements also conflicted with each other. Although the RTM measurements were somewhat closer to the predicted values, the fact

that the failure modes of the shear test were not proper, makes it meaningless to compare these results.

The fact that both tensile and shear stiffness predictions had same values regardless of direction is related to the nature of the UB approach. Therefore it is not surprising that the measurements change with direction while the calculations do not.

4.2.7. Ease of Production

When a production with RTM method is proposed, generally a metal mold is needed. The design and production of the tooling for RTM takes a longer process when compared with the other methods used in this study. When producing larger composite parts, RTM molds are very hard to handle and needs extra tooling such as cranes, etc. Pressure distribution on a large mold must be considered, since the pressure distributions on the mold can deform the mold cavity. Sharp corners must also be considered since resin rich edges can occur in such areas.

When RTM or LRTM are considered the tooling should be analyzed in thermo mechanical point of view, as well as considering the resin flow. Without a flow simulation, dry spots can create problems after production of the molds. When VARTM is to be used, resin transfer can be controlled easily to improve the flow by changing the locations of exit ports, adding flow/vacuum ducts/channels and adding new ports during injection. However, when using VARTM method limited pressure gradient slows down the speed of resin front and vacuum system is sensitive to leakage on mold and tooling, this results in the need of thorough flow analysis or a large quantity of trial and error studies. Honeycomb structures can not be produced with VARTM. When VP is used, flow simulation or decision on locations of exit ports is needed seldom and process is rather straight forward.

In order to produce LRTM pieces, an enduring and flexible upper mold should be designed and produced, which requires high level of skill in LRTM mold production.

Preparation of the fabric requires almost same man hour with VARTM, where VARTM requires more man hour for sealant, peel ply and vacuum bag placement and removal.

For large VP parts, long cycle times are required when compared to VARTM. However, heavy fabrics are not suitable for VP such in the case of injection, which increases man hour cost. Additionally for relatively large structures, the technicians should be rather fast to prevent premature curing of the resin, i.e. while the laminae are still being laid up, before vacuum is applied.

4.2.8. Initial Investment and Production Cost

RTM is the most expensive method for production when compared with other methods considered in this study. An infusion system, a universal oven, a vacuum chamber, a resin chamber and instruments are needed. The tooling has an impact on production cost, especially when small quantities are concerned.

VP and VARTM methods are comparatively cheaper. They need simpler tooling/investment and they are suitable for production in small quantities and for prototyping. Additionally VARTM reduces the quantity of wasted resin. Therefore, VARTM is generally advantageous in cost when compared to VP. However for larger quantities of production the scrap and disposable material amounts become somewhat significant. Although for a high level of production, LRTM can be economically advantageous due to a lower value of waste material; for smaller quantities the man-hour required for mold production becomes an issue. The cost of upper tool (diaphragm) will diminish as the number of parts increases. The usage of consumable materials and high man-hour in VARTM and VP is another disadvantage in pricing when compared to LRTM. For very large parts where VARTM use is essential, generally reusable flexible tooling such as silicon vacuum bags is used [1].

4.2.9. Process Reliability and Labor Effect on Quality

VP is highly affected by labor when quality is concerned. The resin distribution and voids in the structure is highly affected by labor quality. In order to control and decrease void content of the structure, air releaser additives can be used. However, these additives can decrease mechanical properties. Since atmospheric pressure is used, pressure is naturally controlled under normal circumstances such in the case of VARTM and LRTM. However, for large products, product thickness varies with local resin pressure due to gravitational effects and resistance due to resin viscosity, which leads to using less viscous resins, further decreasing the mechanical properties.

In VARTM, RTM and LRTM methods, vacuum is applied prior to resin injection. Therefore, void and resin content are supposed to be not affected by labor quality. However, any possibility of leakage should be controlled.

The number and locations of inlet/exit ports are important when a large scale injection is planned; this becomes an issue for VARTM since the positions of inlet/exit ports are not fixed. Additionally in VARTM method, the lack of borders for the vacuum bags and the flexible nature of these bags require a more qualified and experienced labor because any misalignment of the bleeder or peel ply fabrics cause local flaws which dramatically effect the overall performance of the product. These issues are also valid for VP process.

The processes where a flexible tooling is used, there is an inevitable thickness gradient between the inlet/exit ports, regardless of labor. However this condition could be minimized with careful monitoring and automating of the processes. Since the flexible tool used in LRTM method is relatively stiffer, the thickness gradient is much smaller than other methods.

Since most of the RTM systems are computerized and intensively controlled, labor effect on product is less than other four methods. Temperature of the mold, inlet/exit ports, the value of pressure at any point of the mold and system are monitored and

controlled. Moreover, since the product is mold controlled any thickness gradient that would occur would be insignificant.

For both VARTM and VP methods, the surface quality at one side of the part will be poor and tolerances will be rough for most of the cases. When the product geometry is suitable, it is possible to produce a VARTM or VP product with LRTM method. LRTM will lead to a better surface finish at both sides of the piece.

4.2.10. Environmental Considerations

In Europe toxicological materials are subject to a risk assessment procedure according to European Regulation 793/93. According to this regulation, chemicals have to be risk assessed. Since composites are used in industry, measurements show that environmental considerations in order to lower occupational toxicological gas exposure are becoming more and more successful. This is not only a result of lower gaseous toxicological monomer contents in resins, but also a result of improved and/or new production techniques. Both air samples (ppm level of toxicological gasses in breathing zone air) and biological monitoring (such as mandelic acid and styrene metabolic in post-shift urine or blood) show that closed molding techniques have a major role on this success [70].

When resin transfer techniques are concerned, RTM technique is more advanced, considering the effect on environment. In RTM technique the amount of wasted material is minimal as well as, having a resin mixing chamber and a closed mold, exposure to toxicological chemicals is also in minimum. On the other hand, VP has a maximum impact on environment considering the amount of wasted material (excess resin, wasted bleeder, peel ply, sealants, etc.). In addition employing this process maximizes the exposure of workers to toxic chemicals.

However all the production techniques studied, save VP, are technologically promising and have the advantage of reducing emissions of volatile organic compounds (VOCs) by 90% [71]

CHAPTER 5

CONCLUSION

Composite materials are preferred materials mainly used in high technology industries; where higher performances and lower weights are needed. Fiber reinforced polymer matrix composites are highly favored materials in the wide variety of composites because they are relatively easy of manufacture and are lower in weight. The use of fibers provide an orthotropic material characteristic for these structures, which results in much flexible designs that cannot be obtained with conventional isotropic materials or particle reinforced composites.

The early production techniques used to manufacture composites were rather expensive, both because of the hardware requirements and the expensive raw materials needed. Throughout the years cheaper processes which maintained high performance were developed. The most well known of these techniques are resin infusion techniques. These close mold processes were developed to reduce the tooling and raw material costs, as well as the volatiles which are released when the polymeric resins are cured.

However the advantages of composites come with a price; these materials are difficult to design and characterize. For this reason extensive analytical and numerical models were proposed to help the design process. These models have become more powerful through the years; which are used to predict the structural behavior of the composites as well as the characteristics of processes. For these models to be accurate there has to be an accurate database of material characteristics.

In this study a comparison between the most common resin infusion techniques is made; using the same tooling and keeping the process parameters as constant as the nature of different processes allow. Four processes are examined for their tensile, compressive and shear characteristics. These processes are; resin transfer molding (RTM), vacuum assisted resin transfer molding (VARTM), light RTM (LRTM) and vacuum packaging (VP). Throughout the study another process named modified vacuum packaging (BP) is developed; however the test results show that, BP is an unreliable process and provides low performance in addition generates a high amount of scrap material.

A total of 114 mechanical tests are made; 56 tensile, 36 compressive and 22 shear tests. The test results are summarized in Table 5.1. Additionally the results are compared with a theoretical model, and discussions are made in Section 4.2.

Table 5.1: Summary of Experimental Results

	VARTM	**VP**	**BP**	**RTM$_{(Thick)}$**	**RTM**	**LRTM**
V_f/V_c	54	60	66	44	52	55
Area Density (kg/m^2)	1.89	1.72	1.68	2.27	1.97	1.85
E_{xx} **(GPa)**	51	63	46	50	54	54
E_{yy} **(GPa)**	58	59	48	51	58	56
ν_{xy}	0.31	0.35	0.29	0.11	0.04	0.03
ν_{yx}	0.33	0.34	0.34	0.04	0.03	0.05
G_{xy} **(GPa)**	1.81	1.25	-	-	2.4	1.26
G_{yx} **(GPa)**	0.64	0.84	-	-	2.15	-
UTS$_x$ (MPa)	456	542	450	465	538	511
UTS$_y$ (MPa)	503	597	441	463	548	502
UCS$_x$ (MPa)	61	55	45	94	-	65
UCS$_y$ (MPa)	67	59	56	-	-	74
USS$_x$ (MPa)	60	58	-	67	59	59
USS$_y$ (MPa)	61	58	-	-	67	-

There are two groups of RTM specimens, one ($RTM_{(Thick)}$) produced from a larger mold cavity, the other (RTM) from a smaller one. When the $RTM_{(Thick)}$ specimens are examined, the fiber volume ratios, thus the performances, are observed to be rather low. This situation is a result of the mold controlled nature of RTM process. The RTM specimens were manufactured with a modification in the mold; that is, the mold cavity size was reduced by inserting a thin plate inside; to provide comparable data. The resulting products still have lower fiber content; however, their performance is comparable with the other processes, if not higher. It was noted that RTM, being a more advanced process in comparison, is expected to provide a considerable performance improvement in producing 3 dimensional and complex shaped structures.

Since the process parameters were kept as constant as the process characteristics allowed; the fiber ratios, which depend directly on the characteristics, varied for each process. As stated in Section 4.2 this difference in fiber fractions is used to compare the natures of the processes. It is observed that; the processes which use peel ply have a considerable increase in fiber content. However this is a result of the small amount of layers used in the laminates, which causes the percentage of the resin peeled by the peel ply to be significant throughout the laminate.

Although the measured mechanical performances are directly related to the fiber fraction, RTM and BP processes' performance prove that the results do not depend solely on this parameter. BP plates, which used two peel plies in both surfaces, have the highest fiber ratio while their resulting mechanical performance is the lowest in all examined processes. On the other hand RTM and $RTM_{(Thick)}$ plates possess the lowest fiber fractions, $RTM_{(Thick)}$ being the lower. Both RTM processes' performances are high when compared with other processes which have higher fiber volume ratios. Especially RTM which have a comparable fiber fraction provide the highest performance in most properties.

The VARTM and LRTM processes have similar volume fractions thus provide mechanical performances. VP process has the second highest fiber fraction thus in most investigated mechanical properties, VP proved to have the highest performance. It should be noted that the difference between the performances of RTM and VP processes was not excessive when the difference of the fiber fractions, which is more than 10 percent, is considered.

The results show that, VP, VARTM and LRTM processes are more labor dependent, since VP was expected to have the lowest performance among the three. It was noted that the laborers which manufactured the plates were more experienced in VP process.

The failure shapes observed in the compression tests are rather ill-suited, in majority of the experiments the failure boundary occurred at the contact surface of the compressing tool and the specimen. Therefore, the results can not be defined as ultimate compressive strengths (UTS). It was noted that the measurements are close to the interlaminar shear stress (ILSS) values of previous studies [68]; however no solid link could be established between ILSS and the results.

Additionally the failure shapes of the shear tests are a combination of bearing and shear failure (Figure 4.7). This resulted in a plural number of slopes in the stress strain diagrams. Although the stress results are consistent with ultimate shear strengths (USS) reported in previous studies [68, 69], the moduli are significantly different from both the analytical predictions and the reports of previous studies [69].

The measured ultimate tensile strengths (UTS) and Young's moduli are coherent with low standard deviations and consistent with the literature. However the Poisson's ratios differ in a great extent. The Poisson's ratios of VP and VARTM have about ten times those of RTM and LRTM. It was noted that although the results do not conform to other processes, the standard deviations are somewhat low. Considering the same strain gages and test standards were used for each test, this is a surprising result. Further investigation should be carried on to explain this behavior which could be related to

increased void content or poor wetting which are directly connected to the process characteristics.

For future studies, specimens having more plies can be examined. Additionally, flexural tests can be carried out. Since it is obvious that the compression test apparatus is not appropriate to use with composite materials, another standard can be investigated and the tests can be implemented according to that standard. The shear tests can be made according to the Procedure A of ASTM D4255/ D4255M-01 [64], which can reduce the bearing effect on the test results. Furthermore the apparent effect on Poisson's Ratio can be further investigated. Likewise the processes differences can be investigated in micro scale such as fiber wetting characteristics using Scanning Electron Microscope or void content using non destructive testing methods such as ultrasonic testing.

REFERENCES

1. J. Summerscales and T. J Searle. *Low-pressure (vacuum infusion) techniques for moulding large composite structures*. in *Proceedings of the Institution of Mechanical Engineers, Part L: Journal of Materials: Design and Applications*. 2005: Prof Eng Publishing.
2. S.W. Beckwith and C.R. Hyland, *Resin transfer molding: A decade of technology advances.* SAMPE Journal, 1998. **34**(6): p. 7-19.
3. *Guide to Composite Materials*, in Composite Engineering Materials. SP Systems, 2000
4. W. Li, J. Krehl, J. W. Gillespie, et al., *Process and performance evaluation of the Vacuum-Assisted Process.* Journal of Composite Materials, 2004. **38**(20): p. 1803-1814.
5. Plastech T.T. Ltd, *Light RTM Technology & Tool Training Course Notes* 2006.
6. I. Takashi, K. Yamagishi, I. Okumura, et al., *Smart manufacturing of low-cost integrated panel by resin-transfer molding.* Journal of Advanced Composite Materials, 2004. **13**(1): p. 57-66.
7. J.R. Thagard, O.I. Okoli, Z. Liang, et al., *Resin infusion between double flexible tooling: prototype development.* Composites Part A, 2003. **34**: p. 803-811.
8. M.G. Cooper. *Closed mould processing in the marine industry*. in *Proceedings of the Conference on Marine Composites*. 2003: ACMC/SAMPE.
9. A. Hoebergen, E.C.F.C. Van Herpt, and M. Labordus, *The manufacture of large parts using the vacuum injection technique: practical injection strategies for boatbuilding used in the manufacture of the Contest 55*, in *20th Jubilee International Conference*. 1999, SAMPE Europe: Paris. p. 13–15.
10. J. Scherble and T. Jahn. *New ROHACELL® development for resin infusion processes.* in *Sandwich Structures 7: Proceedings of the 7th International Conference on Sandwich Structures*. 2005. Aalborg University, Aalborg, Denmark.
11. J. Woods, A.E. Modin, R.D. Hawkins, et al., *Controlled Atmospheric Pressure Infusion Process*, International Patent: WO 03/101708 A1
12. M.F. Foley, *The flexible resin transfer molding (FRTM) process.* SAMPE Journal, 1992. **28**(6): p. 15-24.
13. M. Frost, D. Solanki, and A. Mills, *Resin film infusion process of carbon fibre composite automotive body panels.* SAMPE Journal, 2003. **39**(4): p. 44-49.

14. M. Kleinberg, L. Herbeck, and C. Schöppinger, *Advanced liquid resin infusion - A new perspective for space structures*, in *European Conference on Spacecraft Structures, Materials and Mechanical Testing,*. 2002: Toulouse, France.
15. D.A. Papargyris, R.J. Day, A. Nesbitt, et al., *Comparison of the mechanical and physical properties of a carbon fibre epoxy composite manufactured by resin transfer moulding using conventional and microwave heating.* Composites Science and Technology, 2008. **68**: p. 1854-1861.
16. B. Griffiths and N. Noble, *Process and tooling for low cost, rapid curing of composite structures.* SAMPE Journal, 2004. **40**(1): p. 41-46.
17. P. Tan, L. Tong, and G.P. Steven, *Modelling for predicting the mechanical properties of textile composites - A review*. Composites Part A, 1997. **28A**: p. 903-922.
18. N.K. Naik, P.S. Shembekar, and M.V. Hosur, *Failure behavior of woven fabric composites.* Journal of Composites Technology and Research, 1991. **13**(2): p. 107-116.
19. R.A. Naik, *Failure analysis of woven fabric reinforced composites.* Journal of Composite Materials, 1995. **29**(17): p. 2334-2363.
20. W.S. Kuo, *Elastic behavior and damage of three-dimensional woven fabric composites.*, in *The Tenth International Conference on Composite Materials*. 1995. p. 301-308.
21. B.N. Cox, M.S. Dadkhah, and W.L. Morris, *On the tensile failure of 3D woven composites.* Composites, Part A, 1996. **27A**: p. 447-458.
22. N.K. Naik and V.K. Ganesh, *Prediction of on-axes elastic properties of plain weave fabric composites.* Journal of Composites Technology and Research, 1992. **45**(2): p. 135-152.
23. T. Ishikawa and T.W. Chou, *Stiffness and strength behavior of woven fabric composites.* Journal of Materials Science, 1982. **17**: p. 3211-3220.
24. T. Ishikawa and T.W. Chou, *One dimensional micromechanical analysis of woven fabric composites.* AIAA Journal, 1983. **21**(12): p. 1714-1721.
25. B.N. Cox, M.S. Dadkhah, W.L. Morris, et al., *Failure mechanisms of 3D woven composites in tension, compression and bending.* Acta Metallurgica et Materialia, 1994. **42**(12): p. 3967-3984.
26. T.W. Chou and F.K. Ko, *Textile Structural Composites*, in *Composite Materials Series*. 1989, Elsevier: Amsterdam.
27. T. Ishikawa, M. Matsushima, and Y. Hayashi, *Experimental confirmation of the theory of elastic moduli of fabric composites.* Journal of Composite Materials, 1985. **19**(5): p. 443-458.
28. K.L. Reifsnider and F. Mirzadeh, *Compressive strength and mode of failure of 8H Celion 3000/PMR15 woven composite material.* Journal of Composites Technology and Research, 1988. **10**(4): p. 156-164.
29. P.S. Shembekar and N.K. Naik, *Elastic behavior of woven fabric composites: II - Laminate analysis.* Journal of Composite Materials, 1992. **26**(15): p. 2226-2246.

30. N.K. Naik and P.S. Shembekar, *Elastic behavior of woven fabric composites: I - Lamina analysis.* Journal of Composite Materials, 1992. **26**(15): p. 2197-2225.
31. M. Karayaka and P. Kurath, *Deformation and failure behavior of woven composite laminates.* Journal of Engineering Materials and Technology, 1994. **116**: p. 222-232.
32. N.K. Naik and V.K. Ganesh, *Failure behavior of plain weave fabric laminates under in-plane shear loading.* Journal of Composites Technology and Research, 1994. **16**(1): p. 3-20.
33. N.A. Fleck, P.M. Jelf, and P.T. Curtis, *Compressive failure of laminated and woven composites.* Journal of Composites Technology and Research, 1995. **17**(3): p. 212-220.
34. P. J. Kim and D. G. Lee, *Surface quality and shrinkage of the composite bus housing panel manufactured by RTM.* Composite Structures, 2002. **57**: p. 211-220.
35. Y.O. Kas and C. Kaynak, *Ultrasonic (C-scan) and microscopic evaluation of resin transfer molded epoxy composite plates.* Polymer Testing, 2005. **24**: p. 114-120.
36. G. Pinter, E. Ladstatter, W. Billinger, et al., *Characterisation of the tensile fatigue behaviour of RTM-laminates by isocyclic stress–strain-diagrams.* International Journal of Fatigue, 2006. **28**: p. 1277-1283.
37. U. Beier, F. Fischer, J.K.W. Sandler, et al., *Mechanical performance of carbon fibre-reinforced composites based on stitched preforms.* Composites Part A, 2007. **38**: p. 1655-1663.
38. A. D. Kelkar, J. S. Tate, and P. Chaphalkar, *Performance evaluation of VARTM manufactured textile composites for the aerospace and defense applications.* Materials Science and Engineering B, 2006. **132**: p. 126-128.
39. C. Niggemann, Y.S. Song, J.W. Gillespie, et al., *Experimental investigation of the controlled atmospheric pressure resin infusion (CAPRI) process.* Journal of Composite Materials, 2008. **42**: p. 1049-1061.
40. H. Gu, *Tensile and bending behaviours of laminates with various fabric orientations.* Materials and Design, 2006. **27**: p. 1086-1089.
41. N. Himmel and C. Bach, *Cyclic fatigue behavior of carbon fiber reinforced vinylester resin composites manufactured by RTM and VARI.* International Journal of Fatigue, 2006. **28**: p. 1263-1269.
42. T.J. Wu and H.T. Hahn, *The Bearing strength of e-glass/vinyl-ester composites fabricated by VARTM.* Composites Science and Technology, 1997. **58**(9): p. 1519-1529.
43. T. Ishikawa and T.W. Chou, *Elastic behavior of woven hybrid composites.* Journal of Composite Materials, 1983. **16**(1): p. 2-19.
44. T. Ishikawa and T.W. Chou, *Stiffness and strength behavior of woven fabric composites.* Journal of Materials Science, 1982. **17**: p. 3211-3220.

45. T. Ishikawa and T.W. Chou, *In-plane thermal expansion and thermal bending coefficients of fabric composites.* Journal of Composite Materials, 1983. **17**(2): p. 92-104.
46. T. Ishikawa and T.W. Chou, *Non-linear behavior of woven fabric composites.* Journal of Composite Materials, 1983. **17**(5): p. 399-413.
47. H.T. Hahn and S.W. Tsai, *Nonlinear elastic behavior of unidirectional composite laminae.* Journal of Composite Materials, 1973. **7**(January): p. 102-118.
48. T.J. Whitney and T.W. Chou, *Modeling of 3-D angle-interlock textile structural composites.* Journal of Composite Materials, 1989. **23**(9): p. 891-911.
49. Y.C. Zhang and J. Harding, *A numerical micromechanics analysis of mechanical properties of a plane weave composite.* Computer and Structures, 1990. **36**(5): p. 839-844.
50. B.N. Cox and M.S. Dadkhah, *The macroscopic elasticity of 3d woven composites.* Journal of Composite Materials, 1992. **29**(6): p. 785-819.
51. N.K. Naik and P.S. Shembekar, *Elastic behavior of woven fabric composites: III - Laminate design.* Journal of Composite Materials, 1992. **26**(17): p. 2523-2541.
52. N.K. Naik and V.K. Ganesh, *Prediction of thermal expansion coefficients of plain weave fabric composites.* Composite Structures, 1993. **26**: p. 139-154.
53. V.K Ganesh and N.K. Naik, *Thermal expansion coefficients of plain-weave fabric laminates.* Composites Science and Technology, 1994. **51**: p. 387-408.
54. V.K Ganesh and N.K. Naik, *Failure behavior of plain weave fabric laminates under in-plane shear loading: Effect of fabric geometry.* Composite Structures, 1995. **30**: p. 179-192.
55. N.K. Naik and V.K. Ganesh, *Failure behavior of plain weave fabric laminates under on-axis uniaxial tensile loading: II - Analytical predictions.* Journal of Composite Materials, 1996. **30**(16): p. 1779-1822.
56. V.K Ganesh and N.K. Naik, *Failure behavior of plain weave fabric laminates under on-axis uniaxial tensile loading: I - Laminate geometry.* Journal of Composite Materials, 1996. **30**(16): p. 1748-1778.
57. V.K Ganesh and N.K. Naik, *Failure behavior of plain weave fabric laminates under on-axis uniaxial tensile loading: III - Effect of fabric geometry.* Journal of Composite Materials, 1996. **30**(16): p. 1823-1856.
58. V.K Ganesh and N.K. Naik, *Failure behavior of plain weave fabric laminates under on-axis uniaxial tensile loading: I - Laminate geometry.* Journal of Composite Materials, 1996. **30**(16): p. 1748-1778.
59. B.V. Sankar and R.V. Marrey, *A unit-cell model of textile composite beams for predicting stiffness properties.* Composites Science and Technology, 1993. **49**(1): p. 61-69.
60. V.K Ganesh and N.K. Naik, *Failure behavior of plain weave fabric laminates under on-axis uniaxial tensile loading: III - Effect of fabric geometry.* Journal of Composite Materials, 1996. **30**(16): p. 1823-1856.
61. *Metals Handbook*. 8 th edition, Editor. T. Lyman: American Society for Metals.

62. Astm D 3039/ D 3039M - 00, Standard Test Method for Tensile Properties of Polymer Matrix Composite Materials. 10 April 2000
63. Astm D 695 - 02a, Standard Test Method for Compressive Properties of Rigid Plastics. Oct 2002
64. Astm D 4255/D 4255M - 01, Standard Test Method for In-Plane Shear Properties of Polymer Matrix Composite Materials by the Rail Shear Method. Feb 2002
65. Astm E 1356 - 91, Standard Test Method for Glass Transition Temperatures by Differential Scanning Calorimetry or Differential Thermal Analysis. April 1991
66. Astm E 1131 - 86, Standard Test Method for Compositional Analysis by Thermogravimetry. Nov 1986
67. T. Ishikawa, *Anti-symmetric elastic properties of composite plates of satin weave cloth.* Fibre Science and Technology, 1981. **15**(2): p. 127-145.
68. J.W. Weeton, D.M. Peters, and K.L. Thomas, *Engineer's Guide to Composite Materials* edition: American Society for Metals.
69. *Evaluation of mechanical performance*, in Euclid RTP 3.15.1, 'RTM for Aerospace Structural Components'. 2002
70. A. Kasper and J.G.M. Van Rooij, *Trends in Worker Exposure to Styrene in the European GRP Industry.* Reinforced Plastics, 2007. **51**(5): p. 18-25.
71. P. Lazarus, *Infusion!* Professional Boat Builder, 1994. **31**: p. 42-53.